ADAPTIVE PROTECTION FOR RENEWABLE-BASED AC MICROGRIDS IN LOW-VOLTAGE RADIAL NETWORKS

by

Marnó Zietsman

Submitted in partial fulfilment of the requirements for the degree
Master of Engineering (Electrical Engineering)

in the

Department of Electrical, Electronic and Computer Engineering
Faculty of Engineering, Built Environment and Information Technology

UNIVERSITY OF PRETORIA

August 2020

SUMMARY

ADAPTIVE PROTECTION FOR RENEWABLE-BASED AC MICROGRIDS IN LOW-VOLTAGE RADIAL NETWORKS

by

Marnó Zietsman

Supervisor:	Prof. R.M. Naidoo
Department:	Electrical, Electronic and Computer Engineering
University:	University of Pretoria
Degree:	Master of Engineering (Electrical Engineering)
Keywords:	Fault current analysis, low-voltage, optimally sizing, protection re-coordination, radial distribution networks, renewable-based AC microgrids

By placing clusters of renewable-based AC microgrids in low-voltage radial distribution networks, emergent energy demands can be met. However, this leads to fundamental changes and challenges in the topology and protection coordination performance. Protection challenges such as bi-directional current flow, sympathetic tripping, protection blinding, unwanted islanding, system stability, nuisance tripping and prohibition of unsynchronised reclosing may occur. This is due to the complex operation and control of the embedded renewable-based microgrid, causing increased penetration of dynamic fault currents in the radial distribution network. The aforementioned protection challenges prove that existing South African low-voltage protection philosophy standards are unreliable and need to be re-evaluated. It is expected that by optimally sizing and selecting renewable distributed generators, alongside using communication-based intelligent electronic devices and adaptive protection strategies, a hybrid adaptive protection scheme can be outlined and developed for embedded renewable-based AC microgrids in South African low-voltage radial distribution networks.

The developed adaptive hybrid protection philosophy should be able to successfully clear high- and low-impedance faults in a selective, sensitive, speedy and reliable manner. This investigation looks into

the various short-circuit fault current levels experienced in a low-voltage radial distribution network, (namely three-phase, phase-phase, phase-to-ground, and phase-phase-to-ground) when embedded renewable-based AC microgrids are integrated. Three various types of renewable energy sources (namely solar photovoltaic, wind generation and energy storage systems) are modelled and designed to in accordance with the *South African grid code requirements for renewable power plants* and *SANS 10142-1: Wiring of premises* standards, and *NRS 097-2-1: Grid interconnection of embedded generation*. The renewable energy sources and proposed adaptive protection schemes are simulated and validated in a low-voltage radial distribution network with the use of DIgSILENT PowerFactory 2017. The results obtained are used to outline and develop an adaptive hybrid philosophy standard to assist in maintaining the protection coordination between the embedded renewable-based AC microgrid and in-line protection intelligent electronic devices. Additionally, an optimisation function is used to optimise the renewable-based AC microgrid's capacity and power flow, in-turn reducing losses, fault limits, bi-directional power flow, initial cost investments and increasing the voltage profile of the low-voltage radial distribution system. Through this implementation and investigation network efficiency and protection selectivity, sensitivity, stability and reliability of the existing radial low-voltage distribution network, will improve when renewable-based AC microgrids are integrated. This will correct major limitations in the South African low-voltage protection philosophy standards for the development and future introduction of independent power producers in low-voltage radial networks in the utility grid.

LIST OF ABBREVIATIONS

CB	Circuit Breaker
CTI	Coordination Time Interval
CSP	Concentrated Solar Power
ESS	Energy Storage System
FCL	Fault Current Limiter
GM	Gain Margin
IBDG	Inverter-based Distributed Generator
IDMT	Inverse Definite Minimum Time
IED	Intelligent Electronic Device
IEEE	International Electrical and Electronic Engineers
IPP	Independent Power Producer
IRP	Integrated Resource Plan
KCL	Kirchoff's Current Law
LC	Local Controller
LOM	Loss of Main
LV	Low-Voltage
MMS	Microgrid Management System
PCC	Point of Common Coupling
PSM	Plug Multiplier Setting
p.u.	Per Unit
PV	Photovoltaic
RBDG	Rotating-based Distributed Generator
RBM	Renewable-based AC Microgrid
RDG	Renewable Distributed Generator
RDN	Radial Distribution Network
RPP	Renewable Power Plant
THD	Total Harmonic Distortion
TMS	Time Multiplier Setting
SAIDI	System Average Interruption Duration Index
SANS	South African National Standards
STC	Standard Test Condition
WP	Wind Power

TABLE OF CONTENTS

CHAPTER 1 INTRODUCTION

1.1 PROBLEM STATEMENT

1.1.1 Context of the problem

Electricity tariff costs have been increasing in South Africa over the past years, allowing the cost of renewable electricity generation investment to decrease [1]. This makes it appealing to end users, creating a market for small, independent power producers (IPPs) to supply renewable power to low-voltage (LV) distribution networks [1, 2].

Existing LV ($\leq$1 kV) AC distribution networks in South Africa are mainly radial in design and use a centralised single source in-feed generation [1–5]. The LV protection philosophy of such networks depends on fixed-setting protection relay coordination performance, based on inverse definite minimum time (IDMT) curves [6, 7], unidirectional power flow [7, 8], and rely on the assumption that fault levels uniformly decrease as the fault moves further away from the single source in-feed [1, 9, 10]. This philosophy allows optimal time-current grading coordination between the low cost electromechanical protection devices to detect and isolate short-circuit current and earth system faults successfully within the shortest possible time before any damage is caused within the network [1, 2, 7, 11].

The introduction of overly sized and arbitrarily-placed embedded renewable-based AC microgrids (RBM) in LV radial distribution networks (RDNs) will lead to fundamental changes and challenges in the topology and protection performance of the power system [8, 9, 12, 13]. This will affect the existing fixed-setting protection relay IDMT curve coordination performance, which - in succession - will reduce the power system's protection stability, selectivity, reliability, sensitivity and fault clearance speed [1, 3, 8, 13].

The revised 2013 Integrated Resource Plan (IRP) [14] estimates that by 2030, 21% of the total energy generated in South Africa, will be produced by renewable energy sources. This motivates the need for re-evaluation of the existing LV protection philosophy standards [15] to ensure that the full benefits of optimally sized and placed embedded RBMs in South African LV radial networks can be reaped.

1.1.2 Research gap

Emergent energy demands in LV distribution networks can be met environmentally and economically by integrating clusters of RBMs [1, 4, 8, 9, 12]. Yet, the introduction of RBMs in LV radial networks will affect the existing fixed-setting protection device IDMT curve coordination performance [13]. This is due to the penetration of dynamic fault levels caused by the RBMs at fault. This, in turn, causes fundamental changes and challenges in the radial topology and protection performance of the power system [9, 12]. These changes and challenges will discriminate the IDMT curve coordination of existing LV fixed-setting protection devices [15].

By optimally sizing and placing RBMs, alongside with communication-based intelligent electronic devices (IEDs) and adaptive protection strategies, a protection philosophy can be outlined and developed for embedded RBMs in South African LV RDNs. This new, adaptive protection philosophy standard will correct the challenges faced when RBMs are integrated in the South African LV radial network. The introduction of optimally sized and placed RBMs, with adaptive protection capabilities, will lead to the reduction of power system losses, as well as transmission and distribution costs [4, 16]. Power reliability, quality, regulation and stability would also be improved [1, 3, 4, 8, 16].

1.2 RESEARCH OBJECTIVE AND QUESTIONS

This research paper will answer the following questions in order to ensure that an effective, adaptive LV protection philosophy can be investigated, outlined and developed for optimally sized and placed embedded RBMs in South African LV radial networks. By doing so, major limitations in the existing LV protection philosophy standards will be corrected.

1. Can adaptive microgrid protection methods be implemented in an existing South African LV RDN, without affecting existing protection philosophies?

2. How will the adaptive protection coordination affect the existing in-line fixed-setting protection relay coordination (such as fuse-recloser coordination) in the LV RDN when RBMs are integrated and/or removed?
3. Will fuse-relay grading coordination still be required when adaptive protection coordination is applied to the embedded RBMs and LV RDN, using intelligent electronic devices?
4. How will the earthing protection in the existing LV RDN be affected by the introduction of RBM grounding and transient fault penetration?
5. How will the dynamic response, bi-directional power flow and fault penetration levels of various renewable-based generator units (inverter-based distributed generators, rotating-based distributed generators and energy storage systems) affect the IDMT curves of existing fixed-setting coordinated protection relays in the LV RDN?
6. How will an optimisation technique be used to optimally size and place microgrids to pose maximised improvement for system losses, voltage profiles, enhanced system reliability and minimise costs of embedded RBMs in the existing LV distribution network?

By designing a case study, using an existing LV radial network in South Africa and applying the questions being asked above, the answers might be able to assist in developing an ideal LV protection philosophy that will cater for an adaptive protection scheme, used by the RBMs in LV RDNs.

1.3 HYPOTHESIS AND APPROACH

Through the implementation and investigation of an adaptive protection scheme for optimally sized and placed RBMs, the efficiency, protection and reliability of the existing LV radial networks can be improved when RBMs are integrated to or removed from LV RDNs. This will correct both the major limitations in the South African LV protection philosophy standards and enhance the development and future introduction of IPPs to the LV radial distribution utility grid. Many low-end industrial companies and users will benefit from it [9, 17].

In order to prove this hypothesis an LV RDN and multiple RBMs will be modelled, in accordance with *South African grid code regulations for renewable distributed generation* [18], *SANS 10142-1: Wiring of premises* [19] standards and *NRS 097-2-1: Grid interconnection of embedded generation* [20]. A dynamic fault study will be done on the modelled LV radial network to determine the maximum and

minimum fault currents in the network before and after overly sized and arbitrarily-placed embedded RBMs have been integrated. Protection IDMT curve coordination will then be calculated and compared, using the collected simulated data. An optimisation technique will then be used to optimally size the RBMs according to the system constraints gathered from the simulated studies. Protection IDMT curve coordination will then be re-calculated, using the newly simulated data where the RBM is optimally sized and placed in the modelled LV radial network. This approach will assist in outlining the changes and challenges faced when integrating renewable sources in LV radial networks, and the development of the adaptive protection philosophy essential to maintain the protection IDMT curve coordination between the RBM and existing in-line protection devices.

1.4 RESEARCH GOALS

The research goal is to observe the effects of overly sized and arbitrarily-placed RBMs towards the sensitivity and selectivity of the fixed-setting protection relays IDMT curve coordination in LV RDNs. Then, by optimally sizing and placing the RBMs, an adaptive protection scheme can be developed to re-coordinate the IDMT curves of integrated/removed RBMs and the in-line protection devices. In turn, the findings can be used to not only motivate the need to move from fixed-settings protection devices to intelligent electronic devices for there inter-communication qualities, but also to assist in outlining an LV adaptive protection philosophy to be used in South African LV RDNs. The outcome will assist in maintaining the protection coordination between integrated RBMs and in-line protection devices in South African LV RDNs.

1.5 RESEARCH CONTRIBUTION

The research contribution will be based on the effects of overly sized and arbitrarily-placed versus optimally sized and placed RBMs in LV RDNs. An LV adaptive protection philosophy standard for South African LV RDNs is then developed to assist in the re-coordination of protection IDMT curves between the optimally sized and placed RBMs and in-line protection devices. This will allow end users to safely integrate optimally sized and placed RBMs in LV RDNs and achieve the full benefits of renewable distributed generation, while still maintaining protection coordination between the grid-connected RBMs and in-line protection devices.

1.6 OVERVIEW OF STUDY

An LV radial distribution feeder (Feeder A), adapted from an Eskom LV RDN, is modelled in DIgSILENT PowerFactory 2017. Feeder A is an 11 kV, network stepped down to 400 V, using a 200 kVA distribution transformer. The LV side of the distribution transformer supplies four loads at the end of four 1 km lines, respectively. Each load varies between 15∼70 kW.

This study will focus on the impact of overly sized and optimally sized renewable distribution generators (i.e. wind power, photovoltaic and energy storage system) towards the protection IDMT curve coordination of the in-line fuses and fixed-setting protection relays. The renewable distributed generators (RDGs) simulated, are modelled according to the *South African grid connection codes for renewable power plants* [18], *SANS 10142-1: Wiring of premises* [19] standards and *NRS 097-2-1: Grid interconnection of embedded generation* [20] to ensure safe operation and connection to the LV RDN.

The results of this study show how the integrated RBMs discriminate IDMT coordination between the fuse-relay and relay-relay fixed-setting electromechanical protection relays. This motivates the need to move away from existing in-line electromechanical relays to protection IEDs. The IEDs processing - and communication-based capabilities are required to update the coordination of the IDMT curves between the RBM and in-line protection relays. The use of fuse protection closest to the point of connection of the RBM to the LV RDN, is seen to no longer be necessary due to the RBM IED being able to satisfactorily clear in-zone faults. The upstream upstream protection IED is also able to satisfactorily clear system faults, in case the RBM protection IED would fail. Additionally, the study shows that by optimally sizing the RBMs, not only is the fault level contribution to the LV RDN minimised, but also the reduction of investment costs of the RBM. The study concludes and demonstrates that by using an adaptive protection scheme, the in-line LV RDN protection IEDs can successfully be re-coordinated with the RBM IEDs when introduced into the LV RDN.

CHAPTER 2 LITERATURE STUDY

2.1 INTRODUCTION

Power generation industries across the world are experiencing a need for increased power supply in distribution networks, due to continuous population growth. Traditional power generation plants prove inadequate in terms of fuel and construction costs, efficiency, reliability, carbon emissions and various power system losses [3, 4, 9]. However, these emergent energy demands could be environmentally and economically met by designing optimally sized, selected and placed clusters of renewable distributed generators (RDGs) [1, 4, 9, 12, 16]. This can be done by integrating RDGs near end users in a low-voltage (LV) ($\leq$ 1 kV) AC distribution network. Additional benefits include the reduction of power system losses, as well as transmission and distribution costs [4, 16]. Power reliability, quality, regulation and stability would also be improved [1, 3, 4, 12, 16]. Renewable energy sources, such as solar photovoltaic (PV) systems, concentrated solar power (CSP), fuel cells, biomass, gas turbines, hydroelectric and wind power (WP) generation [1–4, 9, 12] are common types of RDGs.

A microgrid is used to assist in controlling multiple numbers of RDGs and energy storage systems (ESS) as a single unit of control [5, 9, 12]. The microgrid optimises reliable voltage security, safety and stability for the user. This is done with the use of local microcontrollers, protection devices, power flow strategies and energy management methods [9, 12, 21]. The microgrid couples RDGs (<100 kVA for LV networks) to a single point of common coupling (PCC), using AC synchronisers, power electronic converters and isolation transformers [1, 6, 12]. It can operate in both stand-alone and grid-connected mode [2, 5, 9, 21]. Power electronic converters are used to convert the DC source generated by a RDG to a grid-synchronised AC voltage. They assist in controlling power-flow, limit stored fault currents, decouple dynamic energy sources from the grid and stabilise the microgrid frequency and voltage when in stand-alone mode [2, 4, 12].

Existing traditional LV distribution networks in South Africa are radial in design and use a centralised single-source in-feed generation [1–4, 6, 7, 21], as shown in Figure 2.1. The LV protection philosophy standards of such networks depend on fixed-setting relay coordination performance, using inverse definite minimum time (IDMT) curves [2, 7], unidirectional power flow [7], and rely on the assumption that fault levels uniformly decrease as the fault moves further away from the single-source [1, 9]. These philosophies allow optimal time-current grading coordination of IDMT curves between the low cost electromechanical protection devices to detect and isolate internal and external faults successfully within the shortest possible time [1, 2, 7, 11, 21].

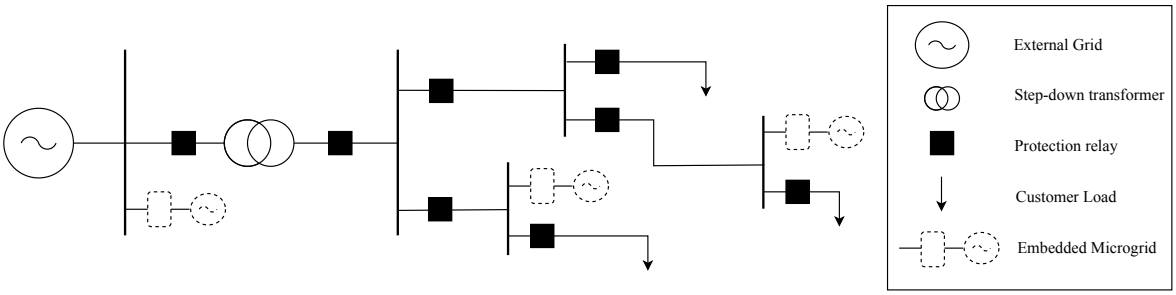

Figure 2.1. Single line diagram of a traditional single-fed LV radial distribution network

The introduction of the renewable-based AC microgrid's (RBM's) complex operation and control [11, 12, 21] in radial distribution networks (RDNs) leads to fundamental changes and challenges in the topology and protection coordination performance [1, 3, 4, 6, 9, 12, 22]. This affects existing protection device IDMT curve coordination performance which, in turn, reduces the power system stability, reliability and quality [1, 3].

Contributing factors include:

- Bi-directional current flow penetration of RDGs in normal and abnormal conditions [1, 3, 9];
- Dynamic response of the various number and types of connected RDG units (IBDGs and RBDGs) [1, 2, 9, 12];
- IBDGs' limiting and RBDGs' high output fault current contribution - between 1.2∼2 per unit (p.u.) inverter rated and 5∼10 p.u. rated current, respectively [1, 9, 12];
- Location placement and capacity of the microgrid in the distribution network [4, 6, 9, 16];
- Microgrid grounding methods [12, 23].

The aforementioned factors result in the following protection challenges to arise:

- Increased and decreased dynamic short-circuit current and overcurrent fault level penetration with respect to mode of operation [1, 3, 5, 7, 9];
- Sympathetic/false tripping [1, 6, 7, 24];
- Nuisance tripping [21, 22];
- Prohibition of synchronised reclosing [6, 22, 24];
- Unwanted islanding [1, 6, 9];
- Protection blinding [1, 3, 6, 22, 23];
- Discrimination of the protection device selectivity (device over-reaching/under-reaching) [3, 6, 12, 22, 24].

These protection challenges prove that existing South African LV protection philosophy standards [15] are unreliable, and need to be re-evaluated before integrating RBMs in traditional LV RDNs.

Directional overcurrent and directional relays [5, 21, 25] with the use of fault current limiters (FCL) [3, 9, 24, 26] are suitable to protect the RBM during overcurrent and short-circuit faults when grid-connected. However, when the RBM is in stand-alone operation, protection must be more sensitive in detecting fault current levels. This is due to short-circuit current magnitudes being significantly smaller than when grid-connected [6, 7]. This makes it the main protection concern, as traditional protection devices either do not respond or take much longer to trip than the required pre-set tripping time [5, 6]. Thus, based on *South African grid connection codes for renewable power plants* (RPP) [18] and *NRS 097-2-1: Grid interconnected of embedded generation* [20], in the event of a fault or disturbance in the distribution network surrounding the RBM, it needs to be disconnected from the utility grid at the PCC. This prevents undesirable microgrid islanding during loss of main (LOM) [1, 2], and ensures that the protection device coordination operates according to the original time-current graded settings [2]. Furthermore, this ensures safe working conditions for line technicians to locate and repair a line fault under substation dead conditions [2]. When disconnected from the utility grid, the stand-alone RBM must prove reliable by supplying power, if un-faulted, to the customers' load, thereby preventing total blackout [2]. Before re-synchronising the RBM to the utility grid, it is also essential to ascertain that voltage magnitude, phase angle and frequency of both energy systems are within acceptable limits [6, 9].

Advances in AC microgrid protection allow safe and reliable operation of both modes of operation. This is vital for maximum effectiveness for a RBM protection philosophy. This can be achieved with the use of communication and sequence component-based intelligent electronic devices (IEDs). Research shows [1, 5, 6, 9, 12] that existing protection methods such as time-overcurrent, differential protection, distance protection, harmonic distortion detection and adaptive protection allow for effective RBM adaptability and improved protection coordination within the LV RDN.

This paper presents a comparative fault and optimisation analysis to develop an effective and reliable adaptive protection coordination philosophy for RBMs, controlling one to multiple RDGs, in the existing South African LV RDNs. While considering the aforementioned effects and challenges of AC microgrids on the existing LV protection philosophy standards, the investigation will follow the requirements as listed for category A1 and A2 ($\leq$ 100 kVA) for LV connected RPPs in distribution networks in accordance with the *South African grid code requirements for RPPs* [18], *SANS 10142-1: Wiring of premises* [19] standards and *NRS 097-2-1: Grid interconnection of embedded generation* [20] to ensure that safety and design standards are met. DIgSILENT PowerFactory 2017 is used to model and simulate selected RDGs (solar PV, WP and ESS) in existing LV radial feeders. These forms of RDGs are selected, due to solar PV and WP being some of the most common renewable sources used in renewable generation and are ideal for the South African climate. Additionally, an efficient ESS can compensate for the very low inertia caused when a new load is added to a power system, where the initial energy balance becomes unstable [9]. Various aforementioned short-circuit fault simulations (namely three-phase, phase-phase, phase-to-ground, and phase-phase-to-ground) will be investigated to observe the effect of fault current penetration levels caused by clusters of RBMs in LV RDNs. With the results and information gathered from the simulations and modelling, an adaptive LV protection philosophy can be outlined and developed to correct the protection challenges faced when optimally sized and placed RBMs are integrated within the South African LV RDNs.

2.2 GROUNDING METHODS FOR AC MICROGRIDS

The primary purpose of system grounding is to minimise the damage to the system in the event of an earth fault. This makes it essential to include suitable RBM grounding methods to ensure optimal performance of protection coordination and personnel safety [12, 23, 24, 27]. The purpose is to ensure that if an earth fault would occur anywhere on the electrical installation, it could be safely discharged

to earth. More importantly, the earth fault current return path ensures that there is sufficient current to allow detection of an overcurrent element [17]. Various ways of grounding the system can each result in different levels of current and voltage stress. Through the use of isolation transformers in RBMs, various wiring configurations and grounding methods can be utilised to connect to the LV RDN [12]. The varieties of system grounding methods can be seen in Table 2.1.

The base impedance of a grounding configuration in a power system determines the desired ground fault levels [27]. High-impedance uni-grounded RBMs are more complex, due to the significant reduction in ground fault values [12, 27]. This poses a safety hazard to personnel and protection devices [12] and affects the operation of grounded RDGs [27]. Using low-impedance grounding will form fault currents high enough for protective relays to detect and isolate, increasing the sensitivity and reliability of the microgrid [12]. Additionally, low-impedance grounding reduces arc flashes and arcing current, which are the common causes of ground faults [12]. Solidly grounded earthing protection does not limit ground fault currents; it merely offers elimination of ground potentials. It also isolates grid-connected RDGs from zero-sequence components [1, 27], enabling the earth fault protection to remain stable.

Research [12, 23, 24] shows that TT and TN-C solid grounding protection earthing methods are commonly used in LV AC distribution networks and remain ideal for LV RBM grounding. Connected RDGs have no influence on the protection earthing system [23]. TT is ideally used for multi-grounding methods, which contain multiple separate neutral grounding points for the RDG, isolation and distribution transformer [12]. TN-C is ideally used for uni-grounding methods where there is only a single common point of neutral grounding configuration between the installed electrical apparatus [12]. With accordance to the *South African grid connection codes for RPPs* [18] and *SANS 10142-1: Wiring of premises* [19] standards, any installation with a neutral point supplied by a combination of transformers and generators located near one another, will be connected to a single neutral bar, that is connected to the consumer's earth terminal and not earthed beyond the earth leakage device. To comply with these standards, TN-C uni-grounding types of solid earthing methods [12, 23] will be considered for the RBM earthing protection, as shown in Figure 2.2. If there are no isolation transformers present in the RBM, neutral points of the IBRGs or RBDGs can be used to configure type I, II or III [12] to allow for effective grounding. An AC system may be said to be effectively grounded when, for all points on the system or specified portion thereof, the ratio of zero-sequence reactance to positive-sequence reactance is not larger than three and the ratio of zero-sequence to positive-sequence reactance is not

Table 2.1. Varieties of system grounding methods

Grounding Method	**Definition**	**Typical levels of available ground fault currents expected**
Solid	No intentional impedance in the grounding path	Same order of ground fault currents as available for three-phase fault -usually in the order of several thousands of ampere
Effective	Based on reduced insulation levels and rated (80%) surge arresters can be used $R_0 \leq X_1$ and $X_0 \leq 3X_1$	
Serving line-ground loads	$Z_0 \geq Z_1$	
Reactance	Intentional insertion of reactance into the system ground path $R_0 \leq 10X_1$	Range from 25% to 60% of the three-phase level - these correspond to X0/X1 ratios of 10 and 3
Low-resistance	Intentional insertion of resistance into the system grounding path $R_0 \leq 2X_0$	From as low as 150 A up to several thousand ampere
High-resistive	The insertion of nearly the highest permissible resistance in the grounding connection $R_0 \geq X_{c0}$	Fault currents up to 50∼100 A - usually less than 10 A
Ungrounded	No intentional grounding connection	Coupled to ground through the distributed capacitance of its phase windings and conductors

larger than one for any condition of operation and for any connected generator capacity [12]. Resistor R_g, reactance X_g or solidly grounded, at the neutral point of the distribution transformer, can be used to assist in achieving effective grounding [12].

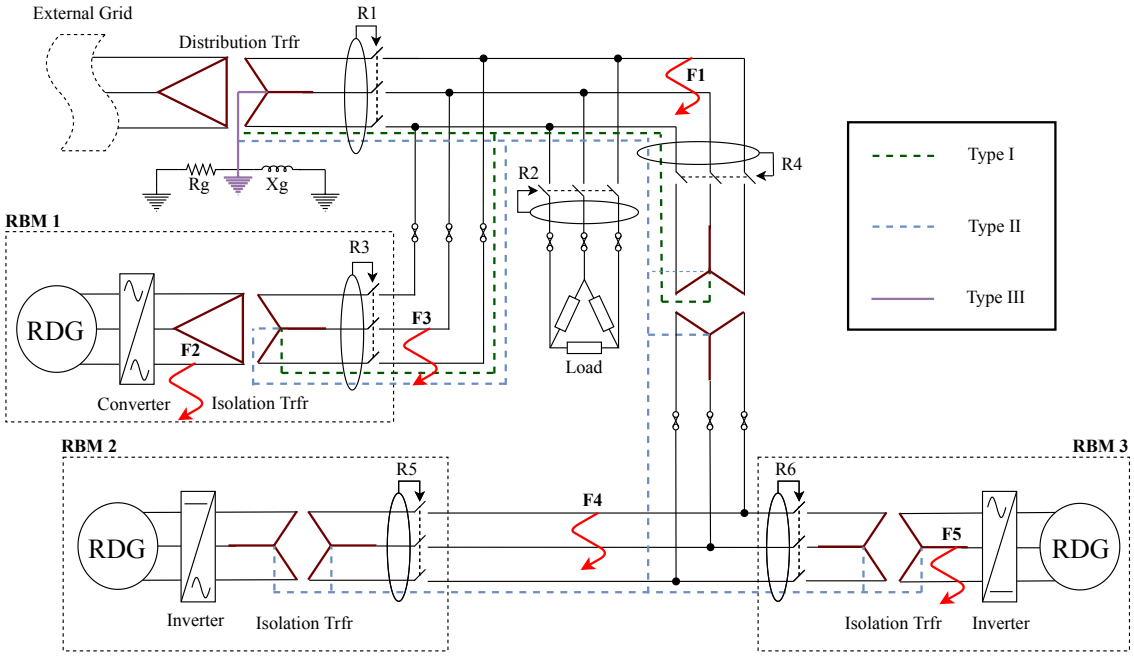

Figure 2.2. Developed LV radial feeder test-bed, with renewable-based AC microgrid and various configuration types of typical uni-grounding methods

2.3 AVAILABLE MICROGRID PROTECTION METHODS

Traditional LV RDNs mainly consist of low-cost protection devices, namely: fuses, reclosers, overcurrent relays and breakers [6, 21]. All of these protection devices' IDMT curves are coordinated to isolate the identified fault, closest to them, in the load feeder of RDNs. Fuses, used to clear permanent faults, are coordinated with upstream reclosers. Reclosers are used to clear transient faults. The coordination between the two ensures adequate protection in the distribution network [1, 9, 21], as shown in Figure 2.3(a). If a permanent fault is detected on the load feeder, the fuses operate first, clearing the fault before the recloser operates on the slow curve. If the fuse fails to clear the fault in time, the recloser will act as back-up protection by operating on the slow curve before locking out, consequently isolating the fault [1, 22]. This device coordination strategy prohibits sympathetic/false tripping and protection blinding [3, 7]. It also decreases maintenance costs and ensures reliability of supply to un-faulted sections in the LV RDN [3, 7].

The RDGs nature dependent dynamic penetration levels cause a traditionally unidirectional power system flow to become bi-directional [3, 6, 22]. The fault current levels become inconsistent and vary according to the RBM's modes of operation. This affects protection coordination performance in LV RDNs [1, 2, 5, 6]. Protection cannot be guaranteed if the fault current levels, flowing through any protection device, are changing continuously [3]. In Figure 2.3(b), the protection coordination discriminates between the primary and back-up relay as the coordination time interval (CTI) is being decreased. This is caused by the continuously changing fault current contribution by the RBM, flowing through any fixed-setting relays, minimising the protection CTI between the in-line relays [10]. This can cause the downstream fuse to blow before the fast trip of the recloser detects the fault upstream, thereby affecting the protection performance coordination of the network. The extent to which the protection coordination between the in-line relays are affected, is dependent on size, location and number of connected RBMs in the LV RDN [4, 16].

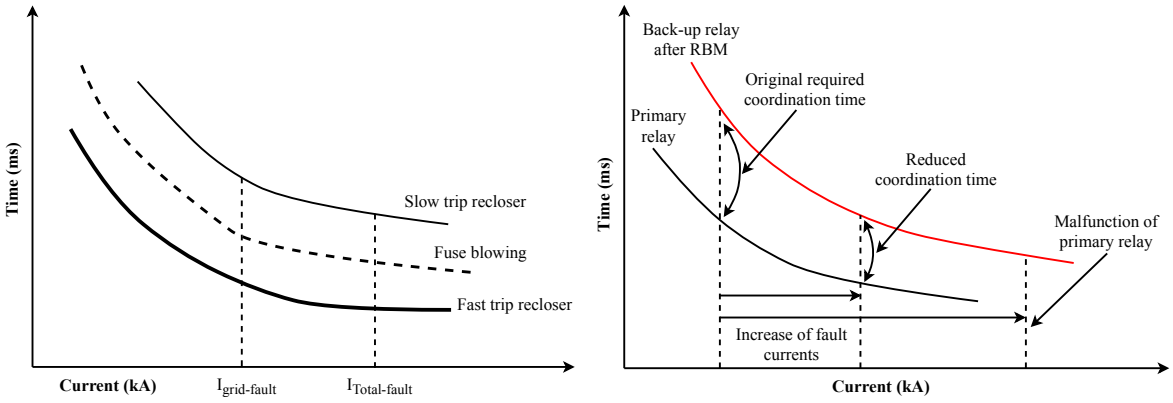

(a) Recloser-fuse coordination curves

(b) CTI between primary and back-up relay

Figure 2.3. Coordination of relay-fuse (a) and CTI miscoordination of primary and back-up relay (b)

To reduce the complexity of RBM protection challenges, communication-based zone protection, using different fault protection techniques with back-up protection, can significantly improve and achieve optimal protection performance for both modes of operation [5, 6, 12, 24, 25, 28]. This will increase the RBM's reliability and safety for both modes of operation.

It is essential that RBM protection philosophy needs to be able to sense downstream fault current when grid-connected. Additionally, the connected RDG units need to have adequate ride through capabilities to prevent false tripping [1, 7]. Load shedding strategies should also be considered when the connected RDG units cannot handle the connected load in either mode of operation [6].

2.3.1 Sequence component-based intelligent electronic devices

Sequence component-based IEDs (zero-, positive- and negative-sequence) are widely-used fault protection devices for stand-alone RBMs [11, 12]. This is due to the lack of need for communication requirements between the protection devices [6, 7]. The protection scheme uses symmetrical current and voltage components to detect phase-to-phase and single-phase-to-ground faults and uses negative-sequence and zero-sequence components, respectively [7, 12]. The application of negative-sequence protection also enhances selectivity of protection [11] to help detect weak, unbalanced faults within the stand-alone system. The reactive part of the negative-sequence impedance, with the use of zero-sequence currents, can assist in determining reverse and forward faults from IBDGs in LV RDNs [6, 7]. A negative-sequence directional element can utilise fault direction to avoid false trips due to low magnitude fault currents when in stand-alone operation [6].

In order to implement sequence-based protection in RBMs, it is known that the transformer windings and RDG units need to be earthed at a single point for zero-sequence components to flow [1, 7]. The single point needs to minimise the number of possible earth paths, simplifying earth-fault detection [1]. The fault responses of inverters are characterised as only positive-sequence sources [1]. During asymmetrical faults, the IBDGs can be controlled to only inject predetermined positive-sequence currents, and will not facilitate negative- or zero-sequence currents [1, 5]. This is not possible with conventional RBDG units [7]. For this case, FCLs can be used to assist in limiting injected fault levels. Additionally, negative-sequence component injection from RBDG units can be filtered out by implanting low-pass filters [5]. By grounding wye (Y_g) points of connected isolation transformers, zero-sequence injection can be minimised [5].

2.3.2 Harmonic distortion detection

Harmonic analysis can be applied to RDG operation to determine system faults through monitoring and comparing total harmonic distortion (THD) threshold values to the voltage and current at the PCC terminal of the RBM [6, 7, 9, 12, 24]. Under normal conditions the distribution network acts as a low-impedance voltage source and the inverter terminals maintain a distortion voltage approximating to zero (THD $\simeq 0$) [24]. During abnormal conditions, the distribution network isolates faulted areas, leaving only local loads. This increases the system's impedance [24]. This characteristic can be used to

enable the RBM IED, with the use of a communication link, to isolate the protection zone closest to the fault when a predetermined threshold value has been met [6]. It is most effective in detecting ground faults in RBMs [12]. Additionally, by using the proportional relationship between zero-sequence and position-sequence currents, harmonic analysis can be done on the fifth harmonic to detect any faults [24]. Harmonic distortion detection is proposed as a back-up protection method since the significant effects of dynamic loads [12] are inappropriate for high-impedance faults [7] and are problematic, with varying fault impedances [6]. These factors can cause nuisance tripping [7].

Embedded RBMs in LV RDNs through power electronic converters are known sources of harmonics [11]. In accordance with the *South African grid connection codes for RPPs* [18], *SANS:10142-1: Wiring of premises* [19] standards, and *NRS 097-2-1: Grid interconnection of embedded generation* [20], limited harmonics are allowed to flow through the PCC, specified by the full operational range of the RDG units when connected [5]. With the use of a frequency selective grounding configuration, IBDGs' harmonics can be limited [27]. This can be done by using a low-impedance path for current harmonics and a low-resistance path for ground fault currents to establish a parallel R-C circuit at the grounded neutral point of the distribution transformer [12, 27], as seen in Figure 2.2.

2.3.3 Differential protection

Differential protection is generally used on substation busbars, microgrids, transmission lines and power transformers as back-up protection for increased reliability [1, 9]. This protection method operates proficiently for internal faults and does not require time-current grading between other protection IEDs [7]. More importantly, this method is not affected by RDG size, type and location [26]. This is due to the method being highly dependent on communication links between protection IEDs [1, 7, 9]. It is based on differential current and symmetrical components, and operates, using Kirchoff's Current Law (KCL) [9, 25]. If any discrepancy is found beyond the set threshold limit, the protection relays send a trip signal to isolate the system fault [1, 7, 9]. It can limit fault current values, and detect bi-directional fault currents and ground faults for both IBDG and RBDG units [12]. This method can be used as primary protection, but back-up protection will be required in case of communications failure between the differential IEDs. Comparative voltage protection, undervoltage, frequency-based and overcurrent voltage protection methods are ideal for back-up protection with differential protection as primary protection [6, 12].

Differential protection may prove ineffective when considering the RBM, switching transients between modes of operation and unbalanced loads [6, 9, 12]. Accuracy can also prove to be a challenge when various current transformer (CT) ratio types are used in the system, where the various power losses can impact on the sensitivity of the differential IEDs [12, 25]. Energy-based differential protection with time-frequency transforms, such as s-transform [7, 12], is suggested to compensate for the increase in DC offset components and operating currents [25]. Implementation of isolation transformers can be used to decay DC components in RDG branches [12]. Other differential protection methods, such as time and impedance-differential-based protection, can assist in decreasing fault clearance time for high current magnitude faults [12, 24]. Sequence component-based differential protection can be used to provide more sensitive protection in the cases of lower current magnitudes and unbalanced faults [12, 24], increasing protection sensitivity and reliability.

2.3.4 Distance protection

Distance protection is an impedance-based protection scheme that offers high selectivity and network stability [7, 9]. The scheme is usually applied to bi-directional power flow systems [9, 26]. The system impedance is calculated at each distance IED, using Ohm's Law [7]. The protection method is reliant on communication links between the IEDs to compare calculated information and send trip commands to relative IEDs to isolate any located faults [9].

Issues may arise in distance relays when high-impedance single-phase-to-earth faults occur in the system [7]. Additionally, when wye connected loads and transformers are connected downstream, the IED tends to operate unnecessarily for ground faults [6, 7]. This is due to low fault impedance appearing at the faulted point, measured by the IED [6]. To overcome this issue, negative-sequence impedance analysis can be implemented at each IED and used to resolve bi-directional faults [6].

Research [6, 12] shows that admittance-based relay can prove to be more effective in AC microgrid protection schemes during both grid and stand-alone operation. This method will be able to detect high and low magnitude fault currents. Under normal conditions, a low-impedance value will be measured by the IED. The relay will only trip when the normalised value becomes larger than the total admittance of the protection zone. The RBMs dynamic operation status can impact on calculated admittance, measured by the distance IED [9, 26]. To help overcome unpredictable dynamic changes,

wide-area monitoring and high frequency current sampling can be used to increase the reliability of the distance protection method [9, 12].

2.3.5 Adaptive protection

Adaptive protection schemes can be introduced to help improve the reliability of existing protection methods by continuously updating characteristics such as voltages, currents and grading settings needed by the protection relay [9, 12, 26]. Adaptive methods mainly comprise of controlling elements, communication links and data arrays between protection IEDs. These are used to calculate and store real-time values to monitor all the protection zones [26, 29]. A hierarchical algorithm is also implemented into the controlling unit to help recognise the network topology by analysing protection device and RDG conditions [2, 12, 30]. With relevant information gathered by the controller, efficient control action methods can be implemented to improve protection settings [1, 12]. Adaptive protection can be implemented in either centralised or decentralised control strategies, each needing different communication methods [6].

2.3.5.1 Centralised protection

Centralised protection utilises only one central controller in the RBM [9]. A microgrid management system (MMS) is used to store real-time updated protection calculation settings in a database [1, 9]. The required measurements are obtained by the protection IEDs and sent to the MMS, using a communication link. [1, 9, 26]. The system fault data and grading settings will update after every RDG disconnection or connection within the RBM and network topology have changed, when integrated into the network [2]. This will help to ensure that protection device coordination is maintained in the distribution network. Communications and remote tripping capabilities between protection IEDs are required to achieve centralised protection [2, 30]. The fact that centralised protection has only one central controller, its failure, or that of the communications system, will hinder the protection of the network [1, 2]. Real-time calculation leaves the centralised protection scheme vulnerable. For example, if the calculations are being updated, instantaneous fault change could occur, rendering the protection devises not being updated, ineffective. [30]. Research [2, 9] suggests that fault settings are to be pre-calculated off-line and stored in an array table to be accessed by the central controller. This will ensure protection reliability.

2.3.5.2 Decentralised protection

Decentralised protection uses multiple controllers with a hierarchical structure for each RDG in the RBM [12, 30]. The scheme can either operate without a communication system, or only use the communication system to exchange local information between individual protection IEDs [12]. It is mainly used for RBMs with multiple RDG units or in remote areas with long distances between RDGs and the RBM [9, 30]. Each RDG unit is individually controlled, using a local controller (LC) [9]. The LC is used to improve the RBM performance and provide maximum power production to the distribution network [9, 25]. By making a single RDG unit the master controller, the frequency and voltage can be maintained when in stand-alone operation [9, 24]. The only downfall to decentralised protection is that each unit is unaware of system-wide variables and other LC actions [9]. Research [9, 12, 24] suggests that a hybrid protection scheme should be used. Commands given by the LC and sent to a central MMS, where system-wide variables can be considered. The MMS can then send modified control commands to the individual LCs if any lack of control is detected.

2.3.5.3 Artificial intelligence

During the planning stage of reinforcing distribution networks, design limits are set to keep the power system operational. Intelligent techniques can be used to optimally size and place RBMs to pose minimised improvement for system losses, voltage profiles and enhance system reliability [4, 16]. Integration of RBMs can be bounded by using power flow equations and inequalities restrictions in a mathematical optimisation problem in order to minimise costs and maximise integration of RDG's power contribution and profits in LV RDNs [4, 16, 29, 31]. Partial swarm optimisation, genetic algorithm and artificial bee colony algorithm are three widely used algorithms for optimal coordination of protection devices [4, 21, 29]. The protection schemes adapt to system changes, obtaining new relay settings as the system topology changes. This is done by formulating the relay coordination setting as an optimisation problem; where the system losses, voltage profile, short-circuit current and capacity factor are set as the objective function. After optimisation, the new time multiplier setting (TMS) can then be calculated off-line and used by the IEDs to update the time-current grading settings [29]. These values can then be stored by the MMS in an on-line array and accessed by the LCs. This will allow for an optimal hybrid adaptive protection coordination method for multiple RBMs, embedded in South African LV RDNs.

2.4 FAULT CURRENT ANALYSIS

To reduce the complexity of the RBM's protection challenges, a hybrid adaptive philosophy with communication-based IEDs and using various zone protection methods, with back-up protection, can significantly improve and assist in achieving optimal protection coordination performance. This will increase embedded RBM reliability and safety for both modes of operation [5, 6, 12, 24, 25]. Renewable generation sources, such as solar PV systems ESS and WP, will be the main focus for the fault current analysis. Short-circuit current levels of each renewable source, along with grid faults, will be investigated to visualise how the existing LV RDN protection coordination will tolerate the increased fault level penetration, contributed by embedded RBMs.

2.4.1 Short-circuit current analysis for renewable distributed generators

By embedding RBMs downstream of the existing LV RDN in-line fixed-setting protection relays, causes the system impedance to decrease; thus increasing the downstream fault current level in the LV RDN. This causes protection miscoordination between the fixed-setting protection relays. The following investigation will look into fault current penetration levels contributed by PV, ESS and WP renewable generation sources.

2.4.1.1 Solar photovoltaic systems

Solar PV, pure DC sources, uses inverters to convert DC to AC power. A relationship between the PV voltage (V_{PV}) and PV current (I_{PV}) can be given by the equation

$$I_{PV} = I_{ph} - I_0[e^{\frac{q(V_{PV}+I_{PV}R_S)}{nkTN_S}} - 1] - \frac{V_{PV}+I_{PV}R_S}{N_sR_{sh}}, \tag{2.1}$$

where

N_s is the number of cells in series,

n the diode factor,

R_s the total series resistance (Ω),

$\frac{kT}{q}$ the ratio between Boltzmann's constant, the temperature (K) and electron charge (eV),

R_{sh} the shunt resistance,

I_{ph} the photo current depending on temperature at the standard level,

I_o the reverse saturation current.

At short-current condition, I_{PV} equals the short-circuit current of the PV cell, and V_{PV} equals zero. At open-circuit condition, V_{PV} equals the open-circuit voltage of the PV cell, and $I_{PV} = 0$. I_{SC} and V_{OC} can be expressed as in (2.2) and (2.3), respectively.

$$I_{SC} = I_{SC(STC)}(1 + K_i(T - T_s)), \tag{2.2}$$

$$V_{OC} = V_{OC(STC)}(1 + K_v(T - T_s)), \tag{2.3}$$

where

K_i $(\%/^\circ C)$ is the temperature coefficient of the PV short-circuit current at the standard test condition (STC),

K_v $(\%/^\circ C)$ is the temperature coefficient of the PV open-circuit voltage at the STC,

T_S is the standard temperature (25 °C),

$I_{SC(STC)}$ is the short-circuit current of the PV calculated in the STC,

$V_{OC(STC)}$ is the open-circuit voltage of the PV calculated in the STC.

2.4.1.2 Energy storage systems

Battery systems are used to absorb excess DC generated voltage. The stored DC voltage can be used to inject power to the system when the voltage output is less than the expected value. This is beneficial to maintain reliability in the system. A DC fault current across the battery terminals (I_{batt}) can be given in equation

$$Ibatt(t) = \frac{V_{batt}}{R_{batt} + R_{line}}(1 - e^{-t\frac{R_{batt}+R_{line}}{L_{batt}+L_{line}}}), \tag{2.4}$$

where

R_{batt} and L_{batt} are the internal resistance induction of the battery system, respectively,

R_{line} and L_{line} are the line resistance and inductance parameters calculated from the battery system to the fault area in the microgrid, respectively,

V_{batt} is the operating voltage of the battery system.

When a new load is added to the power system, the initial energy balance becomes unstable [32]. With the use of an efficient ESS, it can compensate for the very low inertia; accordingly stabilising the power system's energy balance [32].

2.4.1.3 Wind power system

WP is an AC generated power as it uses rotating machines, such as induction generators, to turn mechanical energy into electrical energy. To determine the maximum short-circuit current, the worst-case scenario needs to be considered at the terminal of the rotating generator. Based on an induction synchronous rotating machine, the following equations are expressed:

$$v_s = R_s i_s + \frac{d\psi_s}{dt} + j\omega_s \psi_s, \tag{2.5}$$

$$v_r = R_r i_r + \frac{d\psi_r}{dt} + j(\omega_s - \omega_r)\psi_r, \tag{2.6}$$

$$\psi_s = L_s i_s + L_m i_r, \tag{2.7}$$

$$\psi_r = L_m i_s + L_r i_r, \tag{2.8}$$

$$(L_s = L_{s\sigma} + L_m \, and \, L_r = L_{r\sigma} + L_m), \tag{2.9}$$

where

v_s and v_r are the stator and rotor voltages, respectively [V],

i_s and i_r are the stator and rotor current, respectively [A],

R_s and R_r are the stator and rotor resistance, respectively [Ω],

$L_{s\sigma}$ and $L_{r\sigma}$ are the stator and rotor leakage inductance, respectively [H],

L_m are the magnetising inductance [H],

L_s and L_r are the stator and rotor inductance, respectively [H],

ω_s and ω_r are the stator and rotor angular velocity, respectively [rad/s],

ψ_s and ψ_r are the stator and rotor flux [T].

The stator short-circuit current can be determined, using the transient stator and rotor inductance with the rotor and stator coupling factors $k_r = \frac{L_m}{L_r}$ and $k_s = \frac{L_m}{L_s}$ as given in equation

$$i_s = \frac{\sqrt{2}V_s}{jX^{-}{}_s}[e^{\frac{-t}{T_s^-}} - 1(1-\sigma)e^{j\omega_s t}e^{\frac{-t}{T_r^-}}], \tag{2.10}$$

where

$X_s^- = \omega Ls^-$ being the transient reactance,

V_s is the phase voltage of the stator windings,

T_s^- is the stator time constant for damping of the DC component in the stator windings,

T_r^- is the rotor time constant for damping of the DC components in the rotor windings,

σ is the leakage factor.

$$\sigma = 1 - \frac{L_m^2}{L_s L_r}, T_s^- = \frac{L_s^-}{R_s}, T_r^- = \frac{L_r^-}{R_r}. \tag{2.11}$$

Assuming that the stator voltage has an angle $\alpha + \frac{\pi}{2}$ with respect to the α-stator phase and during the short-circuit occurrence $v_s = j\sqrt{2}V_s e^{j\alpha}$, the short-circuit in the α-phase is given by equation

$$i_{sa} = \frac{\sqrt{2}V_s}{jX_s^-}(e^{\frac{-t}{T_s^-}}cos\alpha - (1-\sigma)e^{j\omega_s t}e^{\frac{-t}{T_r^-}}cos(\omega t + \alpha)). \tag{2.12}$$

Similarly, the short-circuit currents in the stator phase -b and -c can be given by the equation

$$i_{s,max} = \frac{\sqrt{2}V_s}{jX_s^-}[e^{\frac{-T}{2T_s^-}} - (1-\sigma)e^{\frac{-T}{2T_r^-}}], \tag{2.13}$$

where the peak short-circuit current ($i_{s,max}$) can be obtained at the time $t = \frac{T}{2}$ (with T being the period time of the current).

2.4.2 Grid fault current analysis

An adaptive hybrid protection philosophy will be investigated with the use of communication and sequence-based protection IEDs. Applying orders made by an LC and data sent to a central MMS [1, 26, 32], real-time, system-wide variables can be used to calculated, off-line, time-current grading settings. The updated settings can then be stored in an on-line global database. The MMS will send modified control commands to the individual LCs if any lack of control or protection coordination is detected (i.e. integration or removal of RBMs from the LV RDN).

The RBM's dynamic operating nature is caused by the RDG units' dependency on various weather conditions [14]. This dependency is the main contributor to the RBM's topology changes [5, 14]. The pick-up current of the relay settings of the protection relay should be adjustable to the various dynamic fault current penetration levels of the connected IBDG and RBDG. With reference to Figure 2.4, the total fault current seen by relay r can be given by equation

$$I_{fault\,relay\,r} = I_{fault\,grid} + \sum_{i=1}^{n} (k_{ri}\, I_{fault\,RBM_i} RDGi_{status}), \tag{2.14}$$

where

$I_{fault\,relay\,r}$ is the total fault as seen by relay r,

$I_{fault\,grid}$ is the grid fault current contribution to relay r,

n is the total number of connected RDGs,

k_{ri} is the fault coefficient for relay r, caused by the i^{th} connected RBM,

$RDGi_{status}$ shows the connection/disconnection of the i^{th} RDG.

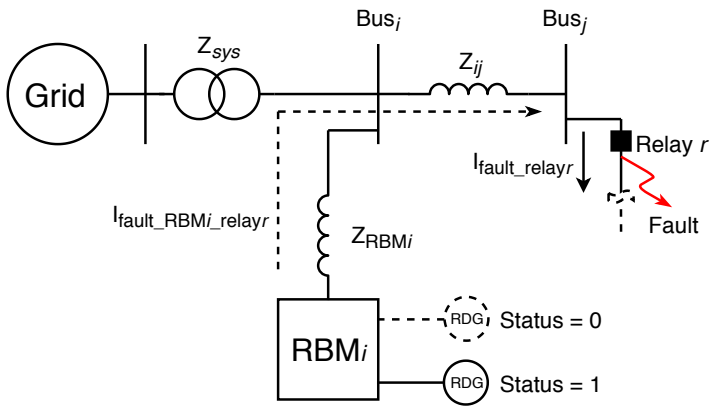

Figure 2.4. Fault current contribution of the i^{th} RBM to the r^{th} relay

Using the Thevenin equivalent and assuming that faults are inside the microgrid, $I_{(fault\,grid)}$ can be be given in equation

$$V_{bus}(F) = V_{bus}(0) - Z_{bus}I_{bus}(F), \tag{2.15}$$

where

$V_{bus}(F)$ and $V_{bus}(0)$ are the phase voltages of the bus during and before the fault, respectively,

$I_{bus}(F)$ is an array of the fault currents flowing out of phases at the bus during the fault,

Z_{bus} is the Thevenin impedance equivalent matrix.

For unbalanced faults, a $\{0\}$ zero- $\{1\}$ positive- and $\{2\}$ negative-sequence Thevenin impedance matrix Z_{bus}^{012} is to be calculated. (2.15) can be rewritten as follows:

$$V_{bus}^{012}(F) = V_{bus}^{012}(0) - Z_{bus}^{012}I_{bus}^{012}(F). \tag{2.16}$$

When $V_{bus}(0)$ are Z_{bus} available, the grid fault current can be calculated as given in equation

$$I_{fault\,grid} = \frac{V_{bus}(0) - V_{bus}(F)}{Z_{bus} + Z_f}, \tag{2.17}$$

where Z_f is the fault impedance.

When calculating the grid fault current contribution to different fault sections inside the RBM (i.e. trunk line/faulted source) (2.17) can be rewritten as follows:

$$I_{fault\,grid} = \frac{V_{th}}{Z_{th}}, \tag{2.18}$$

where

V_{th} is the Thevenin equivalent of the utility grid,

Z_{th} is the Thevenin equivalent from the utility grid to the faulted area.

2.4.3 Calculating fault current coefficients to each protection relay

The system impedance is pre-known at the PCC of the RBM and LV RDN. This can then be used to calculate and update the pick-up current for relay r. An IDMT curve according to IEC60255 will be considered for the adaptive protection relays as given in equation

$$t = TMS\left(\frac{A}{\left(\frac{I_{fault}}{I_{Pick-up}}\right)^{p} + B}\right), \tag{2.19}$$

where

Time multiplier setting (TMS) = $\frac{Trip\ time\ (T)}{Time\ measured\ (T_m)}$,

A = 0.14,

p = 0.02,

B = -1,

I_{fault} is the fault current seen by relay r.

The internal fault current at the terminal of the i^{th} RDG unit can then be calculated in accordance with the pre-specified parameters. The IBDG's positive-sequence fault current in the RBM can be controlled and is limited between 1.2∼2 p.u. inverter rated. RBDGs' high output fault current contribution is between 5∼10 p.u. rated current [1, 5, 12, 32]. Additionally, the inverter can be controlled to only inject positive-sequence components into the RBM. RBDGs generate positive-, negative- and zero-sequence components to correspond with symmetrical and asymmetrical faults [5]. Zero- and negative-sequence

components can be eliminated, using Y_g/Δ isolation transformers (with the Δ connection on the RBM side) and low-pass filters, respectively [5]. The RBDG can be rectified to a DC source to allow an ESS to be applied so that the fault current can be controlled, using an inverter before injecting into the LV RDN.

A fault current coefficient k_{ri} is used to express fault current contribution of the i^{th} RDG to the r^{th} relay, as seen in Figure 2.4 and represented in (2.15). The fault current coefficient will be defined on the base of a three-phase fault, only considering the positive-sequence.

$$k_{ri} = \frac{I_{fault\,RDGi\,relay\,r}}{I_{fault\,RDGi}} = \frac{(\frac{Z_{sys}}{Z_{RDGi}+Z_{sys}})}{I_{fault\,RDGi}}, \tag{2.20}$$

where

$I_{fault\,RDGi\,relay\,r}$ is the fault current contributed by the i^{th} RDG to the r^{th} relay,

Z_{RDGi} is the impedance of the i^{th} relay,

Z_{sys} is the distribution network impedance.

It should be realised that the value of k_{ri} is between 0 and 1. When k_{ri} approximates to 1, the location of the i^{th} RDG is close to the location of the r^{th} relay. When k_{ri} is much less than 1, the fault current contribution of the i^{th} RDG to the relay is small. In general a k fault current coefficient matrix can be used to calculate fault current contributions of numerous RDGs to many relays. There are *'n'* number of RDGs and *'m'* number of relays in the RBM. The same procedure can be applied to unbalanced three-phase faults.

$$K = \begin{bmatrix} k_{11} & \dots & k_{1i} & \dots & k_{1n} \\ : & & : & & : \\ k_{r1} & \dots & k_{ri} & \dots & k_{rn} \\ : & & : & & : \\ k_{m1} & \dots & k_{mi} & \dots & k_{mn} \end{bmatrix}. \tag{2.21}$$

The internal fault currents of the *'n'* number of RDGs can be represented by a [1, n] fault current matrix $I_{fault\,RDG}$.

$$I_{fault\,RDG} = \begin{bmatrix} I_{fault\,RDG_1} \\ : \\ I_{fault\,RDG_i} \\ : \\ I_{fault\,RDG_n} \end{bmatrix}. \tag{2.22}$$

From (2.21) and (2.22), the fault currents produced by the *'n'* number of RDGs seen by the *'m'* number of relays can be given by equation

$$\begin{bmatrix} I_{fault\,\sum_{i=1}^{n} RBM_1\,relay_1} \\ \dots \\ I_{fault\,\sum_{i=1}^{n} RBM_i\,relay_r} \\ \dots \\ I_{fault\,\sum_{i=1}^{n} RBM_n\,relay_m} \end{bmatrix} = \begin{bmatrix} k_{11} & \dots & k_{1i} & \dots & k_{1n} \\ : & & : & & : \\ k_{r1} & \dots & k_{ri} & \dots & k_{rn} \\ : & & : & & : \\ k_{m1} & \dots & k_{mi} & \dots & k_{mn} \end{bmatrix} \begin{bmatrix} I_{fault\,RDG_1} \\ : \\ I_{fault\,RDG_i} \\ : \\ I_{fault\,RDG_n} \end{bmatrix}, \tag{2.23}$$

$$I_{fault\,\sum_{i=1}^{n} RBM_i\,relay_r} = I_{fault\,RDG_1} + \dots + I_{fault\,RDG_n} = \begin{bmatrix} k_{r1} & \dots & k_{ri} & \dots & k_{rn} \end{bmatrix} \begin{bmatrix} I_{fault\,RDG_1} \\ : \\ I_{fault\,RDG_i} \\ : \\ I_{fault\,RDG_n} \end{bmatrix}. \tag{2.24}$$

The grid fault current contribution is not considered in (2.23). Therefore, (2.14) can be rewritten and given in equation

$$\begin{bmatrix} I_{fault\,relay_1} \\ \dots \\ I_{fault\,relay_r} \\ \dots \\ I_{fault\,relay_m} \end{bmatrix} = I_{fault\,grid} + \sum_{r=1}^{m} \sum_{i=1}^{n} (k_{ri}\, I_{fault\,RBM_i}\, RDG_i status), \tag{2.25}$$

$$= \begin{bmatrix} I_{fault\ grid\ relay_1} \\ \dots \\ I_{fault\ grid\ relay_r} \\ \dots \\ I_{fault\ grid\ relay_m} \end{bmatrix} + \begin{bmatrix} k_{11} & \dots & k_{1i} & \dots & k_{1n} \\ : & & : & & : \\ k_{r1} & \dots & k_{ri} & \dots & k_{rn} \\ : & & : & & : \\ k_{m1} & \dots & k_{mi} & \dots & k_{mn} \end{bmatrix} \begin{bmatrix} I_{fault\ RDG1_{status}} \\ \dots \\ I_{fault\ RDGi_{status}} \\ \dots \\ I_{fault\ RDGn_{status}} \end{bmatrix}. \quad (2.26)$$

The fault current contributions between the RBM and LV RDN can be continuously monitored and updated with the use of a communication link between the protection relays. This allows for a secure and adaptive protection method. In case of communication link failure, a RBM back-up protection method should be considered for increased reliability.

2.5 OPTIMISATION ANALYSIS

By optimally sizing and placing the number of embedded RBMs in the LV RDN, it will be possible to reduce power system losses, initial investment costs, fault contribution limits and voltage swell and sag, and improve system voltage profiles, system reliability and stability, voltage regulation and system power factor [10, 16, 23]. Optimally sized and placed RBMs can assist in minimising islanding and in the improvement of the overall protection challenges, as the extent to which the protection coordination is affected, is dependent on size, location and number of embedded RDG units connected to the LV RDN [4, 16, 23].

2.5.1 Optimisation function

Arbitrarily placed RBMs can cause technical problems such as voltage fluctuation, unwanted harmonics and system transients [16, 23]. The RBM can be used during peak times to help reduce peak demands and minimise costs of the end user. Optimally sized and placed RBMs can additionally assist in increasing the system average interruption duration index (SAIDI); thereby improving the network reliability. An objective function can be determined, by using the given equation

$$y = x_1 + x_2 + x_3 + \dots + x_n = \sum_{k=1}^{n} x_k, \quad (2.27)$$

where n is the number of parameters on which the objective function depends.

For this investigation four parameters will be considered, namely system power losses (x_1), voltage profile factor (x_2), short-circuit current factor (x_3) and capacity factor (x_4). The final objective function is given in equation

$$y = x_1 + x_2 + x_3 + x_4, \tag{2.28}$$

where

$$x_1 = \beta_j \frac{P_{Load}^{afterRDG}}{P_{Load}^{beforeRDG}},$$
$$x_2 = \mu_j (V_{bus,j}^{afterRDG})^2,$$
$$x_3 = \eta_j (Fault\,Current\,Limit_j)^2,$$
$$x_4 = \lambda_j \frac{Capacity_j}{S_{base}}.$$

where

β = weight factor of system losses,

μ = weight factor of voltage profile,

η = weight factor of FCL,

λ = weight factor of RDG capacity.

Taking the sum of all values from the objection function (2.28), respectively, the final objective function as give in equation

$$y = \sum_{j=1}^{n} (\beta_j \frac{P_{Load}^{afterRBM}}{P_{Load}^{beforeRBM}} + \mu_j (V_{bus_j}^{afterRBM})^2 + \eta_j (FCL_j)^2 + \lambda_j \frac{CP_j}{S_{base}}). \tag{2.29}$$

2.5.2 Optimisation constraints

The constraints of the system are essential to ensure that maximum performance, power flow, reliability and efficiency of the LV RDN can be achieved. The following constraints can then be set and determined:

2.5.2.1 Weight factor

The weight factors have to be selected in such a way that the sum of all weighted factors must equal one.

$$\beta + \mu + \eta + \lambda = 1, \tag{2.30}$$

where

$$\beta = \frac{P_L^{before\,RDG}}{P_L^{after\,RDG}},$$
$$\mu = \frac{1}{(V_{bus,j}^{after\,RDG} - 1)^2},$$
$$\eta = \left(\frac{I_{FCL,j}^{after\,RDG}}{I_{FCL,j}^{after\,RDG} - I_{FCL,j}^{before\,RDG}}\right)^2,$$
$$\lambda = \frac{S_{base}}{CP_j}.$$

2.5.2.2 Renewable distributed generator capacity constraint

The total load demand of the system should not be less than the total summation of the generated active power by the embedded RDG units. This is to ensure minimal bi-directional power flow in the distribution network.

$$\sum_{j=1}^{g} CP_j \leq P_{Load}, \tag{2.31}$$

where g is the number of connected RBMs.

2.5.2.3 Bus voltage constraint

The bus voltage will vary with an allowable bus voltage tolerance of 5% upper and lower, i.e. $V_{Min} \leq$ 0.95 p.u. and $V_{Max} \leq$ 1.05 p.u.

$$V_{Min} \leq V_{bus,j}^{after\,RDG} \leq V_{Max}. \tag{2.32}$$

2.5.2.4 Short-circuit current constraint

The fault current level must not exceed the allowable overcurrent and earth fault level to ensure safety to the user, and protection of the RBM and LV RDN.

$$I_{FCL,j}^{after\,RDG} < FCI, \tag{2.33}$$

where FCI is the fault current limit of installed devices.

2.5.2.5 Power factor constraint

In accordance with the *South African grid connection codes for RPPs* [18] standard, the RPP will operate at unity measured at the PCC. The power factor of the RDG being installed, may vary within a specified range due to change in loads and type of RDGs embedded in the network.

$$0.98 \leq pf_{RDG,j} \leq 1, j = 1,2,...,g. \tag{2.34}$$

CHAPTER 3 DESIGN METHODS AND PARAMETERS

3.1 CHAPTER OVERVIEW

A comprehensive design method is investigated where design parameters are set in accordance with respective standards and verified by simulating clusters of aforementioned selected RDG types of overly sized and arbitrarily placed versus optimally sized and placed clusters of TN-C Type II uni-grounded RBMs in an existing Eskom LV RDN. Using DIgSILENT PowerFactory 2017, the discriminating effects of the overly sized RBMs on coordinated IDMT curves of the in-line fixed-setting relays can be observed. The RDG S_{base} can then be optimally sized, using the aforementioned optimisation function and constraints. The LV RDN protection relay can then be re-coordinated with and without the optimally sized RBMs, using the new optimised fault levels and the hybrid adaptive protection algorithm. This will allow a detailed observation of the developed hybrid adaptive protection philosophy and ensure it will function as intended when RBMs are being grid-connected or in stand-alone operation.

3.2 DESIGN METHODS

The method to answer the research questions of this study will include designing and simulating clusters of aforementioned selected RDG types of overly sized and arbitrarily placed versus optimally sized and placed clusters of TN-C Type II uni-grounded RBMs in an existing Eskom LV RDN. The design of the RDGs will be in accordance with the *South African grid code regulations for RPPs* [18] standard and *NRS 097-2-1: Grid interconnection of embedded generation* [20]. The wiring of the RBM will be in accordance with the *SANS10142-1: Wiring of premises* [19] standards, to ensure the

safety and connection standard is met when tied to the LV RDN. Additionally, all RDGs above 10 kW must be three-phase units [20].

Using the LV RDN, modelled and simulated in DIgSILENT PowerFactory 2017, the power flow and short-circuit faults of the LV RDN will be recorded for a scenario when the overly sized RBMs, running at full capacity, are in grid-connected and stand-alone mode. This is done to observe the discriminating effects of the overly sized RBMs on coordinated IDMT curves of the in-line fixed-setting relays.

The RDG S_{base} will then be optimally sized, using the aforementioned optimisation function and constraints. This will minimise the economical purchase of the RDG units and unwanted bi-directional power flow, while still maximising the MVA capacity requirements of constraint LV RDNs. The LV RDN protection relay will then be re-coordinated with and without the optimally sized RBMs, using the new optimised fault levels and the hybrid adaptive protection algorithm, as seen in Figure 3.1.

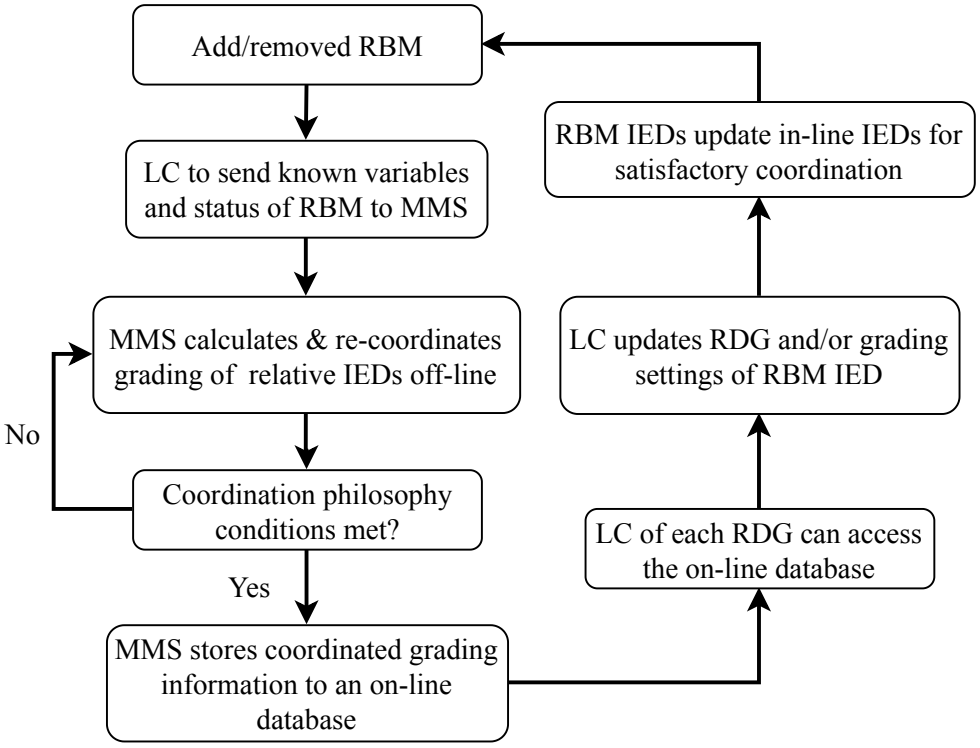

Figure 3.1. Hybrid adaptive protection IDMT curve coordination algorithm

The algorithm will assist in re-coordinating the RBM and in-line protection IEDs for the scenario when RBMs are connected to or disconnected from the LV RDN. The algorithm will calculate the

newly required protection settings off-line, when a change occurs in the LV RDN. Once the calculated protection settings are within the desired limits, they will be stored to an on-line database located in the MMS, reachable by the LCs. The hybrid adaptive protection scheme structure can be seen in Figure 3.2. It is essential for the RBM adaptive protection scheme to be able to sense downstream fault currents when grid-connected.

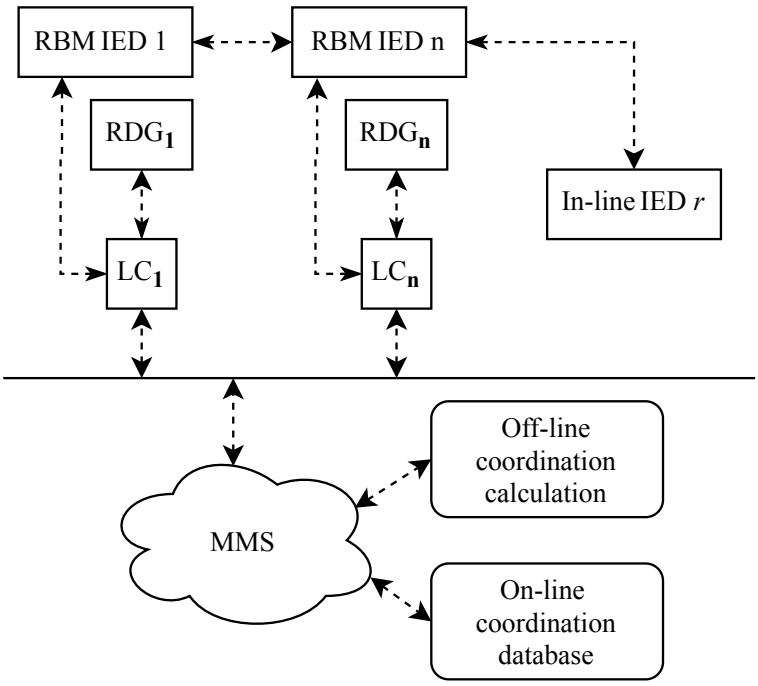

Figure 3.2. Hybrid adaptive protection scheme communications architecture

With reference to the developed LV radial feeder test-bed, as seen in Figure 2.2, the developed adaptive protection scheme will be simulated and tested according to faults F1-F5, as in Table 3.1. This will ensure the hybrid adaptive protection philosophy is functioning as intended when being grid-connected or in stand-alone mode.

Table 3.1. Fault types and location in the developed LV radial feeder test-bed

Fault location		Fault type
F1	LV side of the Dny11 distribution transformer	Three-phase, phase-phase-to-ground, phase-phase, single-phase
F2	LV side of RBM 1 Y/Δ isolation transformer	Three-phase, phase-phase-to-ground, phase-phase, single-phase
F3	Between RBM 1 HV side of isolation transformer and in-line fuse	Three-phase, phase-phase-to-ground, phase-phase, single-phase
F4	Between RBM 2 and RBM 3 HV side of isolation transformer and in-line fuse	Three-phase, phase-phase-to-ground, phase-phase, single-phase
F5	LV side of RBM 3 Y_g/y_g isolation transformer	Three-phase, phase-phase-to-ground, phase-phase, single-phase

3.3 DESIGN PARAMETERS

3.3.1 Renewable energy source design standards

When grid-connected, the RBDG units and IBDG need to have adequate voltage ride through capabilities at the PCC, to prevent false tripping [1, 7], as seen in Figure 3.3. Table 3.2 shows the maximum tripping time for the voltage range at the PCC for the RBM, when grid-connected.

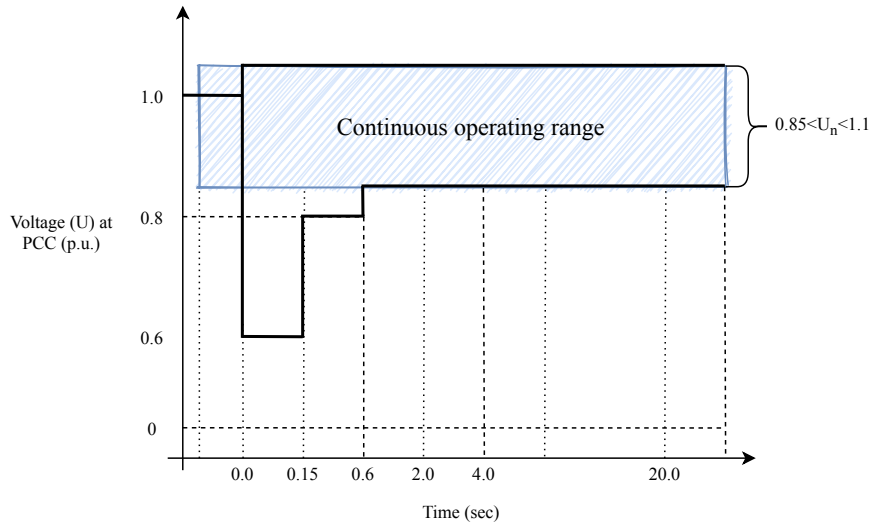

Figure 3.3. Voltage ride through capability for the RPPs of category A1 and A2

Table 3.2. Maximum disconnection times for RPPs of category A1 and A2

Voltage range (at the PCC)	**Maximum trip time (sec)**
V < 50 %	0.2 s
50 % $\leq$ V $\leq$ 85 %	2.0 s
85 % $\leq$ V $\leq$ 110 %	Continuous operation
110 % < V <120 %	2.0 s
120 % $\leq$ V	0.16 s

Load shedding strategies should also be considered when the connected RDG units cannot handle the connected load in stand-alone mode [6]. When islanding operation has been detected, the RBM should disconnect from the grid within 0.2 seconds [18, 20]. For category A, the RDG can only allowed re-synchronising to the LV distribution network 60 seconds at the earliest after disconnection [18, 20]. Before automatic re-synchronising and paralleling the RBM at the PCC, the following conditions need to be met for at least 60 seconds [20]:

- Frequency difference: 0.3 Hz;
- Voltage difference: 5 % of nominal voltage per phase;
- Phase angle difference: 20° (degrees).

The RDG will be designed to withstand a sudden phase jump of up to 20° at the PCC without disconnection or reducing output [18]. The RDG will, after a settling period, resume normal production not later than 5 seconds after a short disturbance in the LV RDN has reverted to normal [18]. It is required that in case of frequency deviations in the LV RDN, the RDG will be designed to be capable to provide frequency response in order to stabilise the grid frequency, as shown in Figure 3.4. The metering accuracy for the grid frequency will be ±10 mHz or better. Once the frequency exceeds 52 Hz or lower than 47 Hz, the RDG will not operate longer than 4 seconds and 200 ms, respectively, before the RBM will be tripped.

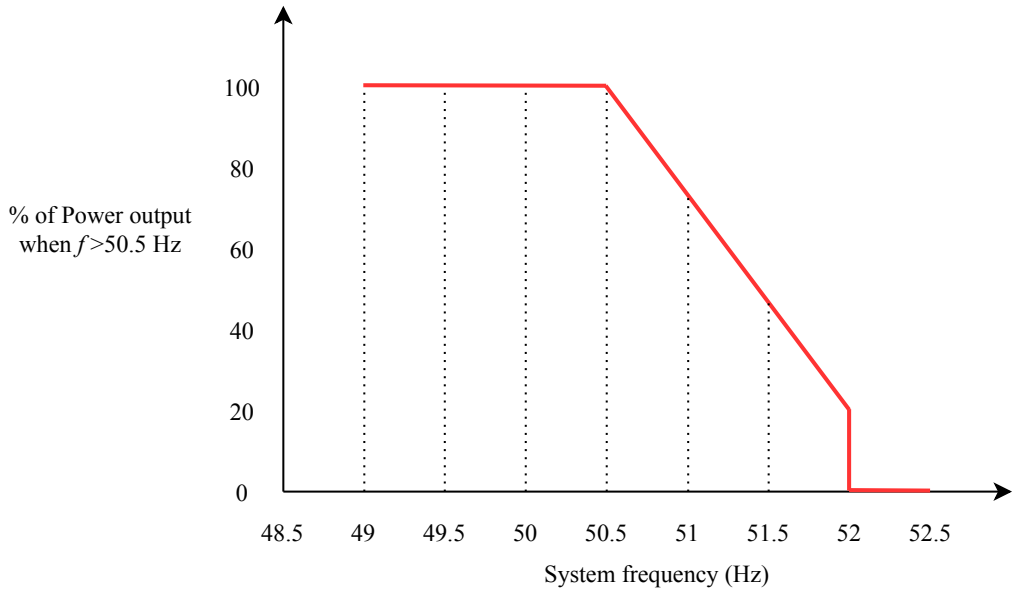

Figure 3.4. Power curtailment during over-frequency for RPPs

The current distortion limit of the RBMs rated current should comply with the *NRS 097-2-1: Grid interconnection of embedded generation* [20] as seen in Table 3.3. The harmonics and inter-harmonics distortion apply up to 3 kHz (50 th harmonic).

Table 3.3. Maximum harmonic current distortion limit of rated current for category A1 and A2

Harmonic order (h)	**h < 11**	**11 ≤ h < 17**	**17 ≤ h < 23**	**23 ≤ h < 35**	**35 ≤ h**
Percentage of rated current (Odd harmonics)	4.0	2.0	1.5	0.6	0.3
Percentage of rated current (Even harmonics)	1.0	0.5	0.38	0.15	0.08
Percentage of rated current (Inter-harmonics)	0.1	0.25	0.19	0.08	0.03
Total demand distortion = 5%					
NOTE 1: Even harmonics are limited to 25% of the odd harmonic limits. NOTE 2: Inter-harmonics are limited to 25% of the odd harmonics limits, and adjusted for the 200 Hz band measurement required by IEC 61000-4-7, except for the lower frequencies, where the flicker contribution is more likely. NOTE 3: Total demand distortion = Total harmonic distortion.					

The power factor of the RBM - in accordance with *NRS 097-2-1: Grid interconnection of embedded generation* [20] - irrespective of the number of phases in which an RBM is connected, will comply to each phase for the system normal conditions when the output exceeds 20% rated of the active power:

- For static power converter and synchronous embedded generators of categories A1 and A2, the power factor will remain above 0.98 and will operate anywhere within the shaded area of Figure 3.5.
- For asynchronous embedded generators of categories A1 and A2, which cannot control the power factor over any range, the power factor will remain above 0.98 and will reach the shaded area of Figure 3.5 within 60 seconds. The power factor will operate anywhere within the shaded area.

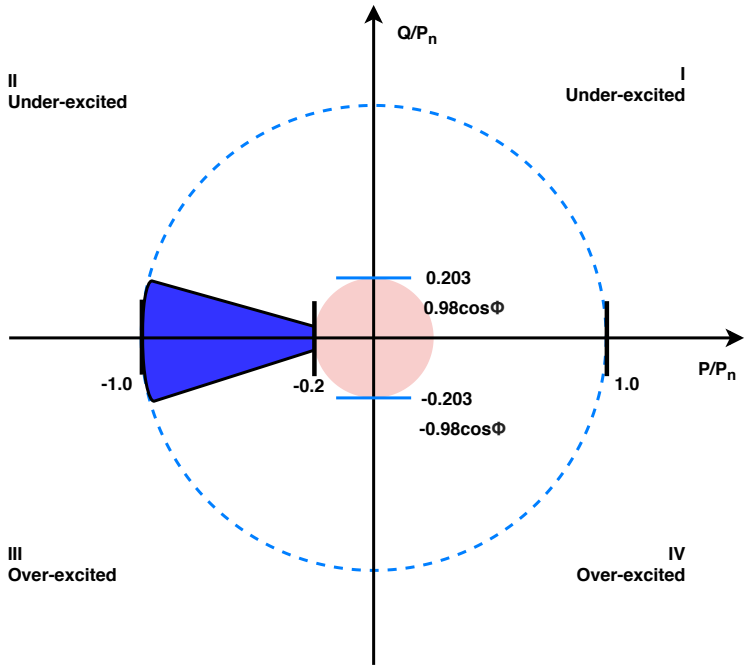

Figure 3.5. Power factor operating requirements for category A1 and A2 (using the load-reference arrows system)

In accordance with *SANS 10142-1: Wiring of premises* [19], each phase conductor of an unearthed or earthed DC system will be protected against overload and short-circuit current by one or more protection devices. Each protection device will have a rated current that does not exceed the lowest of the current capacities, and a minimum short-circuit rating of 2.5 kA [19]. Multiple sources will be protected individually and the protective devices will be located as close as possible to the power source. The earth fault protection will operate at a current related to the earth loop impedance, which will limit prospective touch voltages under short-circuit fault conditions to 25 V for no longer than 5 seconds [19]. The overload, short-circuit and earth leakage protection will follow as per design, described in *SANS 10142-1: Wiring of premises* [19].

The wiring premise of the RBM between the LV RDN and end user can be seen in Figure 3.6. A miniature circuit breaker (MCB), sized to the RDG system accordance to *Applications guide for the protection of LV distribution systems* [17], and *SANS 10142-1: Wiring of premises* [19], will be used for individual protection of each RDG within the RBM. For this study the RBM circuit breaker (CB) will be considered as the PCC, as seen in Figure 3.6.

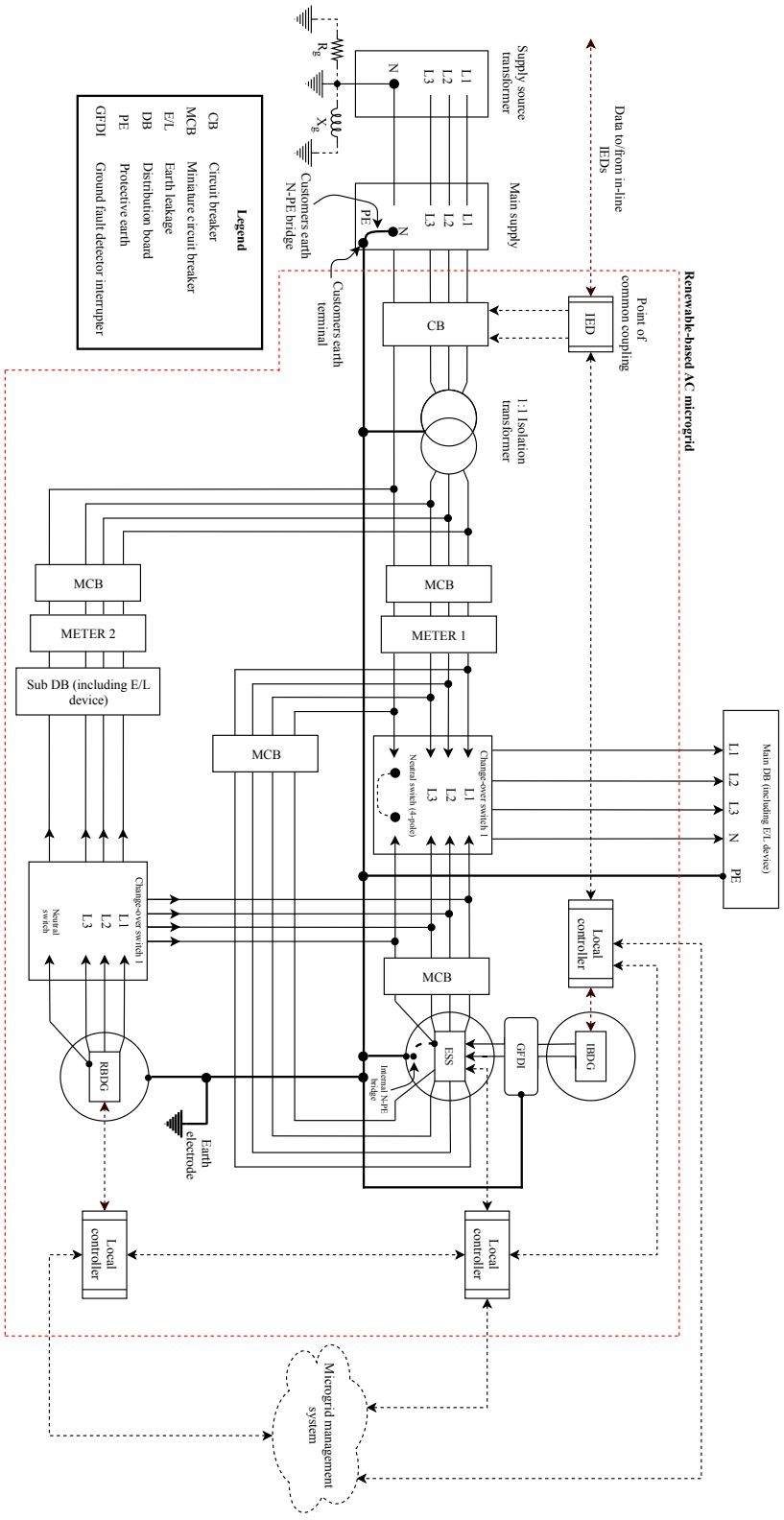

Figure 3.6. Single-line diagram of RBM wiring premise between the LV RDN and end user

3.3.2 Protection IED requirements

The following protection functions are required to select the protection IED needed for the hybrid adaptive protection scheme. Circuit breaker monitoring (ANSI 52) should be included as a protection function of the protection IED. The ANSI codes can be seen in Table 3.4.

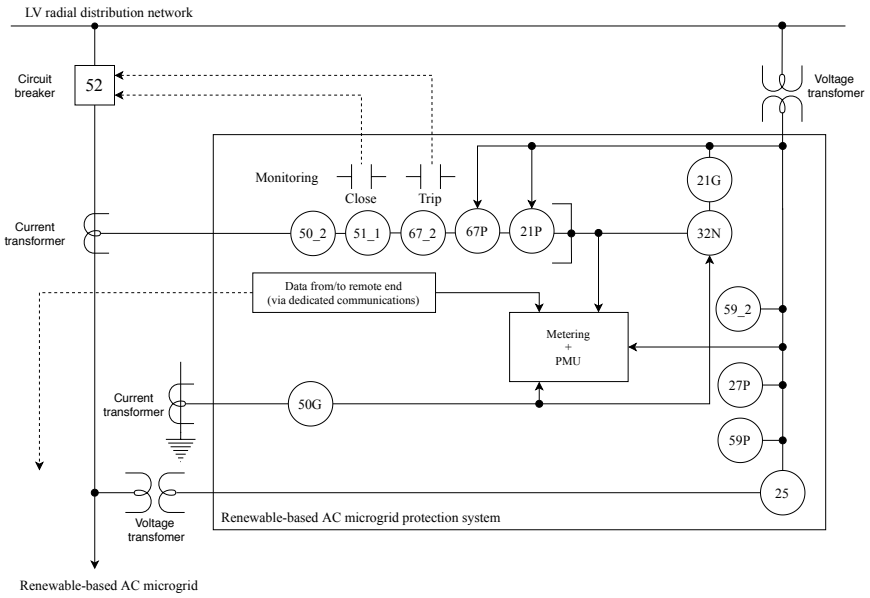

Figure 3.7. Single-line diagram of protection IED functional block diagram

Table 3.4. Required ANSI device numbers and protection functions

ANSI number	Function	ANSI number	Function
21_G	Ground distance	50_2	Negative-sequence instantaneous overcurrent
21P	Phase distance	51_1	Positive-sequence time overcurrent
25	Synchro-check	59P	Phase overvoltage
27P	Phase undervoltage	59_2	Negative-sequence phase overvoltage
32N	Wattmetric zero-sequence directional	67P	Phase directional overcurrent
50G	Ground instantaneous overcurrent	67_2	Negative-sequence directional overcurrent

3.3.3 Low-voltage radial distribution network case study

The results obtained through this case study will be used to develop and outline a hybrid adaptive protection philosophy, with the use of communication links between the protection IEDs, to increase the reliability, speed, sensitivity, stability and selectivity of the protection coordination between the LV RDN and multiple embedded RBMs. The developed hybrid adaptive protection philosophy should be able to successfully clear downstream high- and low-impedance faults in a selective, sensitive and reliable manner, disconnecting the faulted part of the network as quickly as possible, with the smallest number of customers affected.

The case study is simulated in DIgSILENT PowerFactory 2017. The simulation results will analyse the impact of the overly and optimally sized RDGs towards the protection IDMT curve coordination of fixed-setting relays and IEDs in the LV RDN. This case study has been adapted from a local Eskom LV RDN and will be referred to as Feeder A. The single-line diagram of Feeder A can be seen in Figure 3.8. The RDG design details, power flow information gathered and further information used for the case study simulations can be found in Addendum A.

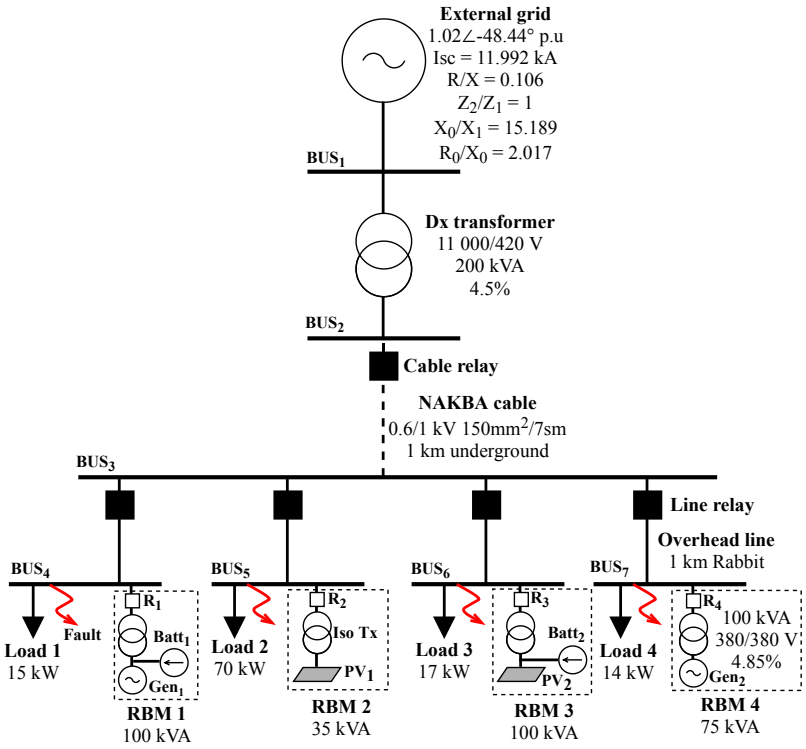

Figure 3.8. Eskom low-voltage radial distribution network [Feeder A]

Feeder A is an 11 kV network, stepped down to 400 V, using a 200 kVA distribution transformer. The LV side of the distribution transformer supplies four loads. Each load varies between 35∼45 kVA. The 400 V aluminum cross-linked polyethylene (XLPE) insulated 150 mm^2 underground cable is rated at 292 A. The overhead lines (Rabbit type aluminum conductor steel reinforced [ACSR]) have a current carrying capacity of 186 A. Based on the cable capacity it will be possible to feed approximately 200 kVA, where each overhead line can approximately feed 140 kVA in the LV RDN before overloading occurs. This is adequate for the RDN component for transferring power to the LV network loads. For simplicity the cable and overhead lines will be 1 km, respectively. All calculations and RDG design can be found in Addendum A.

CHAPTER 4 RESULTS

4.1 CHAPTER OVERVIEW

A simulated case study in DIgSILENT PowerFactory 2017 is carried out to analysis the impact of the aforementioned modelled RBMs in an existing Eskom LV RDN, called Feeder A. In order to get a maximum and minimum fault level understanding of Feeder A, the simulations and grading settings calculations are done with all overly sized RBMs disconnected from the LV RDN, and then with all the connected overly sized RBMs. This will assist in finding the maximum fault level contribution by the embedded RBMs and allow to observe the changes needed to correct the overcurrent IDMT curve coordination between the fixed-setting relays and applied to the protection IEDs. The RBMs can then be optimally sized to meet the optimisation constraints of Feeder A, and be adaptively re-coordinated along with the in-line protection IEDs. The highest and lowest fault levels that are detected by the cable and overhead line 1 protection relay were used to calculate the grading settings needed to successfully clear the fault in Feeder A network. The coordination grading settings are calculated using the bottom-up method where the time multiplier setting (TMS) is set to 0.05 for the in-line overhead line 1 relay and graded with the in-line cable relay, before and after the overly sized RBMs are grid-connected.

It is seen that the selectivity and sensitivity is discriminated between the fixed-settings relays due to the increased fault level contributions of the overly sized grid-connected RBMs, which intern affect the coordination time interval (CTI) and grading margin between the in-line overhead line 1 and cable protection relays, proving protection miscoordination. The protection challenges faced, only motivate the need for IDMT curve re-coordination between the protection devices. This emphasises the need to change from electromechanical fixed-setting relays to protection IEDs for their fast processing - and communication-based capabilities required for a hybrid adaptive protection scheme.

The same coordination philosophy used for the scenario where no RBMs were connected to the LV RDN, is then used to re-coordinated the new in-line cable, overhead line 1 and RBM 1 (R1) protection IEDs, with accordance to the hybrid protection algorithm. Additionally, the optimisation constraint function is applied to size the RDGs according to Feeder A's MVA capacity requirements. After applying the newly sized RBMs to Feeder A, the optimised fault levels are calculated. It is seen, that due to the RBMs S_{base} being recently sized, the fault levels have decreased with all the RBMs connected to Feeder A. This is due to the lower additional impedances of the RBMs when connected to the LV RDN. Additionally, it is seen that when in stand-alone operation, the minimum fault the stand-alone protection IED should be able to detect must be the same minimum fault when grid-connected. This is to ensure that if a switch-onto-fault had to occur during the synchronisation to the grid, the stand-alone settings will be able to sense the lower fault level and successfully trip before any serious damage occurs.

The hybrid algorithm will essentially calculate and store grading settings in setting groups, providing a successful adaptive protection scheme when the RBMs are grid-connected or in stand-alone operation within a LV RDN. Group 1 settings will be when no RBM is connected to the LV RDN. When no RBM is detected in the LV RDN by the LCs at each RBM, the in-line and RBM protection IEDs will be updated/set to group 1 grading settings. Group 2 grading settings will be when one or more RBMs are connected to the LV RDN, as determined by the LCs. It is essential to note that the first RBM connected to the LV RDN will be set as a master. This is done in order for the next grid-connecting RBM to reference and re-coordinate to the existing in-line group 2 cable settings. The overhead line IED and RBM IED will then be graded using the top-down method.

4.2 FEEDER A - CASE STUDY

In order to get a maximum and minimum fault level understanding of Feeder A, the simulations and grading settings calculations will be done with all overly sized RBMs disconnected from the LV RDN, and then with all the connected overly sized RBMs. This will assist in finding the maximum fault level contribution by the embedded RBMs and allow to observe the changes needed to correct the overcurrent IDMT curve coordination between the fixed-setting relays and applied to the protection IEDs. The RBMs can then be optimally sized to meet the optimisation constraints of Feeder A, and be adaptively re-coordinated along with the in-line protection IEDs.

4.2.1 Before embedded renewable-based AC microgrids

The fault level results seen in Table 4.1 and 4.2 has been obtained, using DIgSILENT PowerFactory 2017 before all the overly sized RBMs were integrated to Feeder A, as seen in Figure 4.1. The system fault impedance is calculated at the PCC, as seen in Figure 3.6. The pick-up current at the PCC is used for the grading settings of relay *r*. An IDMT curve according to IEC60255, standard inverse (SI), will be considered for the protection coordination between the protection devices, as in (2.19). The highest and lowest fault levels that will be detected by the cable and overhead line protection relays are used to calculate the grading settings needed to successfully clear the fault in Feeder A network. It can be seen in Table 4.1 that the highest fault level that the cable will experience is the phase-phase-to-ground fault at phase B and the three-phase fault for the overhead lines. It can be seen in Table 4.2 that the lowest fault level that the cable and overhead lines will experience is the single-phase fault. The overcurrent IDMT curves will be investigated for the relay grading settings. For this case study, only the grading for the cable and overhead line 1 will be considered.

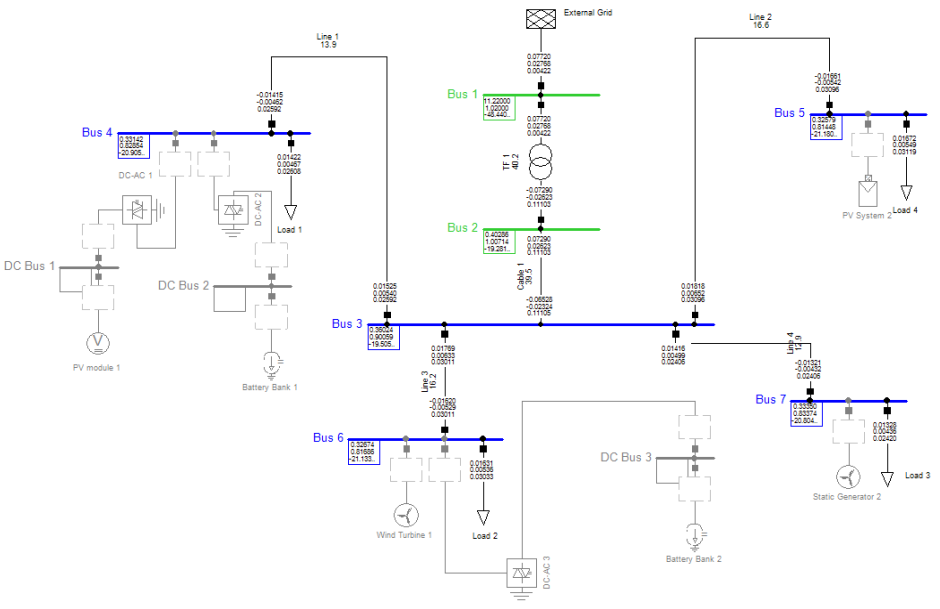

Figure 4.1. Feeder A, modelled in DIgSILENT PowerFactory 2017, with all RBMs disconnected

Table 4.1. Cable and overhead line 1 fault levels before embedded RBMs

	Fault levels				
	3-ph (kA)	**ph-ph (kA)**	**ph-gnd (kA)**	**ph-ph-gnd (kA)**	
Max (@ 1 %)	$[I_{kss}]$	$[I_{kssB}] = [-I_{kssC}]$	$[I_{kssA}]$	$[I_{kssB}]$	$[I_{kssC}]$
Cable	5.9010	5.1110	5.7140	**5.9910**	5.6250
Line 1	**0.9443**	0.8180	0.5053	0.8470	0.8250
Line 2	0.9443	0.8180	0.5053	0.8470	0.8250
Line 3	0.9443	0.8180	0.5053	0.8470	0.8250
Line 4	0.9443	0.8180	0.5053	0.8470	0.8250

Table 4.2. Bus fault levels before RBMs

	Fault levels				
	3-ph (kA)	**ph-ph (kA)**	**ph-gnd (kA)**	**ph-ph-gnd (kA)**	
	$[I_{kss}]$	$[I_{kssB}] = [-I_{kssC}]$	$[I_{kssA}]$	$[I_{kssB}]$	$[I_{kssC}]$
Bus 1	11.992	10.385	1.0240	10.606	10.167
Bus 2	6.1300	5.3080	5.8120	6.1580	6.1400
Bus 3	0.9690	0.8390	**0.5150**	0.8700	0.8450
Bus 4	0.2640	0.2290	**0.1670**	0.2190	0.2530
Bus 5	0.2640	0.2290	0.1670	0.2190	0.2530
Bus 6	0.2640	0.2290	0.1670	0.2190	0.2530
Bus 7	0.2640	0.2290	0.1670	0.2190	0.2530

In order to ensure ideal IDMT curve grading between the cable and overhead line 1 protection devices, the following must be considered, as the ideal CTI between the operation of the protection devices depend upon a number of factors, namely the fault current interrupting time of the circuit breaker (CB), the overshoot time of the relay and measurement errors.

1. The CB interrupting the fault must have completely interrupted the current before the discriminating relay ceases to be energised.

2. The overshoot time is not the actual time during which some forward operation takes place but the time which would have been required by the relay if it was still energising, to achieve the same proportion of operational advance. Relay design is directed to minimising and absorbing these energies, but some allowance is usually necessary.
3. All measuring devices, such as relays and current transformers, are subject to some degree of error. Relay grading settings is carried out, assuming the accuracy of the calibration curves published by manufactures, but since some error is to be expected, some tolerance must be allowed.

After the allowances mentioned above, have been made, the total number to be allowed to cover the items above depends on the operating speed of the CBs and the protection IED performance. Assuming the protection IED and CBs used in this study have low overshoots and fast operation, a grading margin (GM) between 0.35∼0.40 s will be feasible. A safety margin for the pick-up current between 1.05 and 1.3 will be considered to ensure that a satisfactory contact gap (or equivalent) remains between the coordinated relays. Fuses are generally found in LV RDNs and will therefore be considered in this case study. Considering Feeder A, the fuse at bus 4 needs to be the first to clear the fault closest to it before the overhead line 1 relay is required to operate and clear the fault. For satisfactory fuse-relay coordination the following equation will be considered and used to determine the GM required:

$$t^{'} = 0.4t + 0.15, \tag{4.1}$$

where t is the nominal operating time of the fuse.

By following the above mentioned coordination philosophy, the following IDMT curve grading settings can be calculated, using (2.19), with the results being found in Table 4.3.

Table 4.3. In-line group 1 coordination settings for before embedded RBM

Grading settings					
Cable			**Overhead line 1**		
$I_{pick-up} = I_{nom} \times 1.05$ (kA)		0.1166	$I_{pick-up} = I_{nom} \times 1.05$ (kA)		0.0269
Time multiplier setting		0.2645	Time multiplier setting		0.2713
Distance (km)	I_{fault} (kA)	Operating time (s)	Distance (km)	I_{fault} (kA)	Operating time (s)
0.01	5.9910	0.4517	0.01	0.9440	0.5167
0.1	4.1620	0.4994	0.1	0.7657	0.5503
0.2	2.9810	0.5528	0.2	0.6326	0.5848
0.5	1.5720	0.6933	0.5	0.4155	0.6779
0.6	1.3550	0.7363	0.6	0.3728	0.7068
0.8	1.0600	0.8203	0.8	0.3093	0.7625
0.99	0.8720	0.9016	0.99	0.2662	0.8139
ph-gnd	0.5150	1.2277	ph-gnd	0.1670	1.0279

The fuse minimum melting (MM) and total clearing (TC) curves, seen in Figure 4.2, shows where the fuse will operate when a fault occurs. Using (4.1) and the fuse MM as the nominal operating time of the fuse, a TMS value of 0.2713 has been selected for overhead line 1 fixed-setting relay. This will ensure satisfactory tripping coordination to occur between the overhead line 1 relay and 50 A fuse at bus 4. The final IDMT curve coordination between the 50 A fuse, overhead line 1 and cable can be seen in Figure 4.2.

It is essential to note that the TMS should remain above 0.05 to ensure stable operation of the relay. The plug setting multiplier (PSM) should remain above 2, when considering the lowest fault that the relay will clear. This is to ensure that the relay is not too sensitive. Currently the lowest faults PSM for the cable and overhead line 1 relay are 4.4175 and 6.1361, respectively.

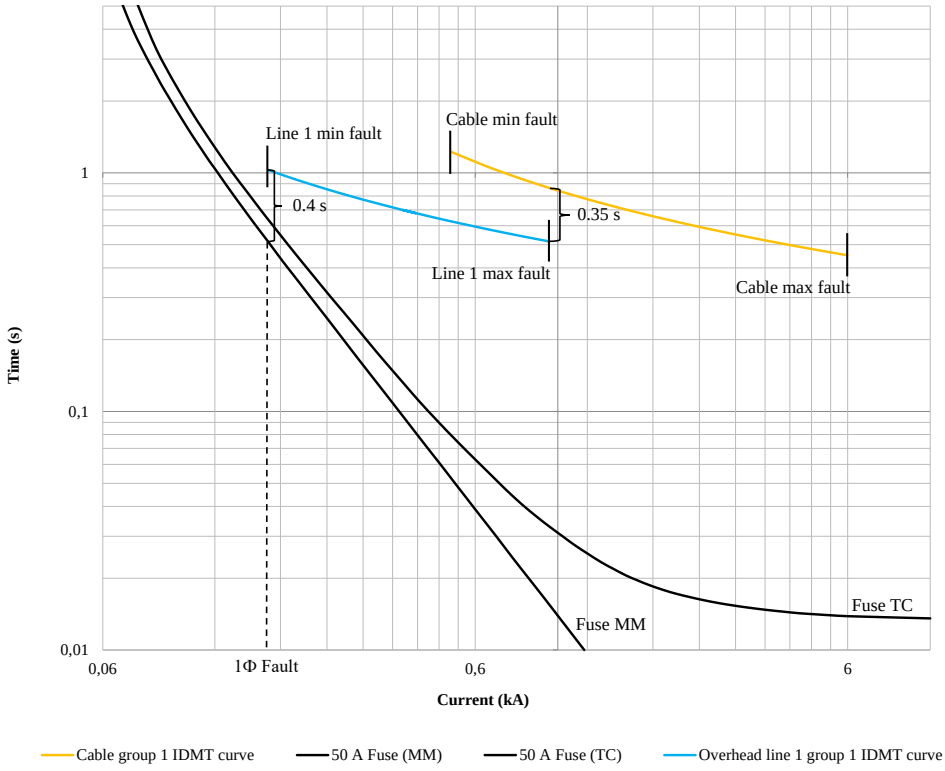

Figure 4.2. IDMT curve coordination between cable, overhead line 1 and 50 A fuse before connecting RBM

4.2.2 After embedded renewable-based AC microgrids

The following simulated fault level results in Table 4.4 and Table 4.5 were obtained, using DIgSILENT PowerFactory 2017 for a scenario when all the RBMs are connected to Feeder A, as seen in Figure 4.3. The existing IDMT curve coordination graded settings, as used when no RBMs are connected, are used to visually understand the entire effects of the embedded RBMs on the in-line fuse, overhead line 1 and cable protection relays. Once the effects have been noted, re-coordination can be implemented, using the hybrid adaptive protection coordination algorithm.

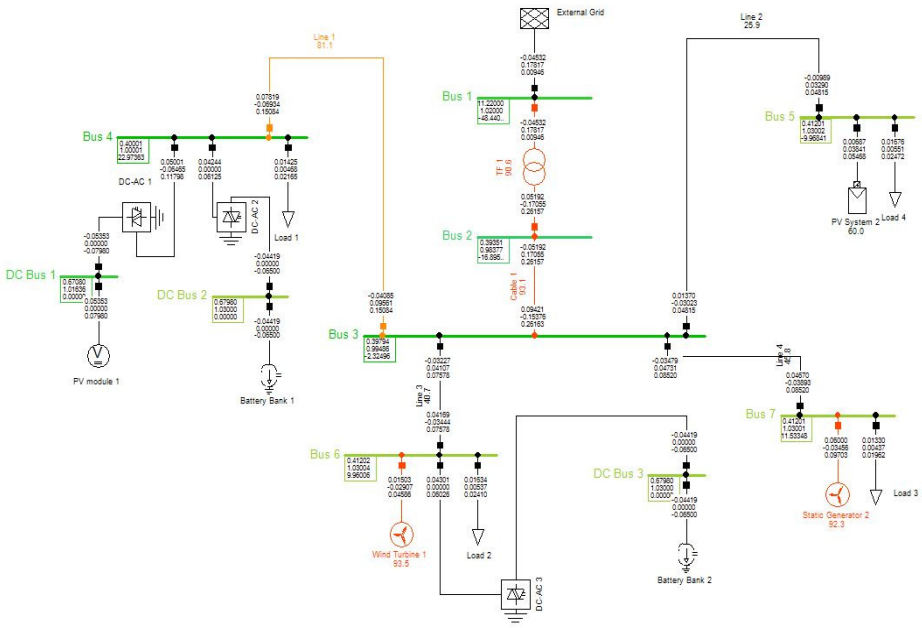

Figure 4.3. Feeder A, modelled in DIgSILENT PowerFactory 2017, with all RBMs connected

Table 4.4. Cable and overhead lines fault levels after embedded RBMs

	Fault levels				
	3-ph (kA)	**ph-ph (kA)**	**ph-gnd (kA)**	**ph-ph-gnd (kA)**	
Max (@ 1 %)	[I_{kss}]	[I_{kssB}] = [-I_{kssC}]	[I_{kssA}]	[I_{kssB}]	[I_{kssC}]
Cable	**6.7211**	5.1190	6.2957	6.001	5.5970
Line 1	**1.7445**	1.3080	0.8188	1.353	1.3170
Line 2	1.7442	1.3000	0.8189	1.3450	1.3090
Line 3	1.7523	1.1005	0.8223	1.1250	1.0880
Line 4	1.7519	1.0960	0.8224	1.1140	1.0770

Table 4.5. Bus fault levels after RBMs

	Fault levels				
	3-ph (kA)	**ph-ph (kA)**	**ph-gnd (kA)**	**ph-ph-gnd (kA)**	
	$[I_{kss}]$	$[I_{kssB}] = [-I_{kssC}]$	$[I_{kssA}]$	$[I_{kssB}]$	$[I_{kssC}]$
Bus 1	12.022	10.404	1.0260	10.625	10.185
Bus 2	6.9500	5.8290	6.7730	6.7620	6.7420
Bus 3	1.7980	1.3600	**0.8340**	1.1400	1.3680
Bus 4	0.5310	0.3830	**0.2800**	0.3660	0.4240
Bus 5	0.5240	0.3890	0.2840	0.3710	0.4310
Bus 6	0.7510	0.5410	0.3950	0.5170	0.5990
Bus 7	0.5000	0.5480	0.4000	0.5240	0.6070

4.2.2.1 Effects of the embedded RBMs on the in-line fixed-setting protection devices

It can be seen in graded settings Table 4.6 and Figure 4.4 how the embedded RBMs are affecting the in-line group 1 grading settings of the cable and overhead line 1 fixed-setting protection relays.

Table 4.6. Affected in-line group 1 grading coordination settings after embedded RBMs

Grading settings					
Cable			**Overhead line 1**		
$I_{pick-up} = I_{nom} \times 1.05$ (kA)		0.1166	$I_{pick-up} = I_{nom} \times 1.05$ (kA)		0.0269
Time multiplier setting		0.2645	Time multiplier setting		0.2713
Distance (km)	I_{fault} (kA)	Operating time (s)	Distance (km)	I_{fault} (kA)	Operating time (s)
0.01	6.7211	-	0.01	1.7446	-
0.087	5.9910	0.4517	0.1	1.4259	-
0.1	5.0786	0.4722	0.2	1.1885	-
0.2	3.9762	0.5062	**0.46**	0.9440	0.5167
0.5	2.5439	0.5822	0.5	0.8012	0.5427
0.6	2.3130	0.6013	0.6	0.7251	0.5598
0.8	1.9960	0.6334	0.8	0.6117	0.5914
0.99	1.7978	0.6584	0.99	0.5348	0.6189
ph-gnd	0.8340	0.9225	ph-gnd	0.2800	0.7959

Due to the additional short-circuit fault level contributed by the RBM, the effects on the IDMT curve coordination of the in-line fixed-setting relays can be seen in Figure 4.4. The increased fault levels in the LV RDN are due to the additional impedances of the connected RBMs. The maximum fault experienced by the cable increased from 5.991 kA to 6.721 kA. The reach of the cable relay moved from 0.01 m to 0.087 m. This can be seen as protection blinding, an incident where the increased fault of this magnitude had to have occurred in Feeder A, the cable fixed-setting relay would not have been able to pick up a fault higher than 5.991 kA, consequently leading to severe equipment damage within the LV RDN. This discriminates the protection coordination sensitivity.

The maximum fault experienced by the overhead line 1 increased from 0.944 kA to 1.7445 kA. This increased fault is seen to have compromised the selectivity between the cable and overhead line 1 protection device due to the decreased CTI (from 0.35 s to 0.225 s). This will cause sympathetic/false tripping. When a fault higher than 0.944 kA would have occurred on the overhead line 1, the overhead line 1 relay would not have operated and would have caused the cable relay to operate instead, which would have been undesirable. This discriminates the protection coordination selectively. The CTI

between the overhead line 1 IDMT curve and 50 A fuse at bus 4 also increased from 0.4 s to 0.574 s. The new coordination time between the fuse and overhead line 1 at 0.28 kA is calculated to be 0.261 s. This shows that if the fuse does not successfully clear the fault closest to it, it will take the overhead line 1 relay 0.313 s longer to operate than what would have been required. This decreased sensitivity could lead to potential damage to equipment connected to the LV RDN.

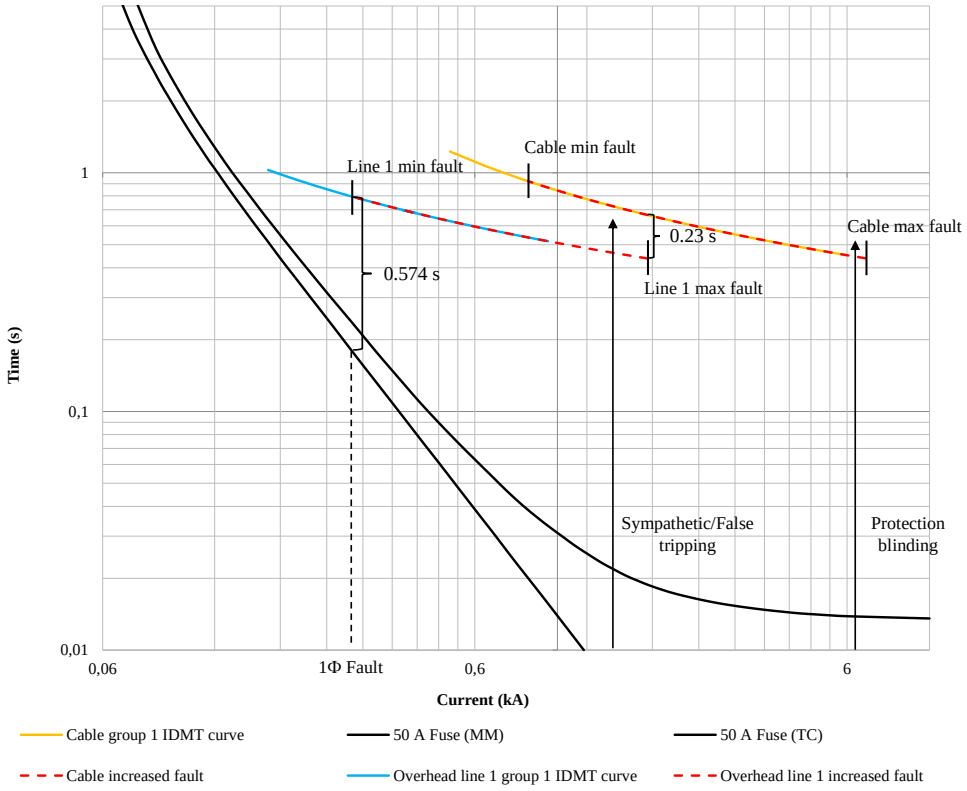

Figure 4.4. Discriminated in-line group 1 grading settings coordination with fuse, after connecting the RBM

All these protection challenges faced, only motivate the need for IDMT curve re-coordination between the protection devices. This emphasises the need to change from electromechanical fixed-setting relays to protection IEDs for their fast processing - and communication-based capabilities required for a hybrid adaptive protection scheme.

4.2.2.2 Re-coordination between in-line protection devices

The same coordination philosophy used for the scenario where no RBMs were connected to the LV RDN, will be used to re-coordinated the new in-line cable and overhead line 1 protection IEDs, with accordance to the hybrid protection algorithm, as seen in Figure 3.1. The highest and lowest fault levels that will be detected by the cable and overhead line 1 protection IED are used to calculate the TMS value required for IDMT curve coordination grading settings needed to successfully clear the fault in Feeder A network. It can be seen in Table 4.4 that the highest fault level that the cable and overhead line 1 will experience, is the three-phase fault. It can be seen in Table 4.5 that the lowest fault level that the cable and overhead line 1 will experience, is the single-phase fault.

Table 4.7. In-line group 1 grading settings corrected after embedded RBMs

Grading settings					
Cable			**Overhead line 1**		
$I_{pick-up} = I_{nom} \times 1.05$ (kA)	0.1166		$I_{pick-up} = I_{nom} \times 1.05$ (kA)	0.0269	
Time multiplier setting	0.2352		Time multiplier setting	0.1839	
Distance (km)	I_{fault} (kA)	Operating time (s)	Distance (km)	I_{fault} (kA)	Operating time (s)
0.01	6.7211	0.3898	0.01	1.7446	0.2969
0.1	5.0786	0.4199	0.1	1.4259	0.3126
0.2	3.9762	0.4501	0.2	1.1885	0.3283
0.5	2.5439	0.5177	0.5	0.8012	0.3636
0.6	2.3130	0.5347	0.6	0.7251	0.3796
0.8	1.9960	0.5633	0.8	0.6117	0.4011
0.99	1.7978	0.5854	0.99	0.5348	0.4197
ph-gnd	0.8340	0.8203	ph-gnd	0.2800	0.5398

The RBM protection IED is fundamentally not coordinated with the in-line protection IEDs and able to successfully synchronise the RBM to the LV RDN. This is done to observe the affected selectivity and sensitivity of the new in-line adaptive protection IEDs without the RBM IED. It can be noted that the new PSM of the cable and overhead line 1 protection IEDs are now 7.154 and 10.288, respectively. It can also be seen in Figure 4.5 that the new CTI between the 50 A fuse and overhead line 1 protection

IED is at the desired 0.261 s, but the CTI between maximum fault that would be experienced by the overhead line 1 and corresponding cable is 0.295 s, which is below the required 0.35 s. This will cause nuisance tripping. To solve this, the pick-up current can be be updated to compensate for the decrease in selectivity between the protection IEDs.

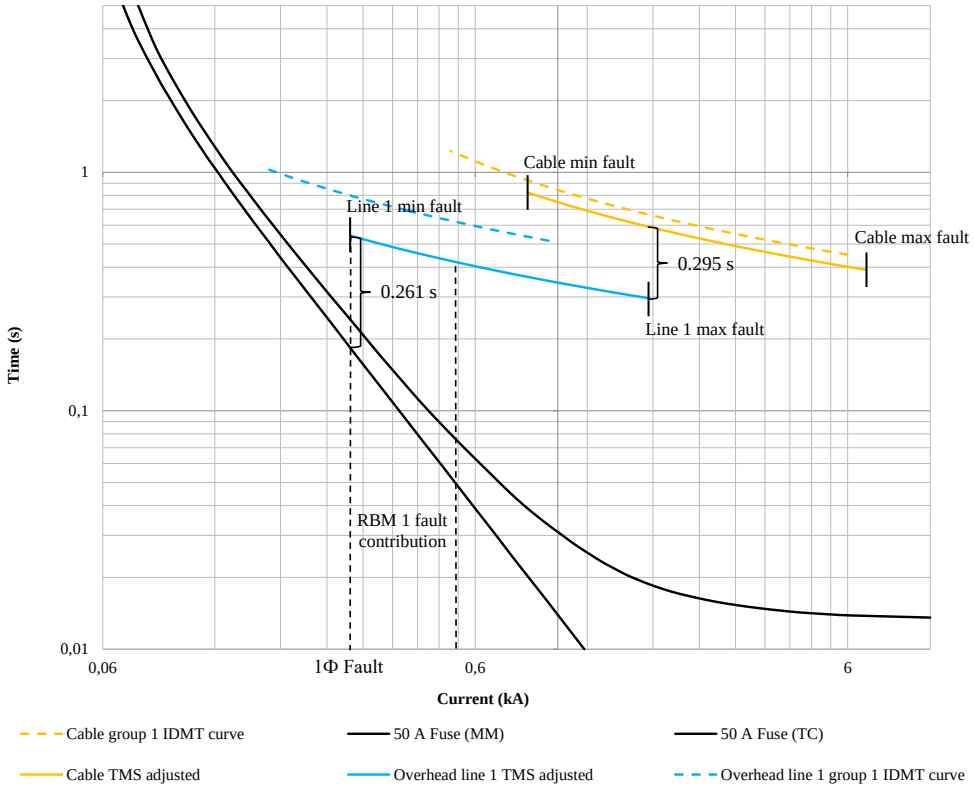

Figure 4.5. In-line group 1 TMS re-coordination between cable and overhead line 1 with fuse, after connecting RBM

It can be seen in Table 4.8 and Figure 4.6 that, although have adjusted both the TMS and pick-up current of the in-line protection IEDs so the CTIs and response time are improved, but the PSM of the cable and overhead line 1 protection IEDs are 3.034 and 1.768, respectively. Additionally, the TMS value of the overhead line 1 protection IED is below 0.05. Both the TMS and PSM are discriminated and show that the overhead line 1 protection IED will be too sensitive for downstream low-impedance faults and will cause sympathetic/false tripping in the LV RDN. The RBM's communication-based protection IED will be coordinated at the PCC, with the in-line protection IEDs. This will improve the sensitivity and selectivity of the IDMT curve grading coordination of the protection IEDs. This will

assist with the decreased selectivity, stability and reliability between the in-line protection IEDs when the RBM IED is not used.

Table 4.8. In-line group 1 TMS and pick-up re-coordination grading settings, after embedded RBMs

Relay settings					
Cable			**Overhead line 1**		
$I_{pick-up} = I_{nom} \times 1.05$ (kA)		0.2747	$I_{pick-up} = I_{nom} \times 1.05$ (kA)		0.1584
Time multiplier setting		0.1203	Time multiplier setting		0.0442
Distance (km)	I_{fault} (kA)	Operating time (s)	Distance (km)	I_{fault} (kA)	Operating time (s)
0.01	6.7211	0.2714	0.01	1.7446	0.1258
0.1	5.0786	0.2983	0.1	1.4259	0.1377
0.2	3.9762	0.3265	0.2	1.1885	0.1504
0.5	2.5439	0.3937	0.5	0.8012	0.1877
0.6	2.3130	0.4117	0.6	0.7251	0.2002
0.8	1.9960	0.4429	0.8	0.6117	0.2258
0.99	1.7978	0.4681	0.99	0.5348	0.2511
ph-gnd	0.8340	0.7979	ph-gnd	0.2800	0.5397

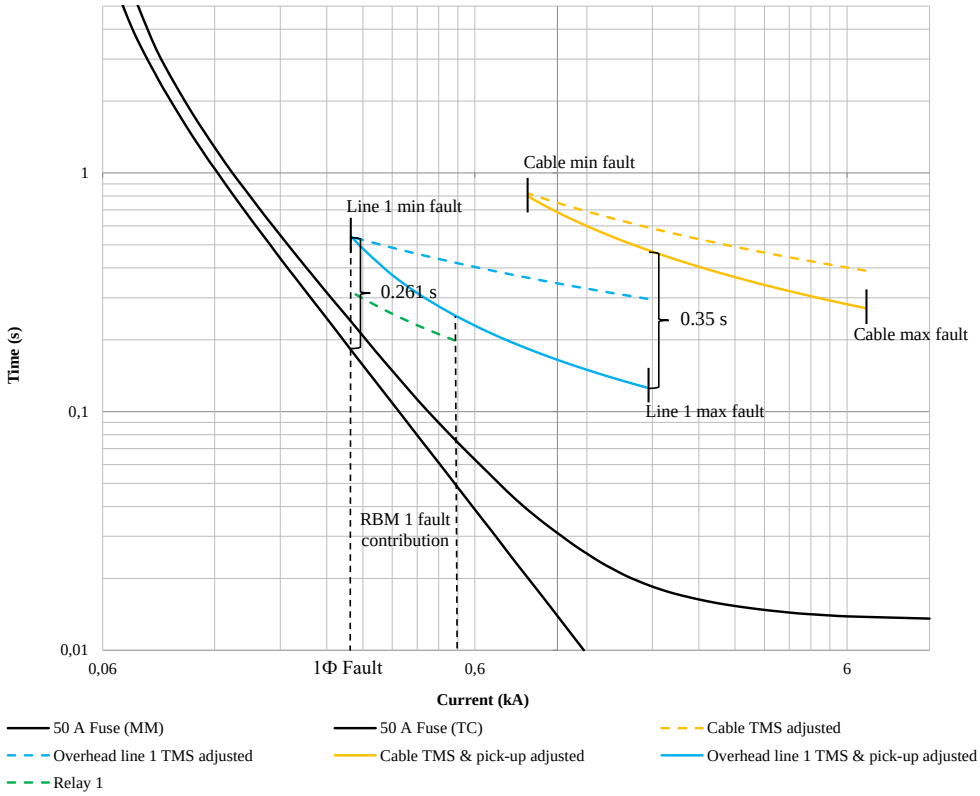

Figure 4.6. In-line group 1 TMS and pick-up re-coordination between cable and overhead line 1 with fuse, after connecting RBM

The RBM 1 IED (R1) TMS is set to 0.05 and can be seen in Figure 4.6. At the moment the RBM is relying on the 50 A fuse to clear any fault at the PCC. This dependency will prove to be expensive, as every time a fault would occur at bus 4, the blown fuse would have to be replaced, causing undesired islanding. Re-sizing the 50 A fuse to 80 A will help overcome this challenge.

4.2.3 After optimally sized renewable-based AC microgrids

After seeing the effects of the overly sized RBMs on Feeder A, the optimisation constraint function can be applied to size the RDGs according to Feeder A's MVA capacity requirements. The increased fault level affects the thermal loading and rating of the overhead lines, in turn affecting the life span of the cable and overhead lines. By optimising the size of the RBMs, lower fault limits can be experienced by

the LV RDN while still benefitting from the advantages of embedded renewable energy in constraint LV RDNs.

The optimisation function was applied to LV side of Feeder A. By solving for S_{base} in the RDG capacity (λ) weight constraint. The weight constraints for bus 2, bus 3 and bus 4, before and after optimisation, can be seen in Table 4.9, Table 4.10 and Table 4.11, respectively. The sized RBMs can be seen in Table 4.12. After applying the newly sized RBMs to Feeder A, the optimised fault levels are calculated and can be seen in Table 4.13 and Table 4.14. It can be seen, that due to the RBMs S_{base} being recently sized, the fault levels have decreased with all the RBMs connected to Feeder A. This is due to the lower additional impedances of the RBMs when connected to the LV RDN. The final grading settings between the RBM IED and in-line protection IEDs can be found in Table 4.15 and Table 4.16. Group 2 grading settings can be seen in Figure 4.7.

Table 4.9. Optimisation function and constraints applied to bus 2

Bus 2 optimisation					
Before	System losses (β)	Voltage profile (μ)	FCL (η)	RDG capacity (λ)	***Total***
Bus 2	0.4303	2.7230	71.8359	1.9693	76.9586
Function y	x_1	x_2	x_3	x_4	
	1.0000	0.4227	3469.86	1.0000	3472.28
After	System losses (β)	Voltage profile (μ)	FCL (η)	RDG capacity (λ)	
Bus 2	-3.2415	2.7778	5.1000	-3.6364	1.0000
Function y	x_1	x_2	x_3	x_4	
	1.0000	0.4444	32.4099	-3.2415	30.6129

Table 4.10. Optimisation function and constraints applied to bus 3

Bus 3 optimisation					
Before	System losses (β)	Voltage profile (μ)	FCL (η)	RDG capacity (λ)	***Total***
Bus 3	0.3842	2.7593	4.7598	1.8013	9.7048
Function y	x_1	x_2	x_3	x_4	
	1.0000	0.4371	15.2339	1.0000	17.6711
After	System losses (β)	Voltage profile (μ)	FCL (η)	RDG capacity (λ)	
Bus 3	-1.0907	2.7778	1.6379	-2.3250	1.0000
Function y	x_1	x_2	x_3	x_4	
	1.0000	0.4444	2.3091	-0.1744	3.5792

Table 4.11. Optimisation function and constraints applied to bus 4

Bus 4 optimisation					
Before	System losses (β)	Voltage profile (μ)	FCL (η)	RDG capacity (λ)	***Total***
Bus 4	0.1424	2.7778	3.9552	0.9206	7.7959
Function y	x_1	x_2	x_3	x_4	
	1.0000	0.4444	1.1152	1.0000	3.5597
After	System losses (β)	Voltage profile (μ)	FCL (η)	RDG capacity (λ)	
Bus 4	2.0096	2.7778	-1.0934	-2.6940	1.0000
Function y	x_1	x_2	x_3	x_4	
	1.0000	0.4444	0.6491	-1.4009	0.6926

Table 4.12. Optimally sized renewable-based AC microgrids

Optimally sized S_{base}					
	$S_{base\ before}$ (kVA)	P_{before} (kW)	$S_{base\ after}$ (kVA)	P_{after} (kW)	Ratio (%)
RBM 1	100.00	89.62	52.00	37.12	0.5200
RBM 2	35.00	-33.33	50.00	-17.69	1.4286
RBM 3	100.00	37.01	50.00	32.96	0.5000
RBM 4	75.00	49.23	60.00	46.11	0.8000

Table 4.13. Cable and overhead line fault levels after optimised embedded RBMs

	Fault levels				
	3-ph (kA)	**ph-ph (kA)**	**ph-gnd (kA)**	**ph-ph-gnd (kA)**	
Max (@ 1 %)	$[I_{kss}]$	$[I_{kssB}] = [-I_{kssC}]$	$[I_{kssA}]$	$[I_{kssB}]$	$[I_{kssC}]$
Cable	**6.1456**	5.1150	5.7566	5.9969	5.6743
Line 1	**1.2608**	0.9453	0.5918	0.9778	0.9518
Line 2	1.5759	1.1745	0.7399	1.2152	1.1827
Line 3	1.2615	0.7955	0.5920	0.8099	0.7833
Line 4	1.2947	0.8099	0.6078	0.8232	0.7959

Table 4.14. Bus fault levels after optimally sized RBMs

	Fault Levels				
	3-ph (kA)	**ph-ph (kA)**	**ph-gnd (kA)**	**ph-ph-gnd (kA)**	
	$[I_{kss}]$	$[I_{kssB}] = [-I_{kssC}]$	$[I_{kssA}]$	$[I_{kssB}]$	$[I_{kssC}]$
Bus 2	6.3548	5.3298	6.1930	6.1829	6.1647
Bus 3	1.4097	1.0717	**0.6572**	1.1111	1.0780
Bus 4	0.3838	0.2768	**0.2024**	0.2645	0.3064
Bus 5	0.4734	0.3515	0.2566	0.3352	0.3894
Bus 6	0.5406	0.3895	0.2844	0.3722	0.4312
Bus 7	0.3695	0.4050	0.2956	0.3872	0.4486

Table 4.15. In-line and RBM group 2 protection settings, after embedded RBMs

Relay settings					
Cable			**Overhead line 1**		
$I_{pick-up} = I_{nom} \times 1.05$ (kA)		0.2101	$I_{pick-up} = I_{nom} \times 1.05$ (kA)		0.1211
Time multiplier setting		0.1616	Time multiplier setting		0.0925
Distance (km)	I_{fault} (kA)	Operating time (s)	Distance (km)	I_{fault} (kA)	Operating time (s)
0.01	6.1456	0.3240	0.01	1.2608	0.2701
0.1	4.6437	0.33543	0.1	1.0305	0.2962
0.2	3.6357	0.3856	0.2	0.8589	0.3243
0.5	2.3261	0.4593	0.5	0.5790	0.4077
0.6	2.1149	0.4787	0.6	0.5240	0.4359
0.8	1.8251	0.5121	0.8	0.4421	0.4940
0.99	1.6438	0.5387	0.99	0.3865	0.5602
ph-gnd	0.6572	1.0252	ph-gnd	0.2450	0.9133

Table 4.16. In-line and RBM group 2 protection settings, after embedded RBMs

Relay settings					
Overhead line 1			**R1**		
$I_{pick-up} = I_{nom} \times 1.05$ (kA)		0.1211	$I_{pick-up} = I_{nom} \times 1.05$ (kA)		0.0718
Time multiplier setting		0.0925	Time multiplier setting		0.05
Distance (km)	I_{fault} (kA)	Operating time (s)	RBM 1	I_{fault} (kA)	Operating time (s)
0.01	1.2608	0.2701	Max fault	0.3838	0.2044
0.1	1.0305	0.2962		0.3650	0.2118
0.2	0.8589	0.3243		0.3250	0.2283
0.5	0.5790	0.4077		0.2950	0.2442
0.6	0.5240	0.4359		0.2650	0.2645
0.8	0.4421	0.4940		0.2250	0.3029
0.99	0.3865	0.5602	ph-gnd	0.2024	0.3342
Min PSM	0.2420	0.9133		0.1670	0.4111

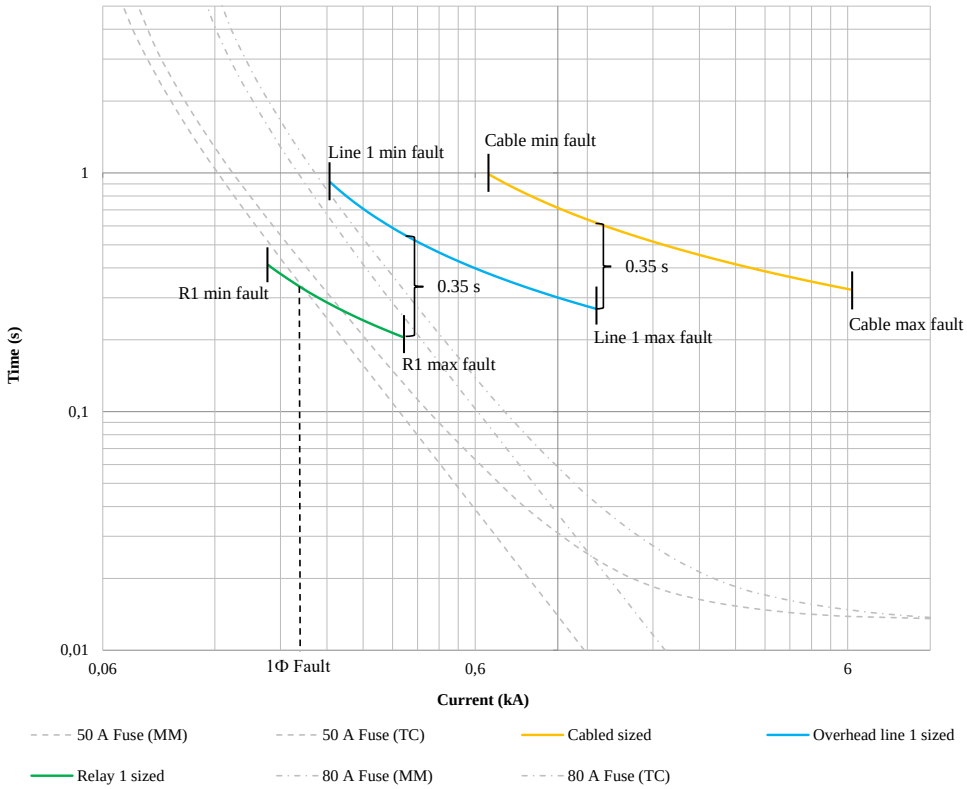

Figure 4.7. Group 2 grading settings for cable, overhead line 1 and relay 1, after optimally-sized renewable-based AC microgrids

The stand-alone grading settings -RBM 1 group 1- can be seen in Table 4.17 and Figure 4.8. The faults used to calculate the the graded settings can be found in Addendum A. When in stand-alone operation, the maximum and minimum fault R1 will detect will be the single-phase and three-phase fault, respectively. However, the minimum fault the stand-alone protection IED should be able to detect must be the same minimum fault when grid-connected, 0.2024 kA. This is to ensure that if a switch-onto-fault had to occur during the synchronisation to the grid, the stand-alone settings will be able to sense the lower fault level and successfully trip before any serious damage occurs. After successful synchronisation and grid stability has been reached for longer than 10 mins [18], the RBM 1 IED can be updated to the calculated grid-connected protection settings (group 2). The CTI between the RBM group 1 and overhead line 1 group 1 IED settings, can be seen in Figure 4.9. The CTI margins between the highest and lowest fault, when grid-connected, are between the recommended 0.35∼0.45 s. This will suffice as the RBM 1 group 1 settings will be able to act as back-up protection for the 10 mins before moving over to group 2 settings. The same can be said about the in-line protection

IEDs. The grid-connected and stand-alone RBM grading settings cover the required protection zone as previously done by the in-line fuse, as seen in Figure 4.7 and Figure 4.8. This shows that the need for the in-line fuse in the LV RDN closest to the RBM is no longer required.

Table 4.17. RBM 1 group 1 grading settings for stand-alone

Relay settings					
R1			**R1 Back-up**		
$I_{pick-up} = I_{nom} \times 1.05$ (kA)		0.0718	$I_{pick-up} = I_{nom} \times 1.05$ (kA)		0.0718
Time multiplier setting		0.065	Time multiplier setting		0.2682
RBM 1 R1	I_{fault} (kA)	Operating time (s)	RBM 1 R1 BU	I_{fault} (kA)	Operating time (s)
ph-gnd	4.4779	0.1112	ph-gnd	4.4779	0.4619
3-ph	1.4876	0.1577	3-ph	1.4876	0.6506
	0.2024	0.5523		0.2024	2.2785

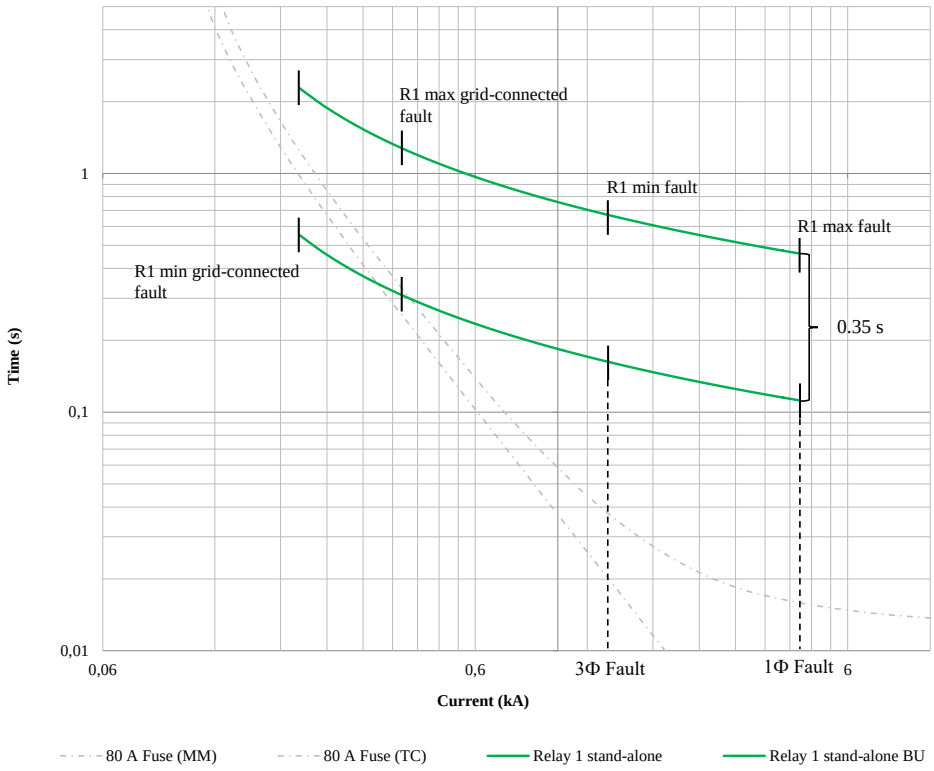

Figure 4.8. RBM 1 group 1 settings coordination for stand-alone renewable-based AC microgrid

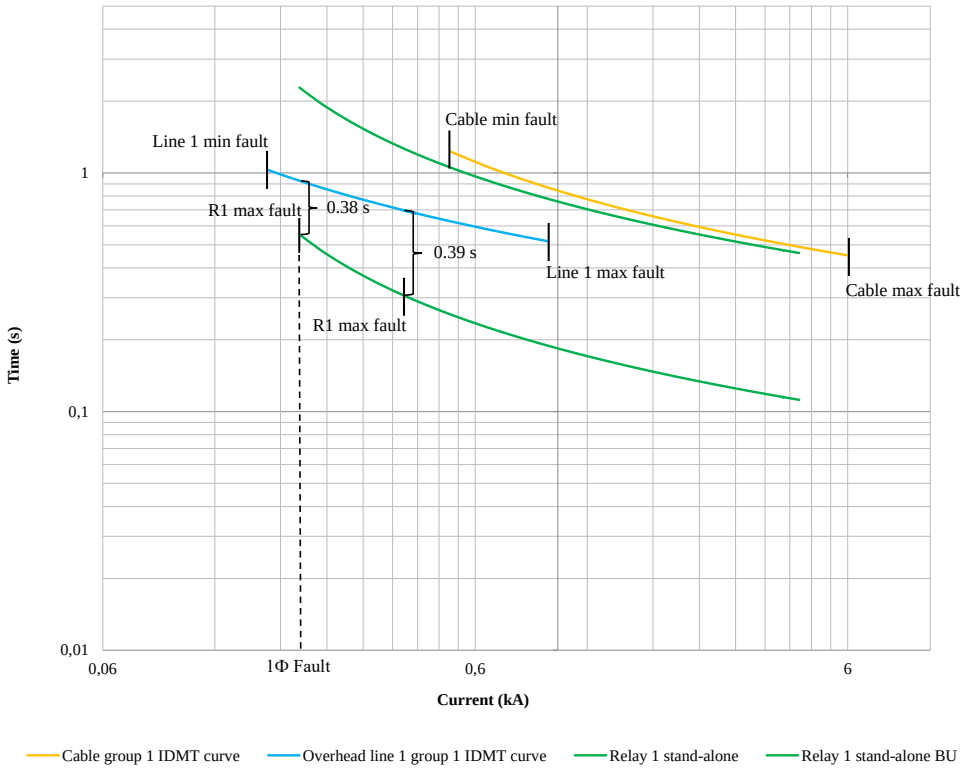

Figure 4.9. CTI between RBM IED group 1 grading settings and in-line IEDs group 1 settings

CHAPTER 5 DISCUSSION

A comprehensive investigation was presented to consider whether RBMs could be integrated successfully in LV RDNs, without discriminating the protection coordination philosophy. This was done by using a hybrid adaptive protection philosophy, to allow for the update of grading settings and re-coordination between the protection IEDs every time a RBM was removed from or integrated into the LV RDN. Additionally, the RBMs were optimally sized and placed in a modelled LV RDN, called Feeder A. An optimisation function was considered, as it could have be used to reduce power system losses, initial investment costs, fault contribution limits and voltage swell and sag, and improve system voltage profiles, system reliability and stability, voltage regulation and system power factor [4, 16, 23]. Optimally sized and placed RBMs can assist in minimising islanding and in the improvement of the overall protection challenges, as the extent to which the protection coordination between the in-line fixed-setting protection devices is affected, depends on size, location and number of connected RBMs in the LV RDN [4, 16, 23].

TN-C Type II uni-grounding protection earthing methods were considered for the electrical installation of the RBM, as seen in Figure 3.6. The purpose was to ensure that if an earth fault would have occur anywhere on the electrical installation, it could have been safely discharged to earth. The single point grounding minimises the number of possible earth paths, simplifying earth-fault detection [1], so that there is sufficient current to allow detection of an overcurrent element [17]. With no isolation transformer, and with the RBM is in stand-alone operation, protection is required to be more sensitive in detecting fault current levels. This is due to short-circuit current magnitudes being significantly smaller than when grid-connected [6, 7]. Implementation of an isolation transformer was then considered, as using low-impedance grounding would have formed fault currents high enough for protective IEDs to detect and isolate the faulted network area, increasing the sensitivity and reliability of the RBM [12]. The Y_g/Δ connected isolation transformer limits the single-phase and phase-to-phase-to-ground fault

current levels contributed, due only to the absence of zero-sequence components of the RBM. The Y_g/y_g isolation transformer grounding allows for low-impedance faults, therefore, significantly higher ground fault levels are present. This assists in the requirement for less sensitive fault detection by the protection IED - in grid-connected and stand-alone mode - thereby preventing additional sensitive CT measurements. Additionally, low-impedance grounding reduces arc flashes and arcing current, which are the common causes of ground faults [12].

The fault responses of inverters are characterised as positive-sequence sources only [1]. During asymmetrical faults, the IBDGs can be controlled to only inject predetermined positive-sequence currents, and will not facilitate negative- or zero-sequence currents [1, 5]. The IBDG's positive-sequence fault current in the RBM can be controlled and is limited between 1.2$\sim$2 p.u. inverter rated. RBDGs' high output fault current contribution is between 5$\sim$10 p.u. rated current [1, 5, 12, 32]. Additionally, negative-sequence component injection from RBDG units can be filtered out by implanting low-pass filters [5]. By grounding wye (Y_g) points of connected isolation transformers, zero-sequence injection can be minimised [5].

For the protection IED functional design, as seen in Figure 3.7, negative-sequence is included as the reactive part of the negative-sequence impedance, with the use of zero-sequence currents, that can assist in determining reverse and forward faults from IBDGs in RDNs [6, 7]. A negative-sequence directional element can utilise fault direction to avoid false trips due to low magnitude fault currents when in stand-alone operation [6]. This is an available option when no isolation transformer is present. Differential protection is not considered - although is not affected by RDG size, type and location [26] - as it may prove ineffective when considering the RBM, switching transients between modes of operation and unbalanced loads [6, 9, 12]. Accuracy can also prove to be a challenge when various CT ratio types are used in the system, where the various power losses can impact on the sensitivity of the differential IEDs [12, 25]. When distance protection is considered, issues may arise in protection IEDs when high-impedance single-phase-to-earth faults occur in the system [7]. Additionally, when wye-connected loads and transformers are connected downstream, the protection IED tends to operate unnecessarily for ground faults [6, 7]. This is due to low fault impedance appearing as the faulted point, measured by the protection IED [6]. To overcome this issue, negative-sequence impedance analysis can be implemented at each protection IED and used to resolve bi-directional faults [6]. Distance protection can only be used as primary protection when fixed-setting protection devices are concerned. Synchro-check capabilities are a requirement to ensure that successful automatic synchronisation to

the grid occurs, in accordance with the *South African grid code regulations for RPPs* [18] standards and *NRS 097-2-1: Grid interconnections of embedded generation* [20].

An adaptive hybrid protection philosophy has been investigated, with the use of communication and sequence-based protection IEDs. The RBM's dynamic operating nature is caused by the RDG units' dependency on various weather conditions [14]. This dependency is the main contributor to the RBM's topology changes [5, 14]. The pick-up current and TMS of the relay settings of the protection IED should be adjustable to the various dynamic fault current penetration levels of the connected IBDG and RBDG. Applying orders made by an LC and data sent to a central MMS [1, 26, 32], real-time, system-wide variables can be used to re-calculate, off-line time-current grading settings. The updated settings can then be stored in an on-line global database. The MMS will send modified control commands to the individual LCs if any lack of control or protection coordination is detected (i.e. integration to or removal of RBMs from the LV RDN). The TMS and pick-up current of the protection IEDs are re-calculated in accordance with the hybrid adaptive algorithm, as seen in Figure 3.1. The algorithm re-calculates the required grading settings to ensure that sufficient coordination between the protection IEDs are kept. The on-line grading settings database updates every time when a RBM has been connected or removed for the LV RDN.

Feeder A (adapted from an existing Eskom LV radial distribution network) and the selected renewable sources (PV, WP and ESS) were designed and modelled in accordance with the *South African grid code regulations for RPPs* [18], *SANS 10142-1: Wiring of premises* [19] standards, and the *NRS 097-2-1: Grid interconnections of embedded generation* [20]. Feeder A is used to observe the effects of RBMs, before and after being optimally, sized using an optimisation function to solve for S_{base}, on the fixed-setting protection devices. This effect motivated the desire to change from electromechanical protection relays to protection IEDs. This is due to the communication between the in-line IEDs and RBM IED requirement, in order to update the re-calculated grading settings needed to re-coordinate the protection IDMT curves for the overcurrent protection element. By optimising the size of the RBMs, lower fault limits can be experienced by the LV RDN, while benefitting from the advantages of embedded renewable energy in constraint LV RDNs, and while proceeding to meet Feeder A's MVA capacity requirements. With the RBMs optimally sized and using the hybrid adaptive protection philosophy, the improvement showed minimised system power losses, enhanced the voltage profile and increased network reliability. Decreased loading capacity was also noted for the cable and overhead line 1, as can be seen in Figure 5.1 and Figure 5.2, respectively. The optimisation weight factors used

in the objection function to minimise S_{base} of bus 2, bus 3 and bus 4 can be seen in Figure 5.3, Figure 5.4 and Figure 5.5, respectively.

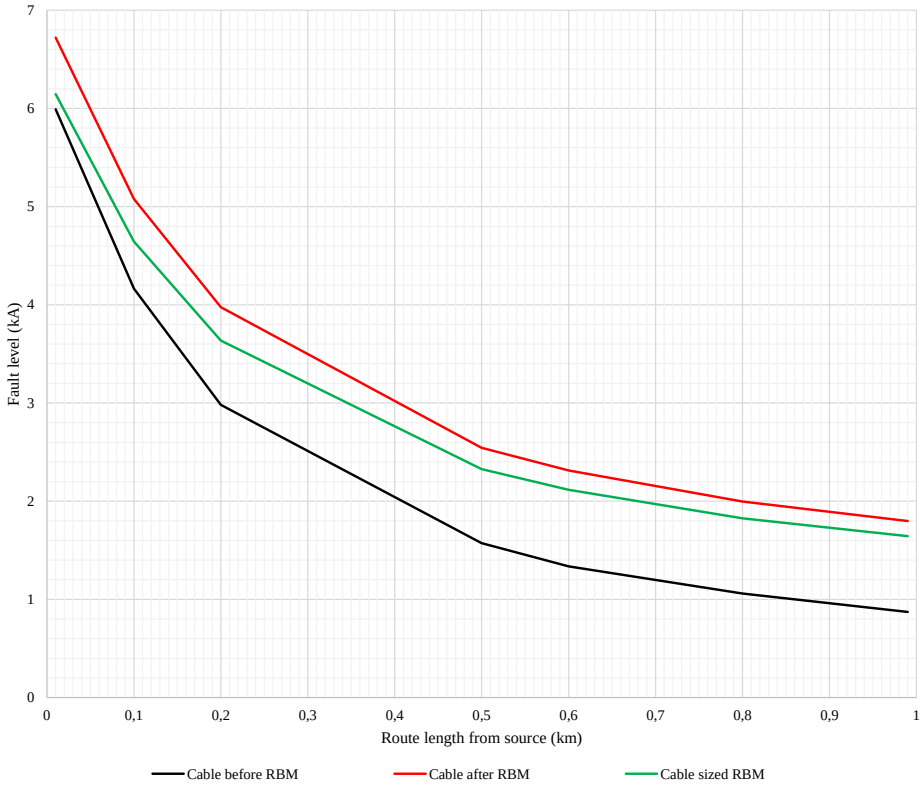

Figure 5.1. Cable fault levels before connected, after connected and optimally sized RBMs

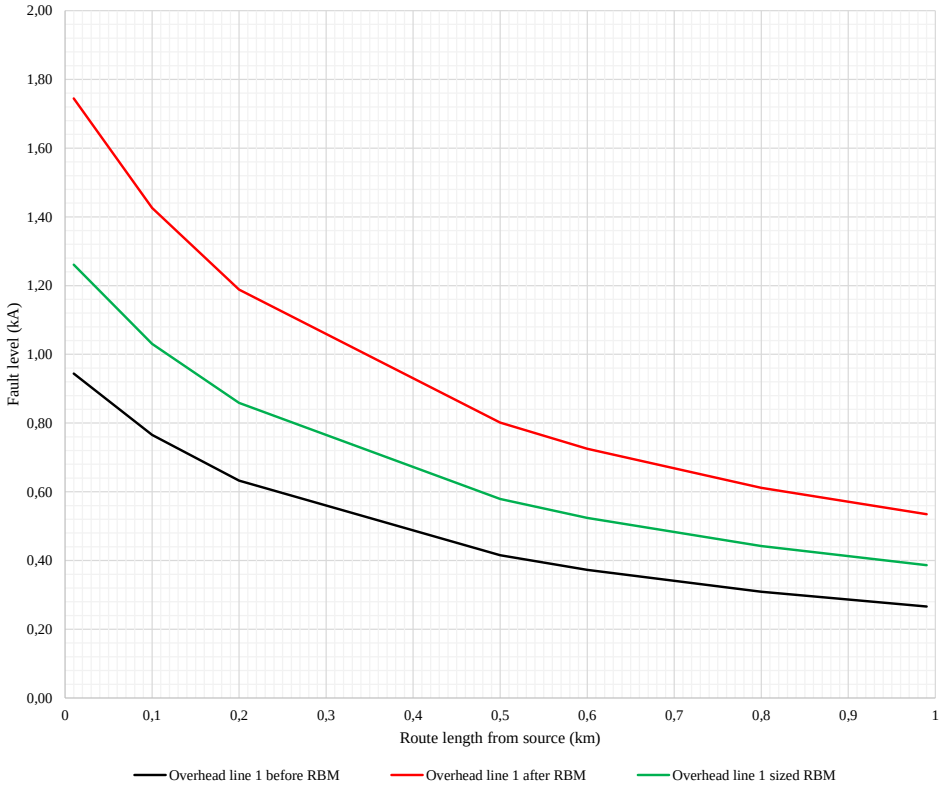

Figure 5.2. Line fault levels before connected, after connected and optimally sized RBM

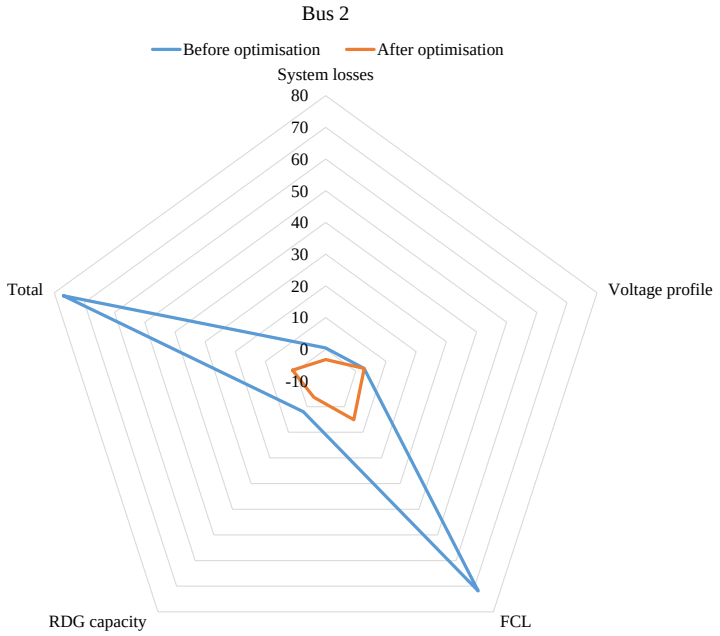

Figure 5.3. Bus 2 weight factors before and after optimisation

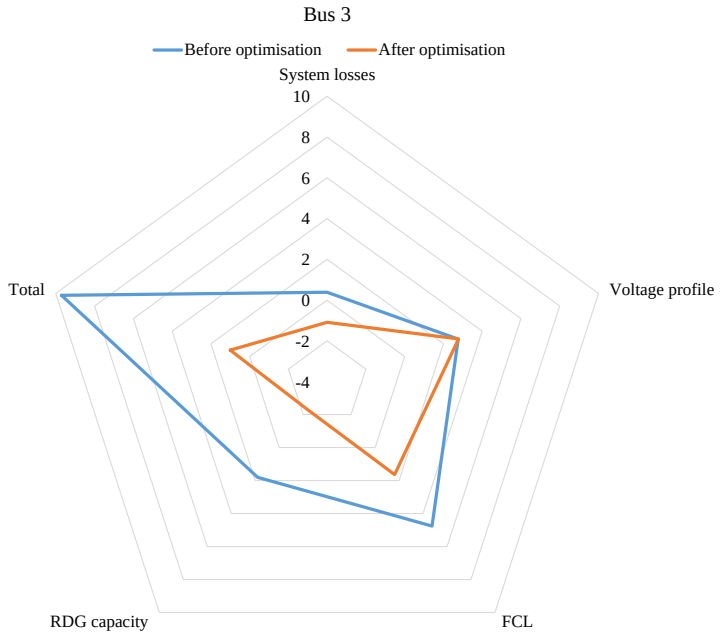

Figure 5.4. Bus 3 weight factors before and after optimisation

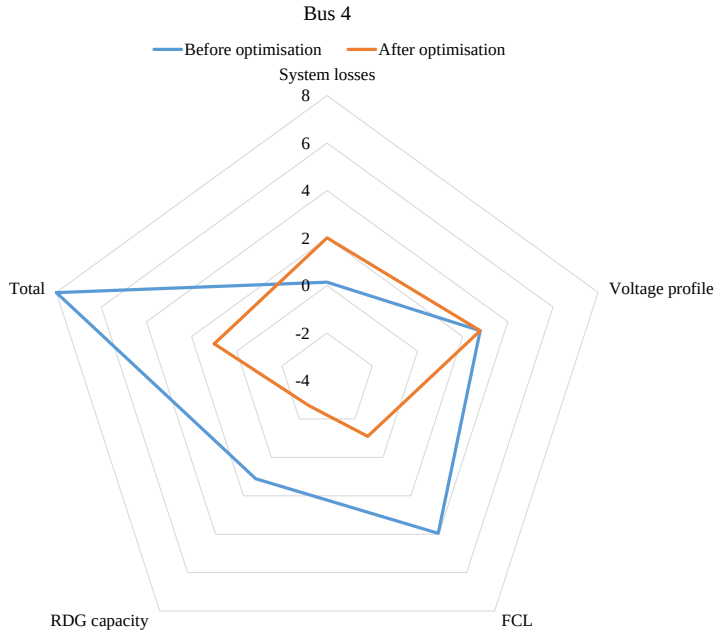

Figure 5.5. Bus 4 weight factors before and after optimisation

The summarised fault levels used for the grading settings can be seen in Table 5.1. The hybrid adaptive protection algorithm was able to successfully re-coordinate the RBM IED and in-line protection IEDs. The summarised grading settings and CTI measurements, for each scenario simulated in DIgSILENT PowerFactory, can be seen in Table 5.2 and Table 5.3.

Table 5.1. Summarised fault levels

	Fault levels					
	Cable		**Overhead line 1**		**RBM 1**	
	$I_{F_{Max}}$ (kA)	$I_{F_{Min}}$ (kA)	$I_{F_{Max}}$ (kA)	$I_{F_{Min}}$ (kA)	$I_{F_{Max}}$ (kA)	$I_{F_{Min}}$ (kA)
Before RBM	5.991	0.8720	0.9440	0.2662	-	-
After RBM	6.721	1.7519	1.7446	0.5348	0.5310	0.2800
Sized RBM	6.1456	0.6572	1.3627	0.2450	0.3838	0.2024

Table 5.2. Summarised grading settings

Grading settings			
In-line IED group 1	**PSM**	**TMS**	**Pick-up**
Cable	4.4175	0.2645	0.1166
Overhead line 1	6.1361	0.2713	0.0269
TMS updated	**PSM**	**TMS**	**Pick-up**
Cable	7.154	0.2352	0.1166
Overhead line 1	10.2880	0.1839	0.0269
TMS and pick-up updated	**PSM**	**TMS**	**Pick-up**
Cable	3.0340	0.1203	0.2747
Overhead line 1	1.768	0.4420	0.1584
Group 2	**PSM**	**TMS**	**Pick-up**
Cable	2.4947	0.1616	0.2101
Overhead line 1	2.0230	0.0925	0.1211
RBM 1	2.3261	0.0500	0.0718
RBM 1 IED group 1	**PSM**	**TMS**	**Pick-up**
Main	2.2641	0.0650	0.0718
Back-up	2.2641	0.2682	0.0718

Table 5.3. Grading coordination time intervals

Coordination time intervals						
	Before RBM		**After RBM**		**After sized RBM**	
	I_{Fault} (kA)	CTI (s)	I_{Fault} (kA)	CTI (s)	I_{Fault} (kA)	CTI (s)
Overhead line 1 max	0.9440	0.3500	1.7446	0.2952	1.2608	0.3500
Cable min	0.5150	0.6007	1.7519	0.2908	0.6572	0.6999
RBM 1 max	-	-	0.5310	0.6486	0.3838	0.3500
Overhead line 1 min	-	-	0.5348	0.6445	0.2450	0.6316

The effects of the embedded RBMs on the settings coordination can be seen in Table 5.2. When applying the hybrid adaptive protection algorithm, it is essential to include the updated pick-current when re-calculating the new TMS. This is to ensure that sufficient sensitivity and selectivity between the protection IEDs are kept when RBMs are removed from or integrated into the LV RDN. The one disadvantage found was that for group settings 2, the overhead line 1 will not be able to detect any fault lower than 0.245 kA, as the PSM value falls below 2. This indicates that when a single-phase fault had to have occurred at bus 4, the overhead line 1 will not be able to act as adequate back-up protection. To help overcome this protection unreliability, a second protection element, such as distance protection, could be updated along with the overcurrent IDMT curves. Where the admittance, measured by the distance IED, will be re-calculated using the hybrid adaptive protection algorithm and sorted on the MMS on-line database. This will assist in a more reliable protection scheme.

The hybrid algorithm will essentially calculate and store grading settings in setting groups. Where group 1 will be when no RBM is connected to the LV RDN. When no RBM is detected in the LV RDN by the LCs at each RBM, the in-line and RBM protection IEDs will be updated/set to group 1 grading settings. Group 2 grading settings will be when one or more RBMs are connected to the LV RDN, as determined by the LCs. The re-coordination grading of the RBMs between the in-line protection IEDs were done, using the bottom-up method. It is essential to note that the first RBM connected to the LV RDN will be set as a master. This is done in order for the next grid-connecting RBM to reference and re-coordinate to the existing in-line group 2 cable settings. The overhead line IED and RBM IED will then be graded using the top-down method. The final grading settings, after optimally sizing the RBMs, for the rest of Feeder A can be found in Addendum A.

CHAPTER 6 CONCLUSION

A comparative analysis and investigation proposal to identify an effective and reliable protection renewable-based AC microgrid scheme, based on the effects and challenges of the existing LV protection philosophy standards, in existing South African LV radial distribution networks, for both grid-connected and stand-alone operation was evaluated. It shows that by integrating optimally selected, sized and placed renewable-based AC microgrids in LV radial distribution networks, emergent energy demands can be achieved, while still maintaining satisfactory protection IED coordination. This can be done by inequality restrictions in a mathematical optimisation function problem in order to minimise initial investment costs and fault level contribution; while maximising integration of renewable-based AC microgrids power contribution and profits in LV radial distribution networks. An hybrid adaptive protection scheme was identified to be most promising in providing safe and reliable renewable-based AC microgrid protection, using communication- and sequence-based relays.

The case study shows how the protection IED overcurrent IDMT curves can be re-coordinated after RBMs have been integrated into or removed from the LV radial network, by adjusting the plug setting multiplier, time multiplier setting and pick-up values of each protection IED. The re-coordinated protection IEDs were able to successfully clear low-impedance faults in a selective, sensitive and reliable manner for both grid-connected and stand-alone renewable-based AC microgrids. The adaptive hybrid protection scheme made use of orders given by an LC and sent data to a central MMS where the MMS calculated off-line, the required protection grading settings for each RBM IED. The off-line calculated grading settings were then stored to an online database, found within the MMS by the LC. The LC applies each group grading setting to their respective RBM IED. The RBM IED communicates to its corresponding in-line protection IED, to allow that protection IED to re-coordinate to its respective RBMs mode of operation. This hybrid adaptive protection strategy proved to be reliable, allowing effective renewable-based AC microgrid adaptability and improvement of protection re-coordination,

along with the in-line protection IEDs. This method will ensure that increased renewable-based AC microgrid reliability, security of supply and efficiency can be achieved. The one disadvantage found in this case study was that the in-line overhead line 1 sensitivity was not satisfactory as it could net detect any fault current under 0.240 kA. Further studies can be done to look at an adaptive distance protection method, using the developed hybrid adaptive algorithm, to solve for the new admittance settings. The adaptive distance protection and adaptive overcurrent protection can be set as main and back-up, respectively, for the renewable-based AC microgrid. This will further enhance the protection reliability of the overall renewable-based AC microgrid system.

REFERENCES

[1] H. L. Van Der Walt, R. C. Bansal, and R. Naidoo, "PV based distributed generation power system protection: A review," *Renewable Energy Focus*, vol. 24, pp. 33–40, 2018.

[2] P. T. Manditereza and R. C. Bansal, "Renewable distributed generation: The hidden challenges - A review from the protection perspective," *Renewable and Sustainable Energy Reviews*, vol. 58, pp. 1457–1465, 2016.

[3] J. M. Abdel-Salam, R. K. A. Abdallah, and M. Hashem, "Improvement of Protection Coordination for a Distribution System Connected to a Microgrid using Unidirectional Fault Current Limiter," *Ain Shams Engineering Journal*, vol. 8, no. 3, pp. 405–414, 2017.

[4] M. H. Pesaran, P. D. Huy, and V. K. Ramachandaramurthy, "A review of the optimal allocation of distributed generation: objectives, constraints, methods, and algorithms," *Renewable and Sustainable Energy Reviews*, vol. 75, no. May 2016, pp. 293–312, 2017.

[5] D. M. Bui and et al, "A Simplified and Automated Fault Current Estimation Approach for Grid-Connected Low-Voltage AC Microgrids," *2016 World Congress Sustainable Technology (WCST 2016)*, pp. 89–101, 2017.

[6] A. A. Memon and K. Kauhaniemi, "A critical review of AC microgrid protection issues and available solutions," *Electrical Power Systems Research*, vol. 129, pp. 23–31, 2015.

[7] J. Kennedy, P. Ciufo, and A. Agalgaonkar, "A review of protection systems for distribution networks embedded with renewable generation," *Renewable and Sustainable Energy Reviews*,

vol. 58, pp. 1308–1317, 2016.

[8] S. Katyara, L. Staszewski, and Z. Leonowicz, "Protection coordination of properly sized and placed distributed generations-methods, applications and future scope," *Energies*, vol. 11, no. 10, pp. 1–22, 2018.

[9] J. B. Brearley and R. R. Prabu, "A review on issues and approaches for microgrid protection," *Renewable and Sustainable Energy Reviews*, vol. 67, pp. 988–997, 2017.

[10] A. Saeed, S. Heresh, and P. Shahram, "Optimal coordination of overcurrent protection in the presence of SFCL and distributed generation," *Turkish J. Electr. Eng. Comput. Sci.*, vol. 26, pp. 2056–2065, 2018.

[11] N. E. Naily, S. Saad, Z. Rajab, and F. Mohamed, "An intelligent protection scheme to mitigate the impact of integrating large share wind energy resources in a weak distribution network," *Wind Engineering*, vol. 41, no. 6, pp. 383–396, 2017.

[12] D. M. Bui, S. L. Chen, K. Y. Lien, Y. R. Chang, Y. D. Lee, and J. L. Jiang, "Investigation on transient behaviours of a uni-grounded low voltage AC microgrid and evaluation on its available fault protection methods: Review and proposals," *Renewable and Sustainable Energy Reviews*, vol. 75, pp. 1417–1452, 2017.

[13] P. Sookrod and P. Wirasanti, "Overcurrent relay coordination tool for radial distribution systems with distributed generation," in *Proceedings of 2018 5th International Conference on Electrical and Electronics Engineering*, ser. ICEEE '18, 2018, pp. 13–17.

[14] "Integrated Resource Plan for Electricity 2010 - 2030," *Department of Energy South Africa*, pp. 1–114, November 2010 (Updated 2013). [Online]. Available: http://www.doe-irp.co.za/content/IRP2010_updated.pdf

[15] B. Mclaren, R. Asmal, P. Moyo, and V. Singh, "Section 3: Low Voltage Protection Philosophy and Reticulation," *Guide Group Technology: Low Voltage Reticulation (Eskom)*, 2012.

[16] P. Prakash and D. K. Khatod, "Optimal sizing and siting techniques for distributed generation in distribution systems: A review," *Renewable and Sustainable Energy Reviews*, vol. 57, pp. 111–130, 2016.

[17] V. Cohen, *Application guide for the protection of LV distribution systems*, 4th ed. Circuit Breaker Industries Ltd, 2006.

[18] "South African Grid Code Requirements for Renewable Power Plants - Version 2.8." [Online]. Available: https://www.sseg.org.za/wp-content/uploads/2019/03/South-African-Grid-Code-Requirements-for-Renewable-Power-Plants-Version-2-8.pdf, Accessed: August, 2020.

[19] "South African National Standards: The Wiring of Premises Part 1: Low Voltage Installations," *South African National Standard (SANS), SANS 10142-1*, Edition 2, 2017. [Online]. Available: https://store.sabs.co.za/catalog/product/view/_ignore_category/1/id/2140452/s/SANS-10142-1-ed-2-00-1/

[20] G. Botha, V. Nundlal, and T. Whittaker, "Grid Interconnection of Embedded Generation Part 2: Small-Scale Embedded Generation Section 1: Utility Interface," Edition 2, 2017. [Online]. Available: https://solar-support.org/files/265/dump

[21] A. R. Haron, A. Mohamed, and H. Shareef, "Coordination of Overcurrent, Directional and Differential Relays for the Protection of Microgrid System," *Procedia Technology*, vol. 11, pp. 366–373, 2013.

[22] S. Javadian, M. Haghifam, M. F. Firoozabad, and S. M. T. Bathaee, "Analysis of protection system's risk in distribution networks with DG," *Electrical Power Energy Systems*, vol. 44, no. 1, pp. 688–695, 2013.

[23] B. Li, Y. Li, and T. Ma, "Research on earthing schemes in LV microgrids," *The International Conference on Advanced Power System Automation and Protection*, vol. 2, pp. 1003–1007, 2011.

[24] S. Hosseini, H. Abyaneh, S. Sadeghi, F. Razavi, and A. Nasiri, "An overview of microgrid protection methods and the factors involved," *Renewable Sustainable Energy Research*, vol. 64,

pp. 174–186, 2016.

[25] K. Lien and et al, "A novel fault protection system using communication-assisted digital relays for AC microgrids having a multiple grounding system," *Electrical Power Energy Systems*, vol. 78, pp. 600–625, 2016.

[26] M. Monadi, M. Zamani, J. Candela, A. Luna, and P. Rodriguez, "Protection of AC and DC distribution systems embedding distributed energy resources: A comparative review and analysis," *Renewable and Sustainable Energy Reviews*, vol. 51, pp. 1578–1593, 2015.

[27] S. Saleh, "On the design and capacity of a grounding configuration for grid-connected DGUs," *IEEE Trans. Ind. Appl.*, vol. 51, no. 6, pp. 5366–5375, 2015.

[28] A. Colmenar-Santos, C. Reino-Rio, D. Borge-Diez, and E. Collado-FernÃąndez, "Distributed generation: A review of factors that can contribute most to achieve a scenario of DG units embedded in the new distribution networks," *Renewable and Sustainable Energy Reviews*, vol. 59, pp. 1130–1148, 2016.

[29] A. Ibrahim, W. El-Khattam, M. ElMesallamy, and H. Talaat, "Adaptive protection coordination scheme for distribution network with distributed generation using ABC," *Electrical Systems and Information Technology*, vol. 3, no. 2, pp. 320–332, 2016.

[30] C. Patil, S. Thale, S. Muchande, and A. Kadam, "A Novel Protection Scheme for DC Microgrid with Hierarchical Control," in *Proceedings of 5th IEEE International Conference on Smart Energy Grid Engineering*, ser. SEGE '17, 2017, pp. 117–122.

[31] R. Li, W. Wang, Z. Chen, J. Jiang, and W. Zhang, "A review of optimal planning active distribution system: models, methods, and future researches," *Energies*, vol. 10, no. 11, pp. 1–27, 2017.

[32] B. Brearley and R. Prabu, "A review on issues and approaches for microgrid protection," *Renewable and sustainable Energy Reviews*, vol. 67, pp. 988–997, 2017.

ADDENDUM A DERIVATION OF HIGHER ORDER MODELS

A.1 CASE STUDY - RDG DESIGNS

The following information was used to design Feeder A, used in DIgSILENT PowerFactory 2017. To ensure minimal bi-directional power flow in the LV RDN, the total load demand of the system should not be less than the total summation of the active power generated by the embedded RDG units.

Table A.1. Case study load demand

Maximum load (kW)	
Load 1	15.00
Load 2	70.00
Load 3	17.00
Load 4	14.00
Total	116.00

Using the RDG capacity constraint and the information in Table A.1, the RDG should be sized, so that the overall power contribution to the network should be less than or equal to 116.00 kW. as in (A.1).

$$\therefore \sum_{j=1}^{4} CP_j \leq 116.00\,kW. \tag{A.1}$$

A.1.1 Solar PV design

In accordance with *SANS 10142-1: Wiring of premises* [19] standards and the *NRS 097-2-1: Grid interconnection of embedded generation* [20], the general requirements for PVs in LV networks, used for the Case study, are as follows, in Table A.2. The specifications were inputted into the simulation requirements, as requested by DIgSILENT PowerFactory 2017.

Table A.2. PV general requirements

Nominal system voltage	400 V
Rated voltage (U_n)	440 V (3-ph)
	252 V (1-ph)
Rated insulation voltage (U_i)	8
Rated impulse withstand voltage (U_{imp})	6 kV
Ambient temperature	- 10 $\sim$ + 40 °C
Rated frequency	50 Hz

For this investigation the Sunpower E20/435 solar panel is used, with specifications and ratings seen in Table A.3.

Table A.3. Sunpower E20/435 solar panel ratings and specifications

Measured at STC, irradiance - 1000 W/m^2 ($G_{a,0}$) 25 °C (T_0^C)			
Parameter	**Symbol**	**Value**	**Unit**
Nominal power	$P_{max,0}^{module}$	435	Watts
Efficiency	η	20.1	%
Rated voltage (Module)	$V_{mpp,0}^{module}$	72.9	Volts
Rated current (Module)	$I_{mpp,0}^{module}$	5.97	Amps
Open circuit voltage	$V_{OC,0}^{module}$	85.6	Volts
Short-circuit current	$I_{SC,0}^{module}$	6.43	Amps
Maximum system voltage		600	Volts
Power	k_p	-0.38	%/°K
Voltage	k_v	-235.5	mV/°K
Current	k_i	3.5	mA/°K
Nominal operating cell temperature	NOCT	45	°C
Number of cells in series	N_{SM}	24	
Number of parallel branches	N_{PM}	2	
Series resistance	R_s^{Cell}	0.04197	Ω

The IBDGs positive-sequence fault current in the microgrid can be controlled and is limited between 1.2∼2 p.u. inverter rated. The total rated output of the photovoltaic system will be designed for 20.88 kW. The inverter ratings can been seen in Table A.4. The specifications were inputted into the simulation requirements, as requested by DIgSILENT PowerFactory 2017.

Table A.4. Inverter ratings

PV inverter	
MPPT working voltage	350 ~800 V_{DC}
Maximum input voltage	1000 V_{DC}
Maximum input current	15 A
Rated output voltage	1.03 p.u. (412 V_{AC})
Maximum output current	29 A
Rated output fault current	2 p.u.
No load losses	0.8 kW
Frequency	50 Hz
Power factor	0.96
Control method	Constant voltage
Pulse width modulation (PWM)	Rectangular

A.1.2 Energy storage system design

The following ESS systems in Table A.5 were used in the Case study. The specifications were inputted into the simulation requirements as requested by DIgSILENT PowerFactory 2017.

Table A.5. Energy storage system specifications

Battery bank 1 specifications [a]	
Maximum voltage	1000 V_{DC}
Rated voltage	400 V_{AC}
Rated current	65 A
Rated power	50 kW
Battery bank 2 specifications (ABB PCS100) [b]	
Maximum voltage	1000 V_{DC}
Maximum current	65 A
Rated power	65 kW
MPPT working voltage for inverter	585 ∼784 V_{DC}
Rated voltage	V_{AC}
Overload capability	10min @ 120 % 30sec @ 150 % 2sec @ 200 %
Internal resistance	0.78 Ω
Inverter losses	1.5 kW
Control method	V_{dc} - Q
PWM	Rectangular

[a] Battery bank 1 has been modelled to inject no reactive support.

[b] Battery bank 2 uses reactive control support.

A.1.3 Wind turbine design

The following wind turbine systems in Table A.6 are used in the Case study. The specifications are used in the simulation requirements, as requested by DIgSILENT PowerFactory 2017.

Table A.6. Wind turbine ratings

Wind turbine 1	
Nominal apparent power rating	35 kVA
Power factor	0.8
Wind turbine type	Type-3 (onshore)
Generator type	Synchronous
Active power	15 kW
Reactive power	11.25 kvar
Voltage rating	400 V
Input mode	P, cos(phi)
R/X ratio	7.33
Control method	Constant-V
Wind turbine 2	
Nominal apparent power rating	75 kVA
Power factor	0.8
Wind turbine type	Type-3 (onshore)
Generator type	Synchronous
Active power	60 kW
Reactive power	45 kvar
Voltage rating	400 V
Input mode	P, cos(phi)
R/X ratio	5.33
Control method	Constant-V

The wind turbine power curve and stochastic wind model as in DIgSILENT PowerFactory 2017, can be seen in Figure A.1 and Figure A.2, respectively.

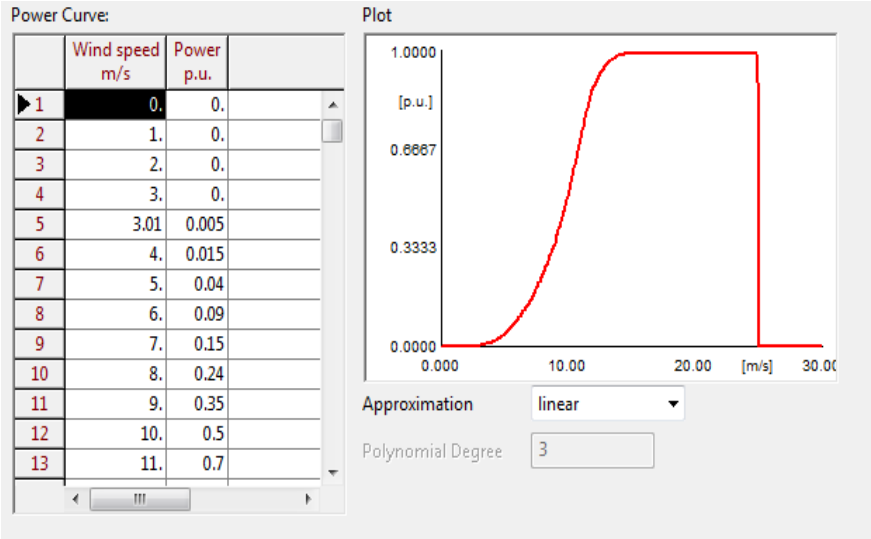

Figure A.1. Wind turbine power curve as in DIgSILENT PowerFactory 2017

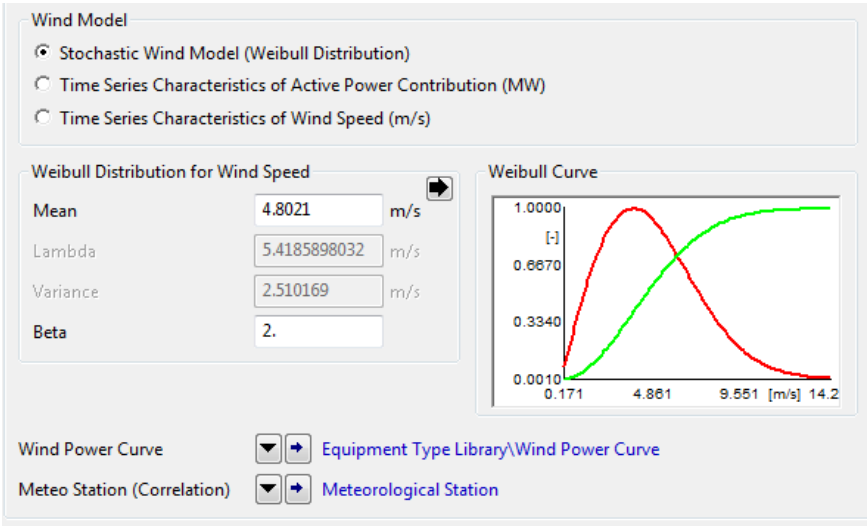

Figure A.2. Wind turbine stochastic wind model as in DIgSILENT PowerFactory 2017

A.1.4 Impedance calculation

In accordance with the *Low-voltage reticulation, section 1: Low voltage overhead reticulation standards* [15], the following distribution and isolation transformer rating has been selected, as in Table A.7 and Table A.8, respectively. The specifications are inputted into the simulation requirements, as requested by DIgSILENT PowerFactory 2017.

Table A.7. Distribution transformer rating

Transformer power rating (S_{rT})	200 kVA
Connection	Dny11
HV voltage rating (U_{HV})	11 kV
LV voltage rating (U_{LV})	420 V
Impedance (U_z)	4.5 %
Copper losses (P_k)	3600 W
X/R ratio	2.592
Type	Oil emerged

With the distribution transformer rating information given in Table A.7, the positive- and zero-sequence components can be calculated as follows:

$$\begin{aligned} Z_{base} &= \frac{U_{LV}^2}{S_{rT}}, \\ &= 0.882\,\Omega, \end{aligned} \tag{A.2}$$

$$\begin{aligned} I_{prim} &= \frac{S_{rT}}{U_{HV}\sqrt{3}}, \\ &= 10.497\,A, \end{aligned} \tag{A.3}$$

$$I_{sec} = \frac{S_{rT}}{U_{LV}\sqrt{3}},$$
$$= 274.93\,A, \tag{A.4}$$

$$X_T = \frac{U_z}{100}\left(\frac{U_{LV}^2}{S_{rT}}\right),$$
$$= 0.03969\,\Omega, \tag{A.5}$$

$$I_{kss}^{''} = \frac{S_{rT} * 100}{U_z U_{rT}\sqrt{3}},$$
$$= 6.465\,kA, \tag{A.6}$$

$$R_k^{''} = \frac{P_k}{3I_{sec}^2},$$
$$= 15.88\,m\Omega, \tag{A.7}$$

$$Z_k^{''} = \frac{U_z U_{LV}^2}{S_{rT} * 100},$$
$$= 39.69\,m\Omega, \tag{A.8}$$

$$X_k^{''} = \sqrt{(Z_k^{''})^2 - (R_k^{''})^2},$$
$$= 36.37\,m\Omega, \tag{A.9}$$

$$\begin{aligned} Z_0 = Z_1 = Z_T &= R + jX_t, \\ &= \frac{0.03969}{2.592} + j0.03969\,\Omega, \\ &= 0.0153 + j0.0397\,\Omega. \end{aligned} \tag{A.10}$$

Table A.8. Isolation transformer rating

Transformer power rating (S_{rT})	100 kVA
Connection	Y_g/y_g - Y_g/Δ
HV voltage rating (U_{HV})	420 V
LV voltage rating (U_{LV})	380 V
Impedance (U_z)	4.85 %
Copper losses (P_k)	1750 W
X/R ratio	1.315
Type	Oil emerged

With the isolation transformer rating information given in Table A.8, the positive- and zero-sequence components can be calculated as follows:

$$\begin{aligned} Z_{base} &= \frac{U_{LV}^2}{S_{rT}}, \\ &= 1.444\,\Omega, \end{aligned} \tag{A.11}$$

$$\begin{aligned} I_{prim} &= \frac{S_{rT}}{U_{HV}\sqrt{3}}, \\ &= 137.46A, \end{aligned} \tag{A.12}$$

$$I_{sec} = \frac{S_{rT}}{U_{LV}\sqrt{3}},$$
$$= 151.93\,A, \tag{A.13}$$

$$X_T = \frac{U_z}{100}\left(\frac{U_{LV}^2}{S_{rT}}\right),$$
$$= 0.07\,\Omega, \tag{A.14}$$

$$I_{kss}'' = \frac{S_{rT} * 100}{U_z U_{rT}\sqrt{3}},$$
$$= 1.700\,kA, \tag{A.15}$$

$$R_k'' = \frac{P_k}{3I_{sec}^2},$$
$$= 25.27\,m\Omega, \tag{A.16}$$

$$Z_k'' = \frac{U_z U_{LV}^2}{S_{rT} * 100},$$
$$= 70.03\,m\Omega, \tag{A.17}$$

$$X_k'' = \sqrt{(Z_k'')^2 - (R_k'')^2},$$
$$= 65.31\,m\Omega, \tag{A.18}$$

$$\begin{aligned} Z_0 = Z_1 = Z_T &= R + jX_t, \\ &= \frac{0.07003}{1.315} + j0.07003\,\Omega, \\ &= 0.0533 + j0.07003\,\Omega. \end{aligned} \tag{A.19}$$

The external source impedance values have been obtained, using DIgSILENT PowerFactory 2017 where the values have been simulated, using the overall system impedance and fault currents at the 132/11 kV substation that supplies Feeder A. The minimum and maximum values have been obtained by simulating the system fault currents under N-1 (where an HV/LV transformer in the distribution substation was switched off), as well as under normal operation conditions, respectively.

Table A.9. External source impedance values

External system voltage	1.02 ∠ -48.44 °	
	Max values	**Min values**
Short circuit power (MVA)	228.4783	165.7763
Short circuit current (kA)	11.992	8.701
R/X ratio	0.106	0.141
Z_1 (Ω)	1.112	1.532
Z_2 (Ω)	1.112	1.532
X_1 (Ω)	1.106	1.525
X_0 (Ω)	16.8	16.8
R_0 (Ω)	33.883	33.883
Z_2/Z_1 ratio	1	1
X_0/X_1	15.189	11.016
R_0/X_0	2.017	2.017

From Table A.9, the zero-, positive- and negative-sequence components are as follows:

$$Z_1 = 0.11536 + j1.10600\,\Omega,$$
$$Z_0 = 0.8Z_1 = 0.09229 + j0.88480\,\Omega. \tag{A.20}$$

Eskom refers to aerial bundled conductors (ABC) with a bare (uninsulated) neutral supporting core for use in overhead single-phase, dual-phase and three-phase LV distribution networks, based on *SANS 1418-1* [19]. The overhead line resistance values have been obtained from the manufacturer's data sheet. Using (A.21), the information in Table A.9 and Table A.10 can be found.

$$Z_0 = R^{'} + (1.571 * 10^{-7} * 2\pi f) + j(2 * 10^{-7} * 2\pi f log\frac{de}{GMR})\,\Omega/m, \tag{A.21}$$

where

earth return of equivalent depth (de) = $\frac{1650}{\sqrt{\frac{\rho}{2\pi f}}}$,

ρ = 100 Ω m,

geometric mean radius (GMR) = $e^{-0.25}r^{'}$,

$r^{'} = F_c\sqrt{\frac{q_n}{\pi}}$,

F_c = Strand lay factor,

q_n = Nominal cross sectional area of conductor in mm^2.

Table A.10. Overhead line ratings

ACSR line type	Rabbit
Overall line distance	1 km
Overall conducting diameter	50 mm^2
GMR	0.00326 m
Rated current	186 A
AC - resistance $R^{'}$ (@ 20 °C)	0.547042 Ω/km
AC - resistance $R_0^{'}$	0.69373 Ω/km
Reactance $X^{'}$	0.384855 Ω/km
Reactance $X_0^{'}$	1.718625 Ω/km
Max operating temperature	80 °C
Susceptance $B^{'}$	3.679125 μS/km
Susceptance $B_0^{'}$	1.501234 μS/km
Max end temperature	50 °C
Rated short-time (1s) current	5.96 kA

Assuming the overhead line has a length of 1 km, the positive- (Z_1) and zero- (Z_0) sequence components can be derived from Table A.10.

$$Z_1 = 0.54704 + j0.38486\,\Omega,$$
$$Z_0 = 0.69373 + j1.71865\,\Omega. \tag{A.22}$$

Table A.11. Underground cable ratings

XLPE cable type	NAKBA 0.6/1 kV 150 mm^2/7sm (aluminum)
Current rating	292 A
Underground current rating	277 A
Overall conducting diameter	150 mm^2
GMR	0.005704 m
Overall cable distance	1 km
AC - resistance $R^{'}$ (@ 20 °C)	0.206 Ω/km
AC - resistance $R_0^{'}$	0.824 Ω/km
Reactance $X^{'}$	0.0819957 Ω/km
Reactance $X_0^{'}$	0.3279823 Ω/km
Max operating temperature	65 °C
Susceptance $B^{'}$	298.4513 μS/km
Susceptance $B_0^{'}$	179.0708 μS/km
Max end temperature	180 °C
Rated short-time (1s) current	12.9 kA
Depth of laying	0.8 m
Cable formation	Trefoil
Soil type	Very dry

Assuming the underground cable has a length of 1 km, the positive- (Z_1) and zero- (Z_0) sequence components can be derived from the Table A.11.

$$Z_1 = 0.20600 + j0.08199\,\Omega,$$
$$Z_0 = 0.82400 + j0.32798\,\Omega, \tag{A.23}$$

Assuming the worst-case fault levels for the PV, Wind turbine and ESS in the RBM, the following zero- and positive-sequence components are determined, using the information given in Table A.3, Table A.4, Table A.5 and Table A.6.

$$Z_1 = 2.10748 + j1.7067\,\Omega,$$

$$Z_0 = 0.8Z_1 = 1.68594 + j1.3654\,\Omega. \tag{A.24}$$

A.1.5 Theoretical fault analysis

The complete zero- and positive-sequence components of the Case study can be seen in Figure A.3. The information will be used to calculate the theoretical fault levels of the LV RDN system with embedded RBMs.

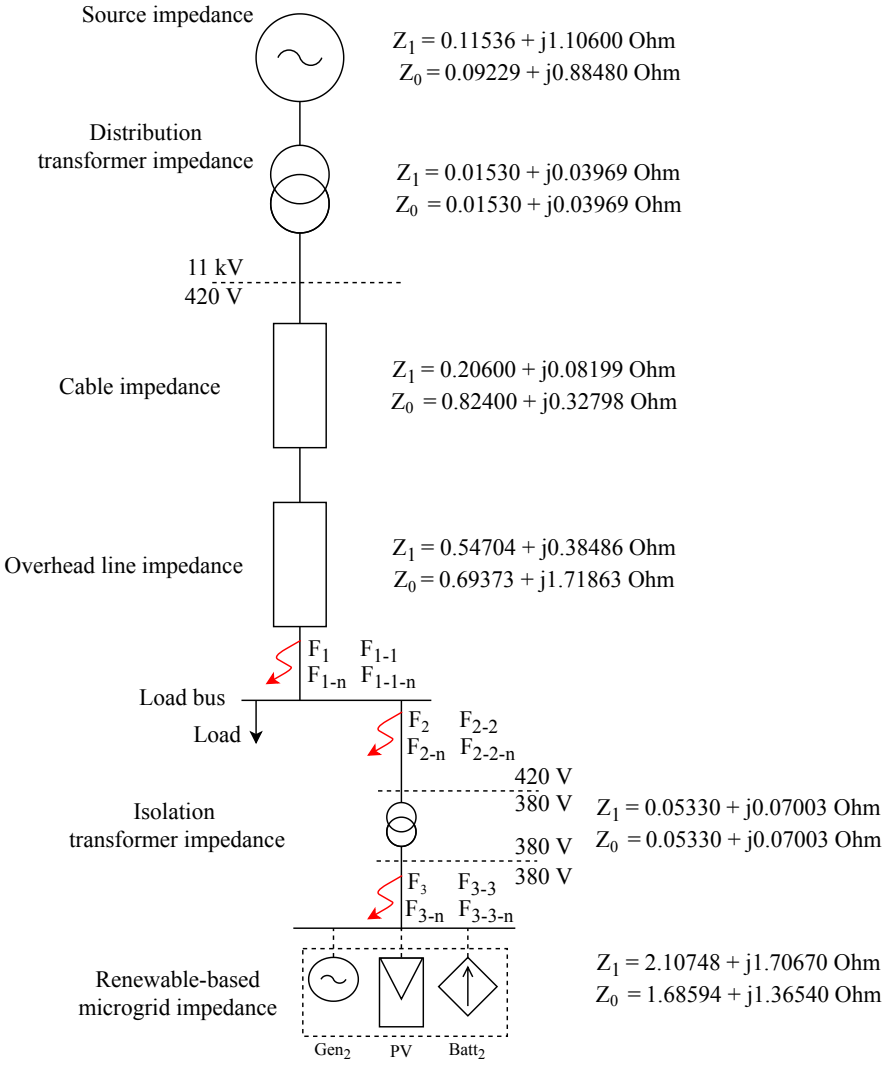

Figure A.3. Single line diagram of overall system impedance values

A.1.5.1 Before embedded RBM fault contribution

Total impedance on HV side:

$$Z_1 = 0.13066 + j1.14569\,\Omega,$$
$$Z_0 = 0.10759 + j0.92449\,\Omega, \tag{A.25}$$

Total impedance on LV side:

$$Z_1 = 0.75304 + j0.46685\,\Omega,$$
$$Z_0 = 1.51773 + j2.04661\,\Omega, \tag{A.26}$$

Total impedance on HV side, referenced to LV side:

$$Z_1 = (0.13066 + j1.14569)(\frac{420}{11000})^2\,\Omega,$$
$$Z_0 = (0.10759 + j0.92449)(\frac{420}{11000})^2\,\Omega, \tag{A.27}$$

Total impedance on LV side:

$$Z_1 = Z_2 = 0.75323 + j0.46852\,\Omega,$$
$$Z_0 = 1.51773 + j2.04661^{(*)}\,\Omega, \tag{A.28}$$

$^{(*)}$Note that the zero-sequence impedance upstream of the distribution transformer has no effect due to the Dyn11 connection.

From the LV RDN impedance values calculated, the following short-circuit calculations can be made: Three-phase (F_1), phase-phase (F_{1-1}), single-phase (F_{1-n}) and phase-phase-to-ground (F_{1-1-n}) faults can be calculated. The faults occur at the end of the 1 km overhead line, as seen in Figure A.3.

$$F_1 = I''_{kss} = \frac{U_{LV}}{Z_1\sqrt{3}},$$
$$= 273.36\angle -31.88^\circ A, \tag{A.29}$$

$$F_{1-1} = I''_{kss_B} = \frac{U_{LV}}{Z_1 + Z_2},$$
$$= 236.74\angle -121.87^\circ A,$$
$$I''_{kss_C} = 236.74\angle 58.12^\circ A, \tag{A.30}$$

$$F_{1-n} = I''_{kss_A} = \frac{U_{LV}\sqrt{3}}{2Z_1 + Z_0},$$
$$= 171.24\angle -44.61^\circ A, \tag{A.31}$$

$$F_{1-1-n} = I''_{kss_B} = \frac{U_{LV}}{Z_1 + (Z_2//Z_0)},$$
$$= 225.03\angle -136.87^\circ A,$$
$$I''_{kss_C} = 262.64\angle 70.92^\circ A. \tag{A.32}$$

A.1.5.2 After embedded RBM fault contribution

RBM referenced to LV RDN side, with no isolation transformer:

$$Z_1 = 2.10748 + j1.70670\,\Omega,$$
$$Z_0 = 1.68594 + j1.36540\,\Omega, \tag{A.33}$$

RBM referenced to LV RDN side, with isolation transform:

$$Z_1 = Z_2 = (0.0533 + j0.07003 + 2.10748 + j1.70670)(\frac{380}{420})^2\,\Omega,$$
$$= (0.04363 + j0.05733 + 1.72517 + j1.39709)\,\Omega,$$
$$= 1.76880 + j1.45442\,\Omega, \tag{A.34}$$
$$Z_0 = (0.0533 + j0.07003 + 1.68594 + j1.36540)(\frac{380}{420})^2\,\Omega,$$
$$= (0.04363 + j0.05733 + 1.38010 + j1.11771)\,\Omega,$$
$$= 1.42373 + j1.17503\,\Omega, \tag{A.35}$$

New Z_{base} value due to different S_{base} of transformers:

$$\begin{aligned} Z^{new} &= Z^{old} * (\frac{S^{new}}{S^{old}})(\frac{V^{old}}{V^{new}})^2, \\ &= 1.444 * (\frac{200\,kVA}{100\,kVA})(\frac{380\,V}{420\,V})^2, \\ &= 2.36409\,\Omega, \end{aligned} \tag{A.36}$$

Total impedance, on LV RDN side with Y_g/Δ connected isolation transformer and embedded microgrid:

$$\begin{aligned} Z_1 = Z_2 &= 1.60198 + j1.14452\,p.u., \\ Z_0 &= 1.72078 + j2.32042^{(*)}\,p.u., \end{aligned} \tag{A.37}$$

$^{(*)}$Note that the zero-sequence impedance of the downstream isolation transformer has no effect, due to the Y_g/Δ connection.

Total impedance on LV RDN side, with Y_g/y_g connected isolation transformer and embedded microgrid:

$$\begin{aligned} Z_1 = Z_2 &= 1.60198 + j1.14452\,p.u., \\ Z_0 &= (1.72078 + j2.32042 + 0.60223 + j0.49703)\,p.u., \\ &= 2.32301 + j2.81745\,p.u., \end{aligned} \tag{A.38}$$

From the LV RDN impedance values calculated, the following short-circuit calculations can be made for the scenario when the RBM would be in grid-connected mode: Three-phase (F_2), phase-phase (F_{2-2}), single-phase (F_{2-n}) and phase-phase-to-ground (F_{2-2-n}) faults can be calculated. The faults occur between the load bus and RBM isolation transformer when grid-connected, as seen in Figure A.3.

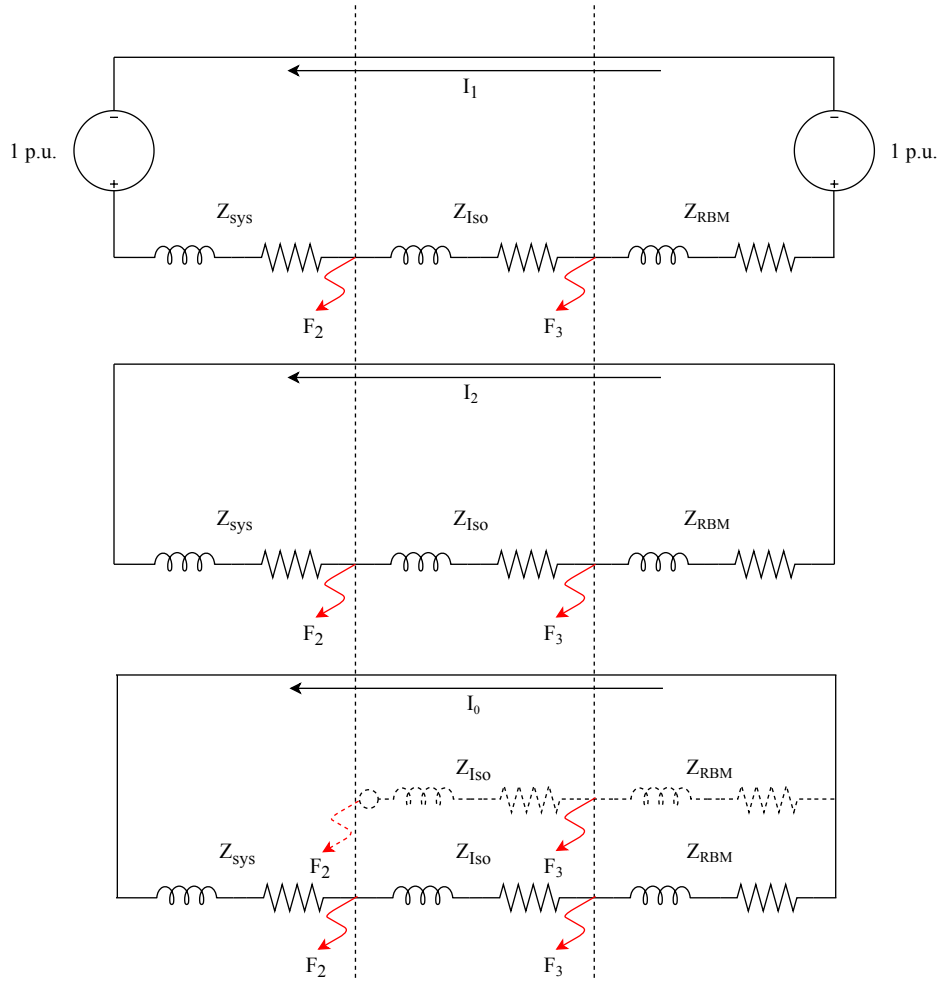

Figure A.4. Single line diagram of overall system sequence components

Faults at F_2, with no connected isolation transformer:

$$F_2 = I''_{kss} = \frac{U_{LV}}{Z_1\sqrt{3}},$$
$$= 209.15\angle -33.64^\circ A, \tag{A.39}$$

$$\begin{aligned} F_{2-2} = I''_{kss_B} &= \frac{U_{LV}}{Z_1 + Z_2}, \\ &= 313.72\angle -123.64^\circ A, \\ I''_{kss_C} &= 313.72\angle 56.36^\circ A, \end{aligned} \tag{A.40}$$

$$\begin{aligned} F_{2-n} = I''_{kss_A} &= \frac{U_{LV}\sqrt{3}}{2Z_1 + Z_0}, \\ &= 502.78\angle -39.26^\circ A, \end{aligned} \tag{A.41}$$

$$\begin{aligned} F_{2-2-n} = I''_{kss_B} &= \frac{U_{LV}}{Z_1 + (Z_2 // Z_0)}, \\ &= 317.23\angle -145.63^\circ A, \\ I''_{kss_C} &= 353.87\angle 75.99^\circ A, \end{aligned} \tag{A.42}$$

Faults at F_2, with Y_g/Δ connected isolation transformer:

$$\begin{aligned} F_2 = I''_{kss} &= \frac{U_{LV}}{Z_1\sqrt{3}}, \\ &= 320.99\angle -35.73^\circ A, \end{aligned} \tag{A.43}$$

$$\begin{aligned} F_{2-2} = I''_{kss_B} &= \frac{U_{LV}}{Z_1 + Z_2}, \\ &= 481.49\angle -125.73^\circ A, \\ I''_{kss_C} &= 481.49\angle 54.27^\circ A, \end{aligned} \tag{A.44}$$

$$F_{2-n} = I''_{kss_A} = \frac{U_{LV}\sqrt{3}}{2Z_1 + Z_0},$$
$$= 371.75\angle -48.94^\circ A, \tag{A.45}$$

$$F_{2-2-n} = I''_{kss_B} = \frac{U_{LV}}{Z_1 + (Z_2//Z_0)},$$
$$= 478.97\angle -125.67^\circ A,$$
$$I''_{kss_C} = 484.02\angle 54.21^\circ A, \tag{A.46}$$

Faults at F_2, with Y_g/y_g connected isolation transformer:

$$F_2 = I''_{kss} = \frac{U_{LV}}{Z_1\sqrt{3}},$$
$$= 320.99\angle -35.73^\circ A, \tag{A.47}$$

$$F_{2-2} = I''_{kss_B} = \frac{U_{LV}}{Z_1 + Z_2},$$
$$= 481.49\angle -125.73^\circ A,$$
$$I''_{kss_C} = 481.49\angle 54.27^\circ A, \tag{A.48}$$

$$F_{2-n} = I''_{kss_A} = \frac{U_{LV}\sqrt{3}}{2Z_1 + Z_0},$$
$$= 554.29\angle -45.91^\circ A, \tag{A.49}$$

$$F_{2-2-n} = I''_{kss_B} = \frac{U_{LV}}{Z_1 + (Z_2 // Z_0)},$$
$$= 466.73\angle -139.09^\circ A,$$
$$I''_{kss_C} = 520.22\angle 66.25^\circ A. \quad \text{(A.50)}$$

Table A.12. Summary of theoretically calculated faults, when grid-connected

Trfr	3-ph	ph-ph	ph-gnd	ph-ph-gnd	
	I''_{kss} (A)	I_{kssB} = -I_{kssC} (A)	I_{kss} (A)	I_{kssB} (A)	I_{kssC} (A)
None	$209\angle -34^\circ$	$313\angle -124^\circ$	$502\angle -39^\circ$	$317\angle -146^\circ$	$353\angle 76^\circ$
Y_g/Δ	$320\angle -36^\circ$	$481\angle -126^\circ$	$372\angle -49^\circ$	$479\angle -126^\circ$	$484\angle 54^\circ$
Y_g/y_g	$320\angle -36^\circ$	$481\angle -126^\circ$	$554\angle -46^\circ$	$466\angle -139^\circ$	$520\angle 66^\circ$

From the LV RDN impedance values calculated, the following short-circuit calculations can be made for the scenario when the RBM would be in stand-alone mode: Three-phase (F_3), phase-phase (F_{3-3}), single-phase (F_{3-n}) and phase-phase-to-ground (F_{3-3-n}) faults can be calculated. The faults occur between the RBM isolation transformer and RBM, as seen in Figure A.3.

Faults at F_3, with no isolation transformer:

$$F_3 = I''_{kss} = \frac{U_{LV}}{Z_1\sqrt{3}},$$
$$= 46.71\angle -39.00^\circ A, \quad \text{(A.51)}$$

$$F_{3-3} = I''_{kss_B} = \frac{U_{LV}}{Z_1 + Z_2},$$
$$= 70.06\angle -129.00^\circ A,$$
$$I''_{kss_C} = 70.06\angle 50.99^\circ A, \quad \text{(A.52)}$$

$$F_{3-n} = I''_{kss_A} = \frac{U_{LV}\sqrt{3}}{2Z_1 + Z_0},$$
$$= 150.13\angle -39.00^\circ A, \tag{A.53}$$

$$F_{3-3-n} = I''_{kss_B} = \frac{U_{LV}}{Z_1 + (Z_2//Z_0)},$$
$$= 84.18\angle -162.67^\circ A,$$
$$I''_{kss_C} = 84.19\angle 84.66^\circ A, \tag{A.54}$$

Faults at F_3, with Y_g/Δ isolation transformer:

$$F_3 = I''_{kss} = \frac{U_{LV}}{Z_1\sqrt{3}},$$
$$= 1.48\angle -52.29^\circ kA, \tag{A.55}$$

$$F_{3-3} = I''_{kss_B} = \frac{U_{LV}}{Z_1 + Z_2},$$
$$= 2.23\angle -142.29^\circ kA,$$
$$I''_{kss_C} = 2.23\angle 37.70^\circ kA, \tag{A.56}$$

$$F_{3-n} = I''_{kss_A} = \frac{U_{LV}\sqrt{3}}{2Z_1 + Z_0},$$
$$= 488.04\angle -39.96^\circ A, \tag{A.57}$$

$$F_{3-3-n} = I''_{kss_B} = \frac{U_{LV}}{Z_1 + (Z_2//Z_0)},$$
$$= 2.72\angle -150.38^\circ\, kA,$$
$$I''_{kss_C} = 2.68\angle 33.35^\circ\, kA, \tag{A.58}$$

Faults at F_3, with Y_g/y_g isolation transformer:

$$F_3 = I''_{kss} = \frac{U_{LV}}{Z_1\sqrt{3}},$$
$$= 1.48\angle -52.29^\circ\, kA, \tag{A.59}$$

$$F_{3-3} = I''_{kss_B} = \frac{U_{LV}}{Z_1 + Z_2},$$
$$= 2.23\angle -142.29^\circ\, kA,$$
$$I''_{kss_C} = 2.23\angle 37.70^\circ\, kA, \tag{A.60}$$

$$F_{3-n} = I''_{kss_A} = \frac{U_{LV}\sqrt{3}}{2Z_1 + Z_0},$$
$$= 4.47\angle -52.26^\circ\, kA, \tag{A.61}$$

$$F_{3-3-n} = I''_{kss_B} = \frac{U_{LV}}{Z_1 + (Z_2//Z_0)},$$
$$= 2.58\angle -172.41^\circ\, kA,$$
$$I''_{kss_C} = 2.57\angle 67.85^\circ\, kA. \tag{A.62}$$

Table A.13. Summary of theoretically calculated faults, when stand-alone

Trfr	3-ph	ph-ph	ph-gnd	ph-ph-gnd	
	I''_{kss} (kA)	I_{kssB} = -I_{kssC} (kA)	I_{kss} (kA)	I_{kssB} (kA)	I_{kssC} (kA)
None	$0.05 \angle -39°$	$0.07 \angle -129°$	$0.15 \angle -39°$	$0.08 \angle -163°$	$0.08 \angle 85°$
Y_g/Δ	$1.48 \angle -52°$	$2.23 \angle -142°$	$0.49 \angle -40°$	$2.72 \angle -150°$	$2.68 \angle 33°$
Y_g/y_g	$1.48 \angle -52°$	$2.23 \angle -142°$	$4.47 \angle -52°$	$2.58 \angle -172°$	$2.57 \angle 68°$

From the theoretically calculated faults, it can be seen that without an isolation transformer present, the fault levels during stand-alone mode are significantly smaller than than when an isolation transformer is present. This high-impedance cause low fault currents, which can go undetected by the protection relay, damaging connected equipment in the LV RDN. The Y_g/y_g connected transformer will be used in the case study, because of the higher single-phase fault level and lower phase-to-phase-to-ground fault level when compared to the Y_g/Δ isolation transformer. With the use of inverters limiting fault current capabilities, the RBMs' high fault contribution can be further minimised. Additionally, with the use of low-pass filters, the negative-sequence components can be filtered out. This will assist in further limiting the RBMs fault contribution to the LV RDN.

A.1.6 Simulation criteria and results

The following results were simulated in DIgSILENT PowerFactory 2017.

A.1.6.1 Results for before embedded RBMs

Table A.14. Customer load flow before embedded RBMs

	P (kW)	**Q (kvar)**	**I_{nom} (A)**	**Power factor**
Load 1	14.22	4.67	26.08	0.95
Load 2	16.31	5.36	30.33	0.95
Load 3	13.28	4.36	24.20	0.95
Load 4	16.72	5.49	31.19	0.95

Table A.15. Bus load flow and fault levels before RBMs

Load flow					
	P (kW)	**Q (kvar)**	**Voltage (p.u.)**	I_{nom} **(A)**	
Bus 1	77.20	27.68	1.02 ∠-48.44°	4.22	
Bus 2	72.09	26.23	1.007∠-19.28°	111.03	
Bus 3	65.28	23.24	0.901∠-19.505°	111.05	
Bus 4	14.15	4.62	0.829∠-20.905°	25.92	
Bus 5	18.18	65.2	0.814∠-20.18°	30.96	
Bus 6	16.20	5.29	0.817∠-21.133°	30.11	
Bus 7	13.21	4.32	0.834∠-20.804°	24.06	
Fault levels (kA)					
	3-ph (kA)	**ph-ph (kA)**	**ph-gnd (kA)**	**ph-ph-gnd (kA)**	
	I_{kss}	I_{kssB}=-I_{kssC}	I_{kssA}	I_{kssB}	I_{kssC}
Bus 1	11.992	10.385	1.024	10.606	10.167
Bus 2	6.13	5.308	5.812	6.158	6.14
Bus 3	0.969	0.839	0.515	0.87	0.845
Bus 4	0.264	0.229	0.167	0.219	0.253
Bus 5	0.264	0.229	0.167	0.219	0.253
Bus 6	0.264	0.229	0.167	0.219	0.253
Bus 7	0.264	0.229	0.167	0.219	0.253

Table A.16. Transformer, overhead lines and cable load flow before RBMs

Load flow				
	P (kW)	**Q (kvar)**	I_{nom} **(A)**	**Loading (%)**
TR HV side	77.2	27.68	42.2	41.3
TR LV side	-72.9	-26.23	111.03	
Cable 1	72.9	26.23	111.05	39.5
Line 1	152.5	54.0	25.92	13.9
Line 2	18.18	6.52	30.96	16.6
Line 3	17.69	63.3	30.11	16.2
Line 4	14.16	4.99	24.05	12.9
(*)Note that the power absorbed is represented as positive and the power injected into the system is represented as negative.				

A.1.6.2 Results for after embedded RBMs

The following results were achieved after connecting all of the designed RBMs to the LV RDN Feeder A in the Case study.

Table A.17. Customer load flow after RBMs

	P (kW)	**Q (kvar)**	I_{nom} **(A)**	**Power factor**	**Max load (kVA)**
Load 1	14.25	4.68	21.65	0.95	82.5
Load 2	16.34	5.37	24.1	0.95	94.6
Load 3	13.30	4.37	19.62	0.95	77
Load 4	16.76	5.51	24.72	0.95	97.02

Table A.18. Bus Load flow and fault levels after RBMs

Load flow					
	P (kW)	**Q (kvar)**	**Voltage (p.u.)**	I_{nom} **(A)**	
Bus 1	-45.322	178.17	1.02 ∠-48.44°	9.46	
Bus 2	-51.92	170.55	0.984∠-16.985°	261.57	
Bus 3	94.21	-153.76	0.995∠-2.325°	261.63	
Bus 4	78.19	-69.34	1.00∠22.974°	150.84	
Bus 5	-9.89	32.90	1.03∠-9.96°	48.15	
Bus 6	41.69	-34.40	1.03∠9.96°	75.78	
Bus 7	49.70	-38.93	1.03∠11.534°	85.20	
Fault levels (kA)					
	3-ph (kA)	**ph-ph (kA)**	**ph-gnd (kA)**	**ph-ph-gnd (kA)**	
	I_{kss}	I_{kssB}=-I_{kssC}	I_{kssA}	I_{kssB}	I_{kssC}
Bus 1	12.022	10.404	1.026	10.625	10.185
Bus 2	6.95	5.829	6.773	6.762	6.742
Bus 3	1.789	1.360	0.834	1.410	1.368
Bus 4	0.531	0.383	0.280	0.366	0.424
Bus 5	0.524	0.389	0.284	0.371	0.431
Bus 6	0.751	0.541	0.395	0.517	0.599
Bus 7	0.500	0.548	0.400	0.524	0.607

Table A.19. Transformer, overhead lines and cable load flow and fault levels after RBMs

Load flow				
	P (kW)	**Q (kvar)**	I_{nom} **(A)**	**Loading (%)**
TR HV side	-45.32	178.17	9.46	90.6
TR LV side	51.92	-170.55	261.57	
Cable 1	-51.92	170.55	261.57	93.1
Line 1	-40.85	95.61	150.84	81.1
Line 2	13.70	-30.23	48.15	25.9
Line 3	-32.27	41.07	75.78	40.7
Line 4	-34.79	47.31	85.20	45.8

Table A.20. Increased fault level contributions

	3-ph (A)	**ph-ph (A)**	**ph-gnd (A)**	**ph-ph-gnd (A)**	
	I_{kss}	I_{kssB} = -I_{kssC}	I_{kss}	I_{kssB}	I_{kssC}
Bus 1	30.00	19.00	2.00	19.00	18.00
Bus 2	82.00	521.00	961.00	604.00	602.00
Bus 3	82.00	521.00	319.00	540.00	523.00
Bus 4	267.00	154.00	113.00	147.00	171.00
Bus 5	260.00	160.00	117.00	152.00	178.00
Bus 6	487.00	312.00	228.00	298.00	346.00
Bus 7	236.00	319.00	233.0	305.00	354.00

A.1.6.3 Results for optimally sized RBMs

Table A.21. Optimisation function and constraints applied to bus 5

Bus 5 optimisation					
Before	System losses (β)	Voltage profile (μ)	FCL (η)	RDG capacity (λ)	***Total***
Bus 5	1.9700	2.8923	4.06178	-2.8383	6.0858
Function y	x_1	x_2	x_3	x_4	
	1.000	0.4909	1.1153	1.000	3.6062
After	System losses (β)	Voltage profile (μ)	FCL (η)	RDG capacity (λ)	
Bus 5	0.6872	2.7778	-4.4435	1.9785	1.000
Function y	x_1	x_2	x_3	x_4	
	1.000	0.4444	3.8546	2.8264	8.1255

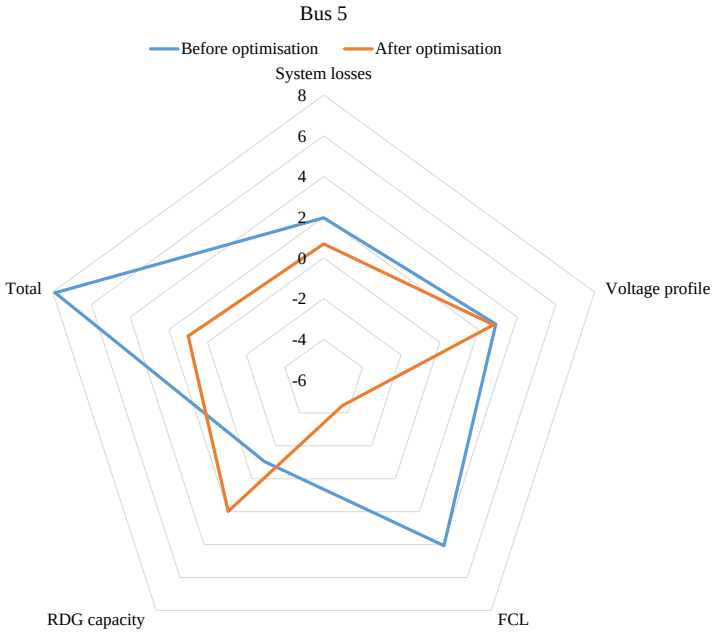

Figure A.5. Bus 5 weight factors before and after optimisation

Table A.22. Optimisation function and constraints applied to bus 6

Bus 6 optimisation					
Before	System losses (β)	Voltage profile (μ)	FCL (η)	RDG capacity (λ)	***Total***
Bus 6	0.3153	2.8923	2.3781	2.0805	7.6662
Function y	x_1	x_2	x_3	x_4	
	1.000	0.4909	1.3412	1.000	3.8318
After	System losses (β)	Voltage profile (μ)	FCL (η)	RDG capacity (λ)	
Bus 6	1.0810	2.7778	0.1752	-3.0339	1.000
Function y	x_1	x_2	x_3	x_4	
	1.000	0.4444	0.2299	-1.5169	0.1574

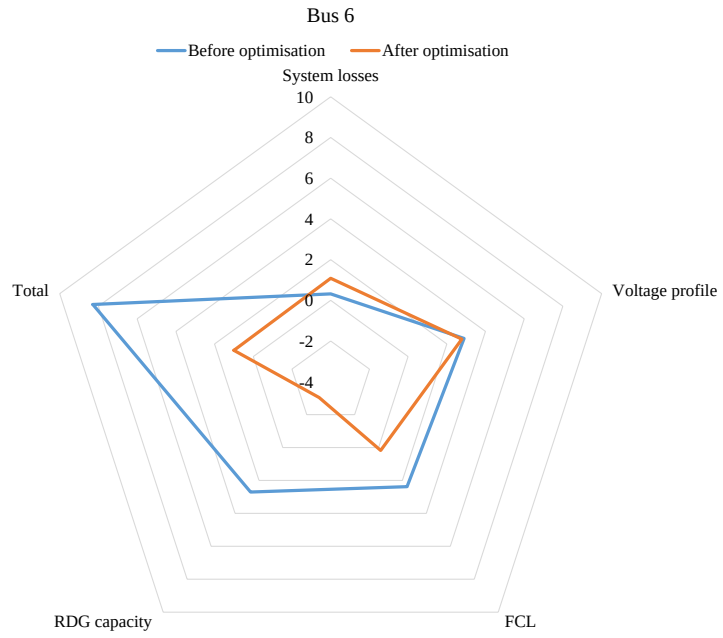

Figure A.6. Bus 6 weight factors before and after optimisation

Table A.23. Optimisation function and constraints applied to bus 7

Bus 7 optimisation					
Before	System losses (β)	Voltage profile (μ)	FCL (η)	RDG capacity (λ)	***Total***
Bus 7	0.2200	2.8923	24.4887	1.9707	9.5718
Function y	x_1	x_2	x_3	x_4	
	1	0.4909	1.1222	1	3.6131
After	System losses (β)	Voltage profile (μ)	FCL (η)	RDG capacity (λ)	
Bus 7	1.0520	2.7778	-1.2032	-1.6267	1
Function y	x_1	x_2	x_3	x_4	
	1	0.4444	0.2353	-1.3012	0.3785

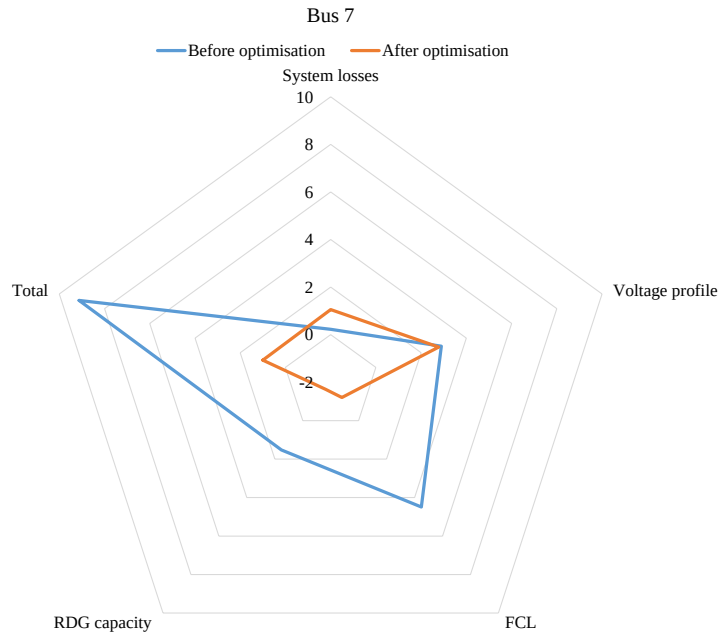

Figure A.7. Bus 7 weight factors before and after optimisation

A.1.7 Grading settings

Table A.24. After optimally sized RBM 1 connected

	Relay 1			
	PSM	T_m	TMS	t
Relay 1	5.3458	4.1062	0.0500	0.2053
Line 1	3.1683	6.0003	0.0925	0.5553
	Line 1			
	PSM	T_m	TMS	t
Relay 1	10.4085	2.9186	0.0925	0.2701
Line 1	6.0023	3.8364	0,.616	0.6201
	Cable			
	PSM	T_m	TMS	t
Cable	29.5261	2.0042	0.1616	0.3240

Table A.25. After optimally sized RBM 2 connected

	Relay 2			
	PSM	T_m	TMS	t
Relay 2	14.9268	2.5202	0.0876	0.2208
Line 2	5.3290	4.1141	0.1387	0.5708
	Line 2			
	PSM	T_m	TMS	t
Relay 2	32.7283	1.9376	0.1387	0.2688
Line 2	6.0246	3.8283	0.1616	0.6188
	Cable			
	PSM	T_m	TMS	t
Cable	29.5261	2.0042	0.1616	0.3240

Table A.26. After optimally sized RBM 3 connected

	Relay 3			
	PSM	T_m	TMS	t
Relay 3	6.2265	3.7581	0.0613	0.2303
Line 3	3.7525	5.2237	0.1111	0.5803
	Line 3			
	PSM	T_m	TMS	t
Relay 3	16.6467	2.4198	0.1111	0.2688
Line 3	6.0246	3.8283	0.1616	0.6188
	Cable			
	PSM	T_m	TMS	t
Cable	29.5261	2.0042	0.1616	0.3240

Table A.27. After optimally sized RBM 4 connected

	Relay 4			
	PSM	T_m	TMS	t
Relay 4	4.8348	4.3724	0.0510	0.2468
Line 3	3.4695	5.5573	0.1074	0.5968
	Line 4			
	PSM	T_m	TMS	t
Relay 4	15.1955	2.5032	0.1074	0.2688
Line 4	6.0246	3.8283	0.1616	0.6188
	Cable			
	PSM	T_m	TMS	t
Cable	29.5261	2.0042	0.1616	0.3240